TRABAJO ESPECIAL DE GRADO

SISTEMAS ÓPTICOS DE TRANSMISIÓN MULTICANAL A LARGA DISTANCIA BASADOS EN RECEPTORES DE TIPO MLSE

Presentado ante la ilustre
Universidad Central de Venezuela
Por el Br. Cook Aguilar, Philippe
Para optar al Título de
Ingeniero Electricista

Caracas, 2008

TRABAJO ESPECIAL DE GRADO

SISTEMAS ÓPTICOS DE TRANSMISIÓN MULTICANAL A LARGA DISTANCIA BASADOS EN RECEPTORES DE TIPO MLSE

Tutor Académico: PhD. Gabriella Bosco
Prof. Guía: Paolo Maragno

Presentado ante la ilustre
Universidad Central de Venezuela
Por el Br. Cook Aguilar, Philippe
Para optar al Título de
Ingeniero Electricista

Caracas, 2008

Cook Aguilar, Philippe

SISTEMAS ÓPTICOS DE TRANSMISIÓN MULTICANAL A LARGA DISTANCIA BASADOS EN RECEPTORES DE TIPO MLSE

Tutor Académico: PhD. Gabriella Bosco. Profesor Guía: Paolo Maragno. Caracas. U.C.V. Facultad de Ingeniería. Escuela de Ingeniería Eléctrica. Ingeniero Electricista. Opción: Comunicaciones. Institución: Politecnico di Torino 2008. Nº pág. 114

Palabras Claves: Dispersión Cromática, Compensación de la dispersión cromática, Sistemas Ópticos de Transmisión, Wavelength Division Multiplexing (WDM), Cross Phase Modulation (XPM)

Resumen. Uno de los principales problemas de la transmisión en fibra óptica es la dispersión cromática. Existen dos tipos de técnicas para compensar los efectos causados por dicho fenómeno. La primera es el uso de fibras compensadoras de la dispersión y la segunda consiste en la compensación electrónica mediante la elaboración de la señal recibida. Entre las distintas técnicas de compensación electrónica existentes, la *Maximum Likelihood Sequence Estimation* (MLSE) es la que ofrece los resultados más prometedores. Ésta técnica trabaja sobre las secuencias de bit recibidas para seleccionar la secuencia transmitida más probable (a través del algoritmo de Viterbi). El objetivo de este trabajo es analizar las prestaciones de distintos formatos de modulación (IMDD, Duobinario, DPSK y DQPSK) en un sistema óptico de transmisión multicanal en presencia de dispersión cromática y efectos no lineales; donde se utilizan conjuntamente las dos técnicas de compensación de la dispersión mencionadas. El estudio del sistema óptico de transmisión se realizó por medio de simulaciones por computador con el programa OptSim y posteriormente los resultados fueron analizados con MATLAB para generar las gráficas del comportamiento del sistema. El resultado fundamental de este estudio es que el uso de receptores de tipo MLSE de complejidad razonable (32 estados) ayuda notablemente a aumentar la tolerancia en el diseño de los parámetros de los mapas de dispersión, aún en presencia significativa del impacto de la XPM. Esto representa una gran ventaja para los sistemas WDM, donde a causa de la pendiente no nula de la curva de dispersión cromática, distintos canales experimentan distintos valores de dispersión "in-line".

Acknowledgments

I wish to thank my supervisors Prof. Gabriella Bosco, Prof. Vittorio Curri and Prof. Pierluigi Poggiolini for giving me the opportunity to carry out my thesis inside their group. I would specially like to thank Prof. Gabriella Bosco for her guidance, encouragement and patience throughout my work.

I would also like to thank my parents, sister and family members for their unconditional love and support throughout these two years which made this journey abroad more comfortable and enjoyable.

Finally I would like to thank my friend Tony and his family in Italy for all their help and support which made me feel at home and as part of their own.

Contents

List of figures

Acronyms

ACS:	Add, Compare and Select
ADC:	Analog-to-Digital Converter
AMZ:	Asymmetric Mach-Zehnder interferometer
ASE:	Amplified Spontaneous Emission
BER:	Bit Error Probability
BPD:	Balanced Photo-Detector
DB:	Duobinary
DCF:	Dispersion Compensating Fiber
DCU:	Dispersion Compensating Unit
DPSK:	Differential Phase Shift Keying
DSF:	Dispersion Shifted Fiber
DQPSK:	Differential Quadrature Phase Shift Keying
DWDM:	Dense Wavelength Division Multiplexing
EDC:	Electronic Dispersion Compensation
EDFA:	Erbium Doped Fiber Amplifier
FEC:	Forward Error Correction
FWM:	Four Wave Mixing
IMDD:	Intensity-Modulation Direct Detection
ISI:	Inter-Symbol Interference
LAN:	Local Area Network
Laser:	Light Amplification by Stimulated Emission of Radiation
LED:	Light Emitting Diode

MLSE:	Maximum Likelihood Sequence Estimation
MZ:	Mach-Zehnder
NRZ:	Non Return to Zero
NZ-DSF:	Non-Zero Dispersion Shifted Fiber
PDF:	Probability Density Function
PMD:	Polarization Mode Dispersion
PRBS:	Pseudo-Random Bit Sequence
OSNR:	Optical Signal to Noise Ratio
RF:	Radio Frequency
RX:	Receiver
RZ:	Return to Zero
SMF:	Single Mode Fiber
SPM:	Self Phase Modulation
SSMF:	Standard Single Mode Fiber
TX:	Transmitter
WDM:	Wavelength Division Multiplexing
XPM:	Cross Phase Modulation
ZDP:	Zero Dispersion Point

Introduction

In the last years, optical communication systems have overcome several obstacles. At the beginning, the biggest problem was the high attenuation introduced by the fiber which made an optical link impossible. Then, in the late 80's when the attenuation problem was solved, the first long distance optical communication systems were born.

With the upgrade of transmission speeds, from 2.5 Gbit/s to 10 Gbit/s for example, chromatic dispersion and non-linear effects become evident. These phenomena present themselves in the form of *Inter-Symbol Interference* (ISI), which strongly impairs the system's performance.

Later, the need for higher capacity gave birth to WDM systems, which allow the expansion of the band without the need to install new stretches of fiber. However, as the spacing between channels decreases, non-linear coupling effects such as *four wave mixing* (FWM) and *cross-phase modulation* (XPM) limit the system's performance.

To assess the problem caused by ISI due to the upgrade of the bit-rate and non-linear effects, different techniques have been developed to be implemented directly on the transmitter or the receiver without touching the transmission channel, thus allowing the use of existing installed fiber.

One of the most important techniques is based on *Electronic Dispersion Compensation* (EDC) at the receiver. It consists on the elaboration of the signal in the electrical domain, after detection with a photodiode.

Amongst the existing EDC techniques, the most promising is *Maximum Likelihood Sequence Estimation* (MLSE) which operates on bit sequences rather than making bit-by-bit decisions based on a fixed threshold level. The MLSE technique selects the most probable sent bit sequence conditional to the received sequence.

This technology is compatible with installed systems and works independently of any other receiver functions, such as *Forward Error Correction* (FEC).

In the existing literature, there are very few papers that study the use of MLSE receivers on dispersion-managed systems, e.g. [8] and [9]. Therefore, the aim of this thesis is to evaluate the effectiveness of the use of MLSE receivers in dispersion-managed multi-channel optical transmission systems working at 10.7 Gbit/s, based on the use of different modulation formats.

This work is structured in eight chapters. In the first chapter, a brief history of fiber optic technology is presented and the structure of a generic optical communications system is explained. In the second chapter, the modulation schemes used in the simulations are presented, these are: *IMDD, Duobinary, DPSK and DQPSK*. In the third chapter, the linear and non-linear optical fiber propagation effects are discussed. In the fourth chapter, the characteristics and functioning of the MLSE technique are presented. In the last four chapters, the results of the system simulations carried out for IMDD, Duobinary, DPSK and DQPSK modulation formats respectively are presented and analyzed.

Chapter 1

Introduction to optical communications systems

Optical communications have evolved out of the necessity for a transmission medium with increased bandwidth capacity. In the last years, optical fiber transmission systems have assumed a predominant position in the realm of high capacity long distance telecommunications.

The success achieved by optical communication systems is due largely to the transmission advantages offered by the fiber, such as:

- Low attenuation, which allows reaching longer distances.
- Immunity to electromagnetic interference, since signals are transmitted as light instead of current.
- Reduced dimensions make possible the grouping of a large number of fibers on a same cable.
- Immense potential bandwidth (50 THz or greater).

In this chapter, a brief history of the evolution of optical communication systems will be presented and the structure of a generic optical transmission system will be explained.

1.1 A brief history of fiber optic technology

As far back as Roman times, glass has been drawn into fibers. Yet, it was not until the 1790s that the French Chappe brothers invented the first "optical telegraph." It was a system comprised of a series of lights mounted on towers where operators would relay a message from one tower to the next. Over the course of the next century great strides were made in optical science.

In the 1840s, physicists Daniel Collodon and Jacques Babinet showed that light could be directed along jets of water for fountain displays. In 1854, John Tyndall, a British physicist, demonstrated that light could travel through a curved stream of water thereby proving that a light signal could be bent. He proved this by setting up a tank of water with a pipe that ran out of one side. As water flowed from the pipe, he shone a light into the tank into the stream of water. As the water fell, an arc of light followed the water down.

In the late 1800's some applications of guided light propagation began to appear as doctors Roth and Reuss, of Vienna, used bent glass rods to illuminate body cavities in 1888. And in 1898, American David Smith applied for a patent on a dental illuminator using a curved glass rod.

Fiber optic technology experienced a phenomenal rate of progress in the second half of the twentieth century. Early success came in the 1950's with the development of the fiberscope, which was an image transmitting device that used the first practical all-glass fiber. However early all-glass fibers experienced excessive optical loss as the signal traveled the fiber, limiting transmission distances.

This motivated scientists to develop glass fibers that included a separate glass coating. The innermost region of the fiber, the core, was used to transmit the light, while the glass coating, the cladding, by having a lower refractive index than the core,

prevented the light from leaking out of the core by reflecting the light within its boundaries.

The development of laser technology was the next important step in the establishment of the industry of fiber optics. In 1960, the first continuously operating helium-neon gas laser is invented and tested. That same year an operable laser was invented which used a synthetic pink ruby crystal as the medium and produced a pulse of light. Semiconductor lasers, which are widely used in fiber optics today, were first developed in 1962.

Because of their higher modulation frequency capability, the importance of lasers as a means of carrying information did not go unnoticed by communications engineers. However, the laser is unsuited for air transmission since it is adversely affected by environmental conditions such as rain, snow and smog. Faced with the challenge of finding a transmission medium other than the air, in 1966 it was proposed that optical fiber might be a suitable transmission medium if its attenuation could be kept under 20 dB/Km. At the time of this proposal, optical fiber exhibited losses of 1000 dB/Km or more. Intuitively, researchers proposed that the high optical losses were the result of impurities in the glass and not the glass itself.

In 1970, the goal of making fibers with attenuation less than 20dB/km was reached by scientists at Corning Glass Works. This was achieved through doping silica glass with titanium.

The early work on fiber optic light source and detector was slow and often had to borrow technology developed for other reasons. For example, the first optical fiber light sources were derived from visible indicators LEDs. But as demand grew, light sources that offered higher switching speed, more appropriate wavelengths and higher output power were developed.

Fiber optics developed over the years in a series of generations that can be closely tied to wavelengths.

The earliest fiber optic systems were developed at an operating wavelength of about 850 nm. This wavelength corresponds to the so called *first window* in a silica-based optical fiber. This window refers to a wavelength region that offers low optical loss. It sits between large absorption peaks caused primarily by moisture in the fiber and Rayleigh scattering.

The 850 nm region was initially attractive because the technology of light emitters at this wavelength had already been perfected in visible indicator LEDs and low cost silicon detectors could also be used. As technology progressed, the *first window* became less attractive because of its relatively high 3 dB/Km loss limit. Then, most companies jumped to the *second window* at 1310 nm with lower attenuation of about 0.5 dB/Km. And in 1977 the *third window* at 1550 nm was developed. This window offered the theoretical minimum optical loss for silica-based fibers, about 0.2 dB/Km [1].

The erbium-doped fiber amplifier (EDFA), which reduced the cost of long-distance fiber systems by eliminating the need for optical-electrical-optical repeaters, was invented in 1986 by David Payne of the University of Southampton and Emmanuel Desurvire at Bell Labratories. Based on Desurvire's optimized laser amplification technology, the first transatlantic telephone cable went into operation in 1988.

In the 90’s the technique of Wavelength Division Multiplexing (WDM) is introduced. The optical fiber industry has continued its advance with the development of new types of fibers and optical components that keep raising the bar in terms of efficiency and capacity.

In the last decade researchers have explored new ways to improve optical communication systems such as innovative modulation formats, dispersion compensation and distributed amplification (RAMAN amplifier).

The tendency in recent research is to accomplish the implementation of most of the functions of a network in the optical domain.

1.2 A generic optical communications system

A generic optical communications system consists of a transmitter, an optical fiber (that constitutes the channel) and a receiver. A simple scheme of this system is shown in *Figure 1.1*.

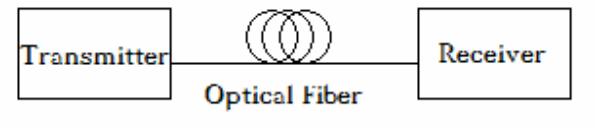

Figure 1.1. Generic optical communications system

1.2.1 The optical transmitter

The optical transmitter transforms the electric signal applied at its input into an optical signal suitable for propagation on the fiber.

There are two types of transmitters: those based on direct modulation and those based on external modulation.

- Transmitter based on direct modulation

  When using a direct modulation transmitter, the digital signal containing the information to be transmitted guides the optical source between two levels representing the "1" and "0" via an electronic driver, so the signal comes out already modulated in intensity as shown in *Figure 1.3*. A direct modulation transmitter is represented in *Figure 1.2*.

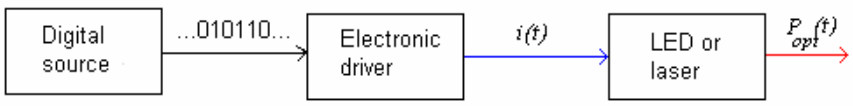

Figure 1.2. Direct modulation transmitter

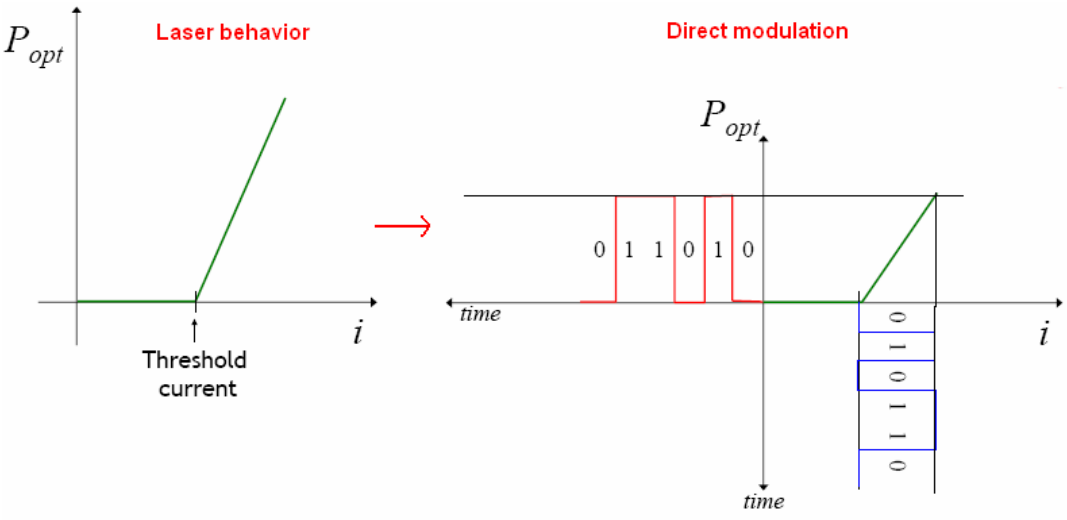

Figure 1.3. Direct modulation

This type of transmitter is cheap and easy to implement, but a small variation of the current that controls the optical source causes a variation on the phase and frequency of the output signal. This means that the modulated signal occupies a wide bandwidth and is more susceptible to chromatic dispersion.

For this reasons, direct modulation is used on low bit-rate short distance systems such as Local Area Networks.

- Transmitter based on external modulation

  In this case, the optical source is kept at constant power to provide a stable output which is modulated externally. The external modulator modulates the phase, polarization or intensity of the constant power optical signal according to the digital signal to be transmitted. The structure of an externally modulated transmitter is shown in *Figure 1.4*.

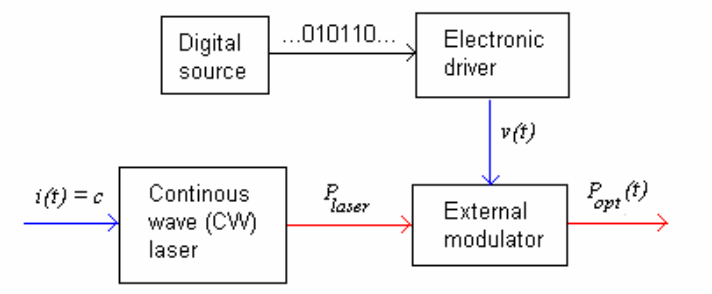

Figure 1.4. Externally modulated transmitter

The external modulation generates a narrower band signal than the direct modulation, and it yields better results regarding chromatic dispersion, but yet, it is more costly.

This type of modulation is used for long distance transmissions and in DWDM systems.

Any type of transmitter is based on an optical source. Optical sources are active devices which emit electromagnetic radiation at the optical frequencies. These can be classified in *Light Emitting Diodes* (LED) and *Light Amplification by the Stimulated Emission of Radiation* (LASER).

- LED

Light Emitting Diodes work thanks to the phenomenon of *spontaneous emission*. This phenomenon consists of the spontaneous drop of an electron from a high energy level E_2 to a low energy level E_1, generating in consequence a photon with energy E_2-E_1. The frequency of the generated photon is determined by Planck's law:

$$h \cdot f_{photon} = E_2 - E_1 \qquad (1.1)$$

In the LED photons are generated in a random manner in every direction and in an ample range of frequencies, but only a fraction of photons emitted couple on to the fiber.

As a first approximation the optic output power is proportional to the injected current.

$$P_{out} = k \cdot I(t) \qquad (1.2)$$

The LED has a low output power, a low modulation velocity and its use in optical systems brings strong limitations caused by dispersion due to the fact that the output signal bandwidth is wide. Consequently, they are used in low cost applications, typically with multimode fibers, in short distances (1 Km maximum) and low bit-rates (up to 155 Mbit/s).

- LASER

In a semiconductor laser, photons are generated in a p-n junction polarized directly. Then, these photons are forced to transit in the inner structure several times by using some type of partially reflector filter placed on both its sides. During transit, the photons are amplified by the effect of the *stimulated emission*.

In the stimulated emission, an electron drops from the conduction band to the valence band due to the interaction with an incoming photon, and consequently a photon with the same frequency and phase of the incoming one is generated. This phenomenon is represented in *Figure 1.5*.

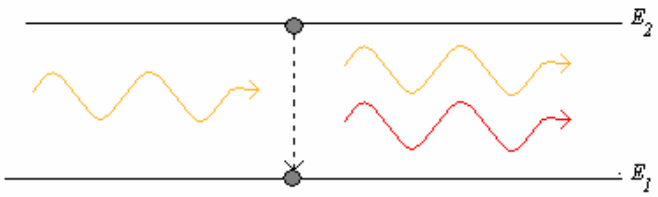

Figure 1.5. Stimulated Emission

There are different laser technologies, but all of them allow us to transmit at a larger distance and with a higher modulation speed than the LED, and also the signal they produce has a narrower spectrum so that tolerance to chromatic dispersion increases. Thus, the laser is used as an optical source is systems which require better performance.

1.2.2 The optical fiber

The optical fiber is a dielectric waveguide with a cylindrical geometry which is made with highly pure silica. In the fiber's structure two sections can be recognized: the inner part which is where the light travels called *core* and the outer part called *cladding* which has a refractive index lower than the core. This structure may be observed in *Figure 1.6*.

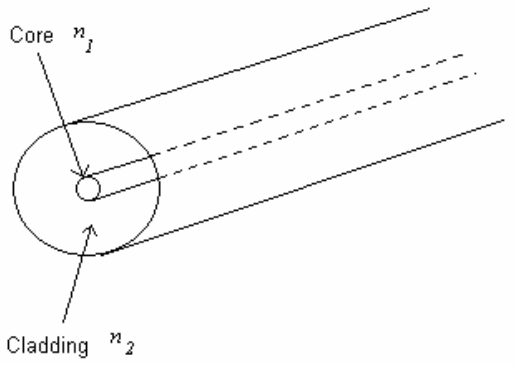

Figure 1.6. Optical fiber

The functioning principle of the fiber is based in what happens when a ray of light strikes a boundary between two different materials. As is observed in *Figure 1.7*, when a ray of light strikes the boundary between two mediums that have different refractive indexes ($n_1 > n_2$) this is partly reflected and partly transmitted according to Snell's law:

$$n_1 \sin(\alpha) = n_2 \sin(\beta) \tag{1.3}$$

where α is the angle of incidence with respect to the normal to the surface and β is the angle that the transmitted ray forms with this normal.

The angle β increases when α increases up to the limit value of β=π/2, at which there is no transmitted ray. This is the phenomenon of *total reflection*, and the *critical angle* is the angle of incidence above which the total reflection occurs, this angle is represented as:

$$\alpha_L = \arcsin\left(\frac{n_2}{n_1}\right) \tag{1.4}$$

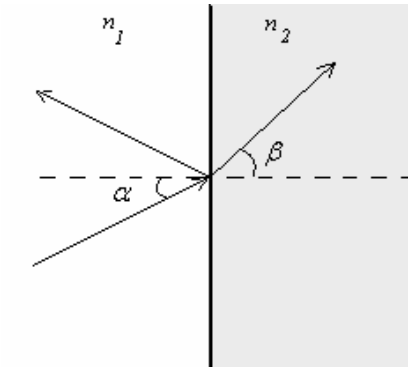

Figure 1.7. Incidence of a ray of light at a boundary between two mediums

The light transmission in the inner part of the fiber is based on the phenomenon of total reflection, which is produced when the ray strikes the surface between the core and the cladding. The concept of *fiber acceptance angle* is then introduced: all angles smaller than the acceptance angle are guided (this is to say, they have total reflection). The fiber acceptance angle is represented as:

$$\theta = \sqrt{\frac{n_2^2 - n_1^2}{n_0}} \tag{1.5}$$

where n_0 is the refractive index of the medium external to the fiber.

The light rays which enter with an incidence angle larger than the acceptance angle will strike the surface between the core and the cladding with an angle smaller than the critical angle and a part will be transmitted to the cladding not allowing for total reflection. This phenomenon is shown in *Figure 1.8*.

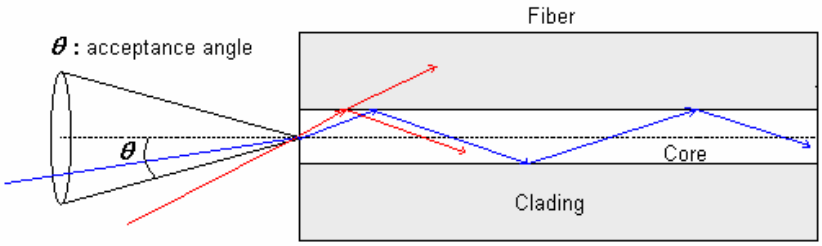

Figure 1.8. Cone of acceptance

There are two basic types of fiber: multimode fiber and single mode fiber [2]:

- Multimode fiber

  This fiber was the first to be manufactured and commercialized, and its denomination simply refers to the fact that numerous light rays (modes) are carried simultaneously through the fiber. Modes result from the fact that light will only propagate in the fiber core at discrete angles within the cone of acceptance. This fiber type has a much larger core diameter compared to the single mode fiber and is easiest to couple to other components.

  Multimode fiber is best designed for short transmission distances, and is suited for use in low cost LAN systems.

- Single mode fiber

  In the single mode fiber just one mode is carried along the fiber's axis. Single mode fiber allows for a higher capacity to transmit information because it can retain the fidelity of each light pulse over longer distances, and it exhibits no dispersion caused by multiple modes. Single mode fiber also enjoys lower attenuation than multimode fiber.

Single mode fiber is best designed for longer transmission distances, making it suitable for long distance telephony and multichannel television broadcast systems, and, in general, high capacity data transmission.

Single mode fiber has gone through a continuing evolution for several decades now. As a result, there are three basic classes of single mode fiber used in modern telecommunications systems:

- Standard Single Mode Fiber (SMF)

  It's the oldest and most widely deployed type. These fibers were initially intended for use near 1310 nm, and later the 1550 nm systems made these fibers less desirable due to their very high dispersion at this wavelength.

- Dispersion Shifted Fiber (DSF)

  To address the problem of the high dispersion at 1550 nm of the SMF, manufactures developed the DSF, which moved the zero dispersion point to the 1550 nm region.

- Non Zero Dispersion Shifted Fiber (NZ-DSF)

  Years later, scientists would discover that while DSF worked extremely well with a single 1550 nm wavelength, it exhibits serious non linearity impairments when multiple, close-spaced wavelengths in the 1550 nm region were transmitted in DWDM systems. To address this shortcoming, the NZ-DSF was introduced. Some of the non-linear effects affect the system mainly when chromatic dispersion is low. The NZ-DSF presents highly enough dispersion as to reduce the impact of its non-linear effects, and at the same time low enough as to limit the linear distortion of the signal.

1.2.3 The optical receiver

The optical receiver has the function of converting the optical received signal in an electrical signal, and, when observing this signal in a one bit period it must determine which of the two possible bits "0" or "1" was transmitted.

Generally, the receiver is formed by: an optical filter, a photodiode and an electric receiver.

The optical filter has the functions of extracting a desired wavelength from the WDM comb and of cutting out the noise introduced by amplifiers and interference of adjacent channels.

The photodiode has the function of converting the received optical power into an electric current which will later enter the electric receiver.

In the electric receiver, the decisions about the received bits are taken. The process of incoherent demodulation called *Direct Detection* is in principle very simple: the receiver detects the presence or absence of optical power in the bit slot. In order to guarantee that the sampling instant be the closest to the optimal instant, which corresponds to the instant of larger aperture of the eye diagram, a circuit is necessary to recover synchronism. Yet, in the case of coherent demodulation, a circuit which nears phase recovery is necessary.

In the signal reception procedure errors are obviously produced, because the signal is affected by phenomena which impair the system's performance (for instance ASE noise, the shot noise, the thermal noise, the distortion due to non linear effects and the ISI). These phenomena must be taken into account in the system's design phase so that a given *Bit Error Rate* (BER) may be reached.

Among the parameters which describe the system's performance we may recognize: the BER (which is typically 10^{-12} for high speed optic systems), the Q factor, which is a

sort of signal-to-noise ratio, and the sensitivity, which is the receiver power necessary to obtain a prefixed BER.

Chapter 2

Optical modulation formats

Optical modulation is the process of converting digital information into an optical format suitable for transmission through the fiber.

There are two possible ways to modulate the optical source. One is to do it directly, which only allows to modulate the amplitude of the signal, and the other one is to modulate the optical source externally, which allows modulating the amplitude, phase or polarization of the signal.

Direct modulation is easier to implement and the components needed to produce it are cheaper, but its performance in terms of spectral occupancy, noise and chirp is poor. For these reasons, direct modulation is used for low-cost, low bit-rate systems implemented on Local Area Networks.

On the other hand, external modulation offers a better performance due to the fact that the laser's output power is kept constant, thus providing stability that decreases excessive chirp. This improvement in performance allows external modulation to achieve higher bit-rates and reach greater distances. Due to its added complexity and components, external modulation is more expensive than direct modulation.

In this chapter four different digital modulation techniques are presented, these are: *Intensity Modulation Direct Detection* (IMDD), *Duobinary* (DB), *Differential Phase-Shift Keying* (DPSK) and *Differential Quadrature Phase-Shift Keying* (DQPSK).

2.1 IMDD

This is the easiest modulation format to implement. Information is coded in the intensity of the optical signal: if a bit slot contains power, that bit is a "1", and if it does not contain power then the bit is a "0".

The simplest way to implement such format is to switch on and off the optical source, which corresponds to the direct modulation of the laser. This was the base for a first generation of optical systems.

Later, in order to enhance the system's performance, external modulation was introduced. In this type of modulation, the laser is kept at a constant current giving place to a very stable output power which is later modulated with an external modulator as is shown in *Figure 2.1*.

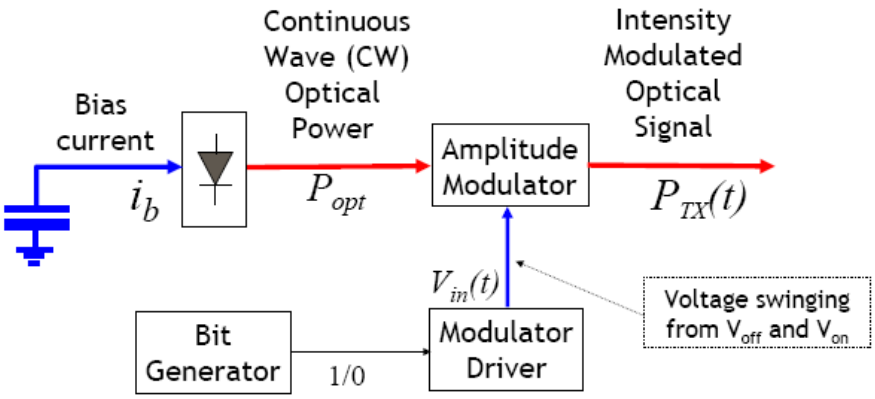

Figure 2.1. IMDD transmitter with external modulation

The most used modulator is the *$LiNbO_3$ Mach-Zehnder modulator*. The basic structure of this modulator comprises two waveguides, two Y-junctions and a RF/DC electrode. The optical signals launched into the modulator are equally split into two waveguides at the first Y-junction on the substrate. When voltage is not applied to the RF electrode, the two signals are recombined at the second Y-junction in phase and coupled into a single output. In this case the output signal is recognized as a "1". When voltage is applied to the RF electrode, the refractive index is changed due to electro-optic effects and the phase of the signal in one arm is advanced and the phase of the signal in the other arm is retarded, and when the two signals are recombined at the second Y-junction they are lost. In this case the output signal is recognized as a "0". The voltage difference which induces the "0" and the "1" is called driving voltage, and is an important parameter when designing the modulator.

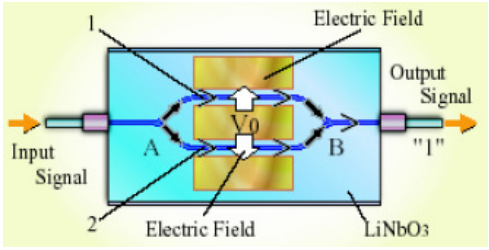

Figure 2.2. Mach-Zehnder modulator

Intensity modulation may be implemented with two types of coding which are differentiated according to the type of pulse used for transmission. The RZ (*Return to Zero*) coding uses a pulse that returns to zero within the bit slot, and the NRZ (*Non Return to Zero*) coding uses pulses that have the same duration as the bit slot. In *Figure 2.3* and *Figure 2.4,* two bit sequences representing the mentioned types of coding are shown.

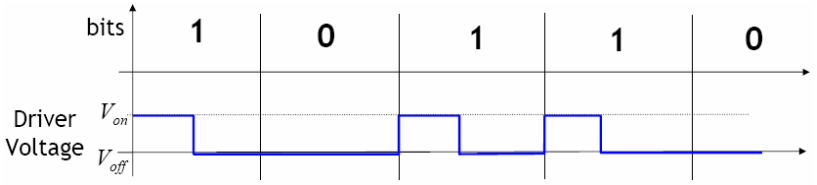

Figure 2.3 RZ encoding

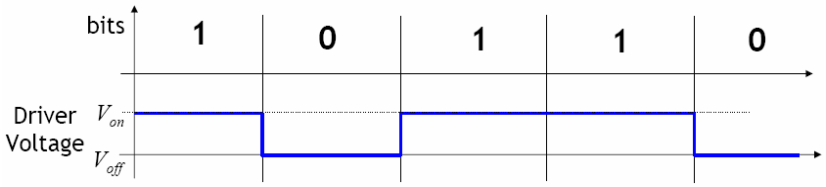

Figure 2.4 NRZ encoding

NRZ encoding has the advantage of being easy to implement and of having a small spectral occupancy (favouring the presence of many channels) which make it the standard of optical communications. On the other hand it has a higher impact on the non-linearities of the fiber.

RZ encoding has the advantage of a reduced effect on the non- linearities of the fiber. But it has the disadvantage of ample spectral occupancy and a more complex implementation.

For all modulation formats based on Intensity Modulation the receiver set-up is like the one shown in *Figure 2.5*.

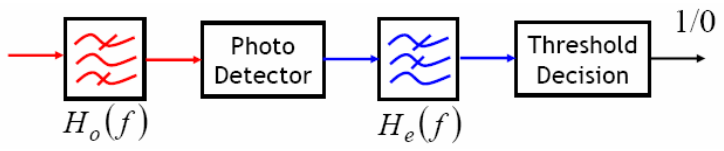

Figure 2.5. Typical IM receiver

2.2 Duobinary

Duobinary modulation belongs to a family of systems referred to as *partial response*, in which the bit sequence is manipulated in different ways before being sent to the fiber. With this modulation scheme, the signal transmitted at a certain time depends on both the bit at that time and on one or more of the previous bits. This scheme has a very good spectral efficiency as it transmits R bits/s using less than R Hz of bandwidth.

This modulation format can be seen as a DPSK scheme where a certain bit correlation or interference is introduced at the transmitter. Due to this introduced correlation, the Duobinary pulses will have ISI. However, it is introduced in a controlled manner so that it can be removed at the receiver in order to recover the original signal. The Duobinary modulation scheme is shown in *Figure 2.6.*

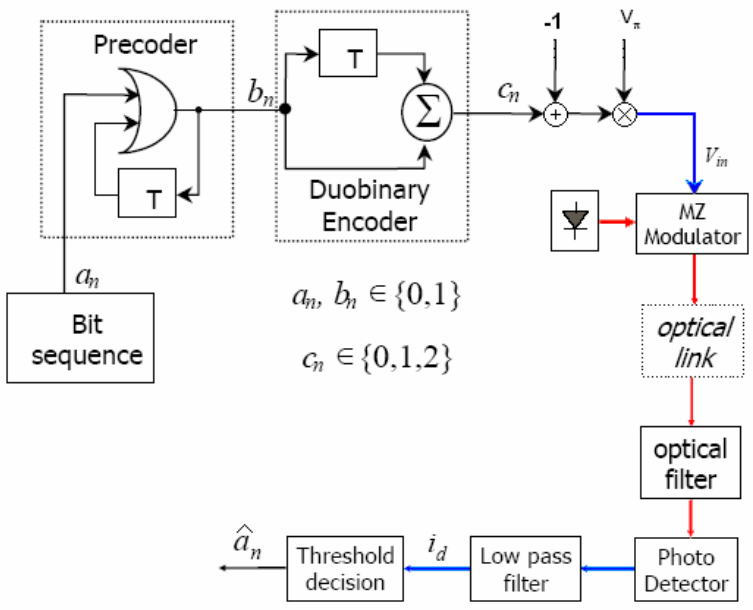

Figure 2.6. Duobinary modulation scheme

As it may be seen, the data sequence goes through a precoder, in which an XOR logic operation takes place between the current bit and the previous output bit from the precoder. The precoder's output is then sent into the encoder where the addition of the current bit and the preceding bit takes place, thus generating a signal which has three levels "0", "1" and "2". After the encoder, a -1 is added to shift the signal and make it symmetric with respect to the level "0". As a result, the signal shown in *Figure 2.7* is obtained. At this point, the signal is multiplied by V_π to then control a Mach-Zehnder modulator.

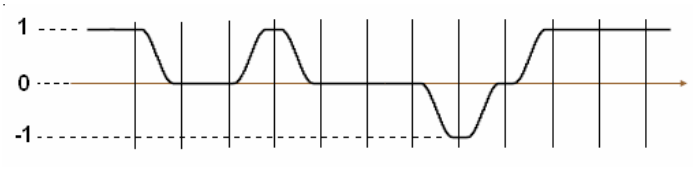

Figure 2.7. Duobinary three level signal

The Duobinary receiver is a conventional single-photodiode receiver that looks at power, converting again the three levelled signal into a two level signal, as it is seen in *Figure 2.8*.

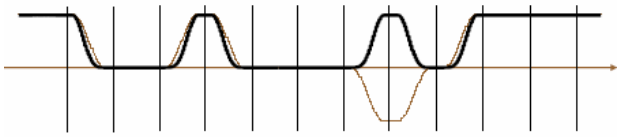

Figure 2.8. Duobinary two level signal

2.3 Optical phase modulations

There are two fundamental ways to represent a data sequence through the phase of a signal. The first way is to change the phase of a carrier signal according to the variations of the data sequence. This scheme uses a finite number of phases to represent different transmitted symbols. The receiver determines the phase of the received signal and maps it back to the symbol it represents, thus recovering the original data. This requires the receiver to be able to compare the phase of the received signal to a reference signal, such receiver is called coherent. And the second way is to differentially encode the data sequence and then modulate the phase. In this case, a non-coherent receiver is used since the phase between two successive received symbols is compared and used to determine what the data must have been. This modulation scheme is called differential.

In the first case, there is an ambiguity of phase if the constellation is rotated by some effect in the communications channel. This problem can be overcome by using the data to change the phase rather than set the phase; this is equivalent to using a differential modulation format.

In this section two differential modulation formats will be presented, these are: *Differential Phase Shift Keying* (DPSK) and *Differential Quadrature Phase-Shift Keying* (DQPSK).

2.3.1 DPSK

In this modulation scheme a binary “1” may be transmitted by adding 180° to the current phase and a binary “0” by adding 0° to the current phase. A modulated signal is shown in the *Figure 2.9*. It is assumed that the signal starts with *zero phase* and there is a phase shift at t=0.

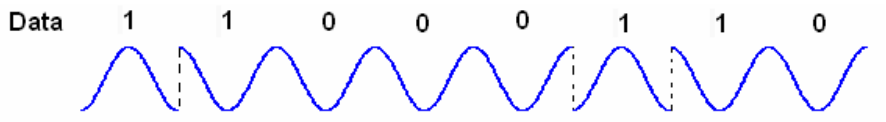

Figure 2.9. Modulated DPSK signal

A DPSK modulation may be implemented in two different ways. An intensity modulator or a phase modulator as shown in *Figure 2.10* may be used. Using a phase modulator, the information is transferred within the signal's phase (while amplitude remains constant), controlling the modulator with a tension in the interval $0/V_\pi$. On the other hand, if an intensity modulator is used, the tension controlling it swings in the interval $-V_\pi/V_\pi$.

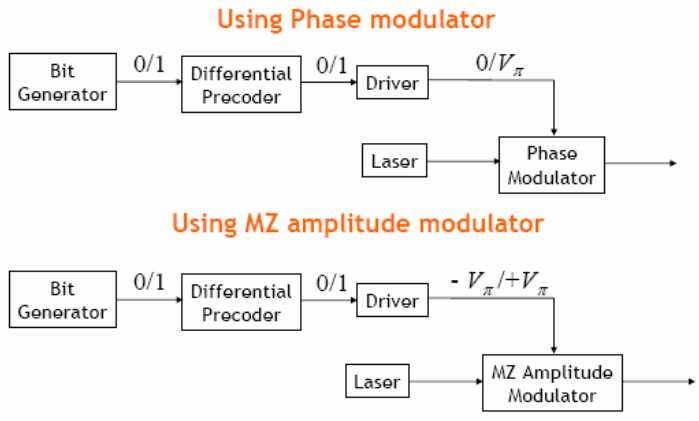

Figure 2.10. DPSK transmitters

In the differential precoder the XOR operation is performed between the transmitted bit and the precoder's previous output bit. The precoder is shown in *Figure 2.11.*

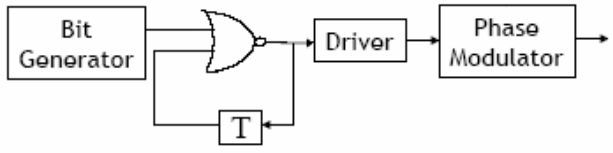

Figure 2.11. DPSK precoder

The DPSK receiver is shown in *Figure 2.12.* It consists of an *Asymmetric Mach-Zehnder Interferometer*, which delays one bit in one arm so two bits can be compared at the same time, and a *balanced photo detector* (BPD), which should be perfectly balanced (have identical responsivity) in order to avoid problems. In principle, DPSK can be detected using only one photodiode on either output of the interferometer, but the two ports form slightly different signals which produce different "eyes" and the balanced photo detector sums the "eyes" reinforcing each other.

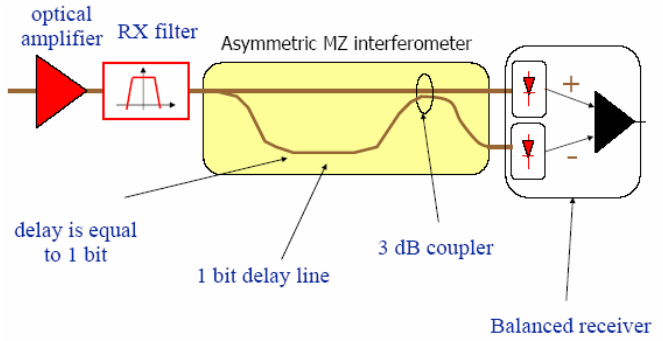

Figure 2.12. DPSK receiver

It is important to point out that the DPSK reduces the impact of the fiber non linearities and avoids coherent reception, but it needs a precoder at the transmitter and an asymmetric interferometer and an expensive balanced photo detector at the receiver.

2.3.2 DQPSK

This scheme is a 4-level differential phase modulation. With a "conventional" binary modulation scheme, the transmitter has to emit as many pulses per second as the bit rate, but with a 4-signal scheme that ratio is halved. This halves the spectral width and therefore the bandwidth efficiency greatly increases.

The DQPSK transmitter generates an optical signal by encoding the information in the differential optical phase Δθ between successive symbols, where Δθ may take one of the four values [0, π/2, π, 3π/2]. Each phase corresponds to a different symbol, composed of two parallel bits (called in-phase and quadrature respectively). A modulated signal is shown in *Figure 2.13*. It is assumed that the signal starts with *zero phase* and there is a phase shift at *t*=0.

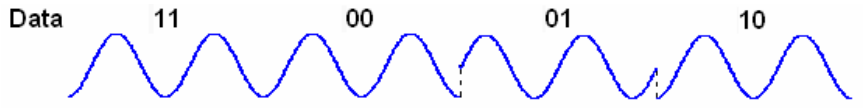

Figure 2.13. Modulated DQPSK signal

The schematic of a typical DQPSK transmitter is shown in *Figure 2.14.* The MZ driving voltage is in the range [-Vπ, Vπ]. The signals from the upper and lower branches are combined through an optical coupler after adding an optical phase shift equal to π/2 to the lower branch. Given the differential nature of the decoding in DQPSK, a precoder is required at the transmitter in order to provide a direct mapping of data from the input to the output. The structure of the precoder is shown in *Figure 2.15* where the following input/output relationship is implemented:

$$\begin{aligned} p_k &= \overline{(a_k \oplus b_k)} \cdot (a_k \oplus p_{k-1}) + (a_k \oplus b_k) \cdot (b_k \oplus q_{k-1}) \\ q_k &= \overline{(a_k \oplus b_k)} \cdot (b_k \oplus q_{k-1}) + (a_k \oplus b_k) \cdot (a_k \oplus p_{k-1}) \end{aligned} \tag{2.1}$$

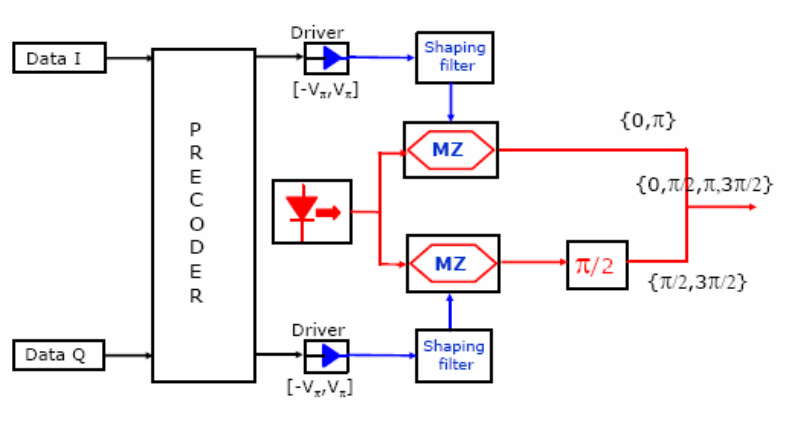

Figure 2.14.Typical DQPSK transmitter schematic

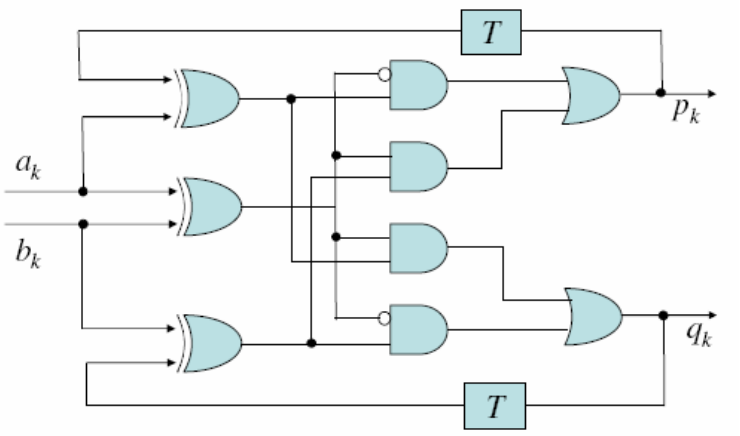

Figure 2.15. DQPSK precoder structure

The DQPSK receiver demodulates the received optical signal, generating two parallel electrical signals $y^I(t)$ and $y^Q(t)$. The receiver shown in *Figure 2.16* consists of an optical filter, a pair of AMZ interferometers with a differential delay ideally equal to the time duration of a transmitted symbol, each followed by a BPD consisting of two photodetectors (one for each output branch of the AMZs), connected so as to subtract their currents from each other, then followed by a post-detection electric filter. The

differential optical phase between the interferometer's arms should be set to π /4 and - π /4 for the upper and lower branches respectively.

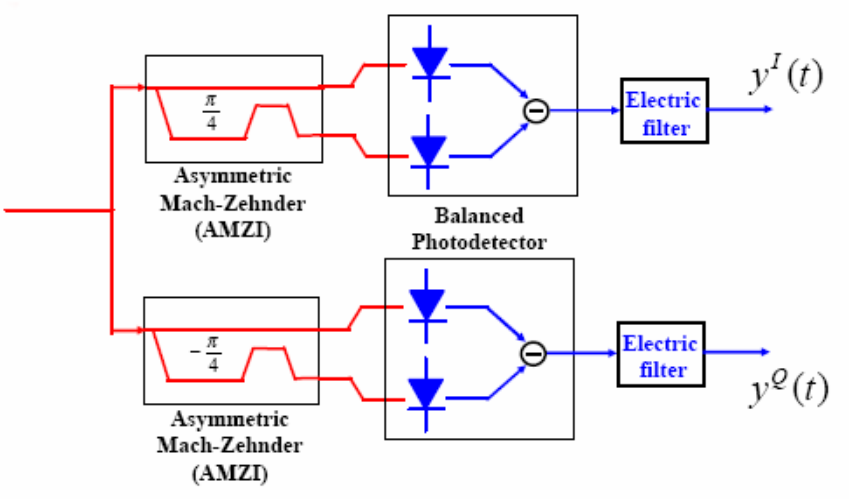

Figure 2.16. DQPSK receiver

If E(t) is the optical field at the output of the receiver's optical filter, the signals at the output of the upper AMZ can be written as:

$$\begin{aligned} E_1(t) &= \tfrac{1}{2}\left[E(t) + \gamma E(t - T_{AMZ})\mathrm{e}^{j\,\pi/4}\mathrm{e}^{j\,\delta\phi}\right] \\ E_2(t) &= \tfrac{1}{2}\left[E(t) - \gamma E(t - T_{AMZ})\mathrm{e}^{j\,\pi/4}\mathrm{e}^{j\,\delta\phi}\right] \end{aligned} \tag{2.2}$$

where $\delta\Phi$ is a quantity that can be controlled, typically by thermal adjustment of the AMZ. $\delta\Phi$ can be transformed into a frequency detuning parameter Δf of the AMZ transfer function through the relation:

$$\Delta f = \frac{\delta\phi}{4\pi} B_R \tag{2.3}$$

where B_R is the bit rate, which for DQPSK is equal to twice the symbol rate S_R. The value Δf = 0 corresponds to perfect tuning of the AMZ.

The AMZ delay error is defined as:

$$\delta T_{AMZ} = T_{AMZ} - T \tag{2.4}$$

where T_{AMZ} is the delay introduced by the AMZ between its two asymmetric arms and $T = 1/S_R$ is the symbol time. For optimal reception, it should be $T_{AMZ} = T$, resulting in $\delta T_{AMZ} = 0$.

γ can take on values in the range $\{0,1\}$ and is related to the AMZ extinction ratio ε through the following relationship:

$$\varepsilon = (1 + \gamma)^2 / (1 - \gamma)^2 \tag{2.5}$$

According to this definition ε belongs to the interval $\{1,\infty\}$, where the extremes mean no extinction at all and ideal (infinite) extinction ratio, respectively. Note that physically speaking ε represents the highest possible power ratio that one could obtain between the two outputs of the AMZ, in CW.

The electrical signal at the output of the BPD can be written as:

$$V(t) = \frac{1}{2}\left[R_1|E_1(t-\tau_1)|^2 - R_2|E_2(t-\tau_2)|^2\right] \tag{2.6}$$

where R_1 and R_2 are the BPD individual branch responsivities, while τ_1 and τ_2 are the delays (optical or electrical) accumulated between the AMZ output and the BPD electrical subtraction stage. The BPD amplitude imbalance is defined as:

$$K = \frac{R_1 - R_2}{R_1 + R_2} \tag{2.7}$$

This parameter has range{-1,1} and the extremes correspond to only the lower or the upper branch of the BPD being operational, whereas the value K = 0 corresponds to perfect balance. We also define:

$$\delta T_{BPD} = \tau_1 - \tau_2 \qquad (2.8)$$

representing the signal delay imbalance at the photodetector's current subtraction stage in the BPD. Such imbalance is typically due to different pigtail lengths connecting the AMZ ports to the BPD inputs and of course $\delta T_{BPD} = 0$ is the optimum value.

In the following, it will be assumed that the RX parameters are perfectly tuned, i.e. $\Delta f = 0$, $\varepsilon = \infty$, $\delta T_{AMZ} = 0$, $K = 0$ and $\delta T_{BPD} = 0$.

It is important to point out that the DQPSK modulation format has the advantages of having reduced bandwidth requirements and of increasing the tolerance to chromatic dispersion and fiber non linearities, but it needs a complex precoder at the transmitter side, and two asymmetric interferometers and two expensive balanced photodetectors at the receiver.

Chapter 3

Optical fiber propagation effects

In an optical transmission system, when the signal propagates through the fiber, linear and non linear propagative phenomena are manifested. The linear effects may be modelled by a transfer function which is independent of the input signal; but the non linear effects depend on the input signal and cannot be modelled by a transfer function.

3.1 Linear effects

Considering the propagation of the optical field through a single mode fiber, and neglecting the non linear effects for now, the evolution of the amplitude along the propagation coordinate *z* is given by the wave equation:

$$\frac{\partial E}{\partial z} = -\alpha(\omega)E - j\beta(\omega)E \tag{3.1}$$

where α(ω) is the attenuation constant and β(ω) is the propagation constant.
This equation admits the analytic solution:

$$E(\omega, z) = E(\omega,0)e^{-\alpha(\omega)z}e^{-j\beta(\omega)z} = E(\omega,0)H_F(\omega, z) \tag{3.2}$$

where $H_F(\omega)$ is the fiber's transfer function.

In the following, the attenuation and the dependence of the propagation constant on the frequency, which generates the chromatic dispersion, will be analyzed separately.

3.1.1 Attenuation

The attenuation introduced by a fiber span is defined as the ratio between the power at the beginning of the fiber and the received power at the end of it.

When a signal propagates through the fiber, part of its energy is absorbed by the material, which generates a loss in the signal power.

The attenuation is caused by phenomena such as the Rayleigh scattering and infrared absorption, which depend on the material and are due to the presence of imperfections and impurities. The attenuation also depends on the wavelength, the type of fiber and the possible mechanical strains applied to it.

As it can be seen in *Figure 3.1* the attenuation has an absolute minimum of 0.2 dB/Km around 1550 nm, and a relative minimum of 0.4 dB/Km around 1300 nm. These wavelengths define the spectral windows in which the fiber is used.

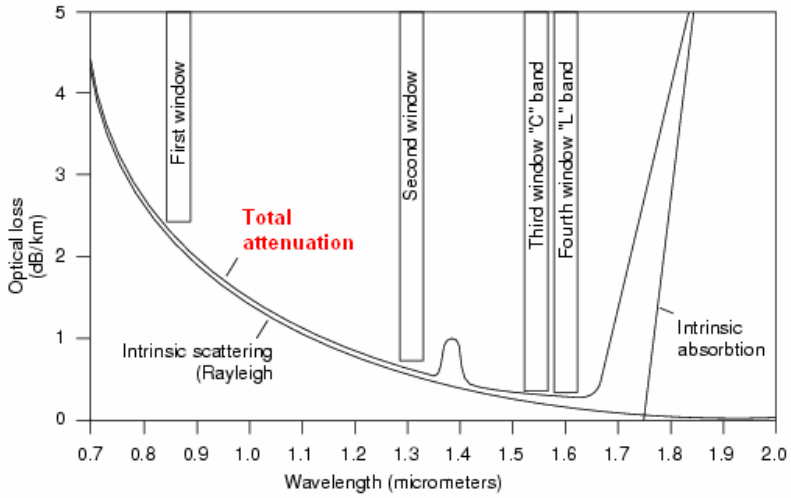

Figure 3.1. Attenuation of a single mode fiber

The attenuation can be considered constant in the bandwidth used for the transmission; thus the dependence of the attenuation on the wavelength can be neglected. So, under this hypothesis, the attenuation is a non distortional effect.

3.1.2 Chromatic dispersion

The propagation constant depends on the wavelength, meaning that the signal's different spectral components propagate with different velocities.

In consequence, the received signal is distorted. Pulses widen in time and interfere with adjacent pulses, so the eye diagram closes itself. This phenomenon is called Intersymbol Interference (ISI), which reduces the performance of the system. The dispersion limit, which is the maximum distance at which the system is still capable of working, decreases as the bit rate increases.

Dispersion has two contributions, the material dispersion and the waveguide dispersion. The material dispersion is caused by the dependence on the frequency of the material's refractive index. On the other hand, the solution of the propagation equation for the fundamental mode gives origin to a dependence of the group velocity on the frequency; this is the waveguide dispersion, this depends on the project parameters and can be controlled. The total chromatic dispersion is approximately the addition of these two, as shown in *Figure 3.2*.

The study of chromatic dispersion may be approached by developing Taylor's series of the propagation constant around the central frequency. We obtain:

$$\beta(\omega) \cong \beta_0 + \beta_1 \cdot (\omega - \omega_0) + \frac{\beta_2}{2} \cdot (\omega - \omega_0)^2 + \frac{\beta_3}{6} \cdot (\omega - \omega_0)^3 + \ldots \qquad (3.3)$$

with

$$\beta_i = \left(\frac{\partial}{\partial \omega} \right)^i \beta(\omega) \Bigg|_{\omega=\omega_0} \qquad (3.4)$$

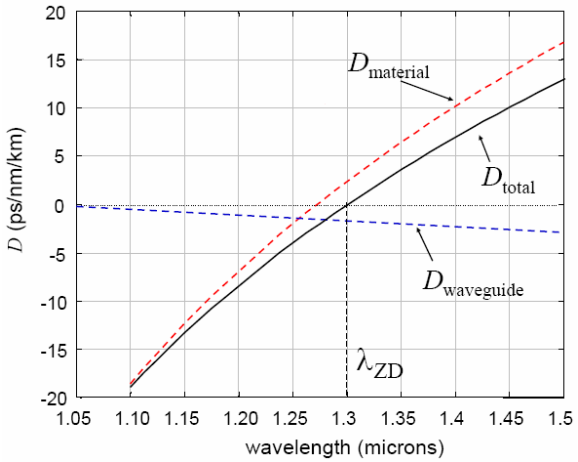

Figure 3.2. Total chromatic dispersion for G. 652 fiber

The term $\beta_0 = \beta(\omega_0)$, at a given distance z, determines a constant phase rotation which doesn't distort the pulse.

The term β_1 introduces a delay τ_g, known as *group delay*, which is substantially the propagation delay of the pulses:

$$\tau_g(\omega_0) = \beta_1 z = \left.\frac{\partial \beta}{\partial \omega}\right|_{\omega=\omega_0} z \tag{3.5}$$

This delay, proportional to z, is independent of the frequency, which means that also β_1 does not contribute to the distortion of the pulse.

The term β_2, on the other hand, causes a delay which depends on the frequency and is proportional to z.

Considering the contribute of β_2, the total delay is:

$$\tau_g(\omega) = \tau_g(\omega_0) + \beta_2 \cdot (\omega - \omega_0) \cdot z \tag{3.6}$$

where $\tau_g(\omega_0)$ represents an average group delay which is independent of the frequency, and the second term originated by β_2 is a delay which takes a different value for each spectral component of the transmitted pulse.

The constant β_2 can be positive or negative; then, two cases may be considered:

- *Normal Dispersion Regime* (β_2>0)*:* In this case, spectral components with larger frequencies propagate with a lower velocity than the spectral components with smaller frequencies.
- *Anomalous Dispersion Regime* (β_2<0)*:* In this case, the spectral components with larger frequencies propagate more rapidly.

The measure of dispersion in the optical fiber is generally expressed by means of the *D* parameter, which is related to β_2 by the following relation:

$$D = \beta_2 \cdot \left(-\frac{2\pi c}{\lambda^2} \right) = -0.785 \cdot \beta_2 \quad \left[\frac{ps}{nm \cdot Km} \right] \tag{3.7}$$

For example, at a wavelength of 1550 nm standard SMF fibers have $\beta_2 \cong$ -20 ps^2/Km and $D \cong$ 16 ps/nm/Km, and so they operate in an anomalous dispersion regime.

The delay introduced by β_3 is also dependent on the frequency, and so it causes the distortion of the impulse waveform:

$$\tau_g \beta_3 = \frac{1}{2} \beta_3 \cdot (\omega - \omega_0)^2 \cdot z \tag{3.8}$$

But as β_3 takes very small values, its contribution may generally be neglected.

3.1.2.1 Dispersion compensation

Chromatic dispersion is a phenomenon which may be compensated. There are several different techniques for compensating dispersion; these may be classified in optical and electronic compensation.

Optical compensation consists in introducing, after each fiber span, a particular fiber called *Dispersion Compensating Fiber* (DCF), which by having a dispersion *D* with opposite sign to the preceding fiber, cancels the phenomenon of dispersion achieving a value of accumulated dispersion theoretically equal to zero. Nevertheless, in the presence of non-linear phenomena, dispersion compensation is more complicated, and must be achieved by using dispersion maps obtained by means of numerical simulation. In addition to the DCF, *Dispersion Compensating Units* (DCU) can be placed at the beginning and end of the link to further adjust the dispersion compensation values. A DCU is formed by winding a first optical fiber and second optical fiber into coil shapes and storing them in a case. The first optical fiber has a negative chromatic dispersion D_1 and a negative dispersion slope S_1 at a wave length in use. The second optical fiber has a positive chromatic dispersion D_2 and a positive dispersion slope S_2 at the wavelength in use.

A generic dispersion compensated system is shown in *Figure 3.3.*

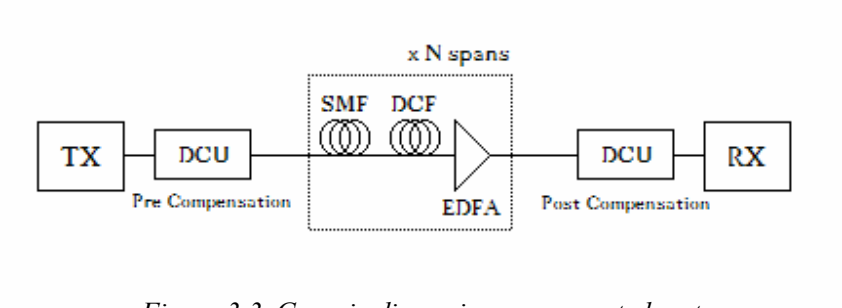

Figure 3.3. Generic dispersion compensated system

On the other hand, electronic compensation is achieved through an equalizer placed at the receiver. One of the most effective ways to electronically compensate dispersion is based on a technique called *Maximum Likelihood Sequence Estimation* (MLSE), this method will be presented in Chapter 4.

3.1.2.2 Dispersion maps

Dispersion maps are graphics that show the systems accumulated dispersion as a function of the total length. The three basic parameters on which dispersion maps depend are: pre-compensation dispersion (D_{pre}), in-line dispersion compensation (D_{IL}) and post-compensation dispersion (D_{post}). An example of a dispersion map is shown in *Figure 3.4*.

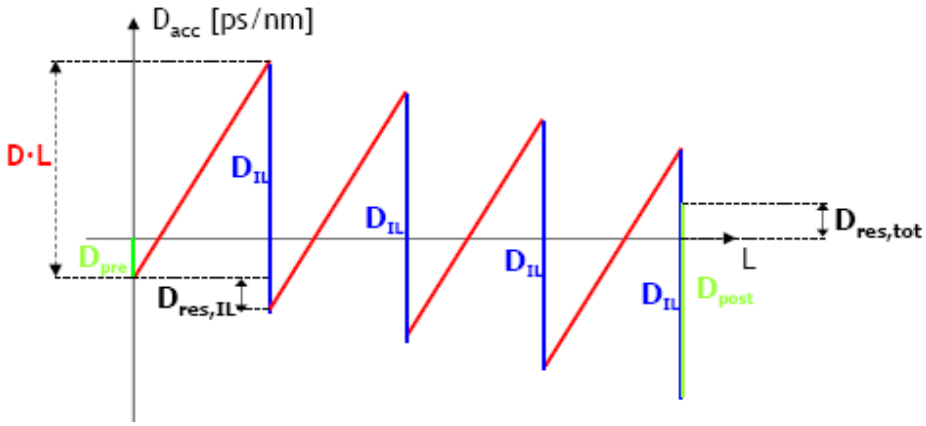

Figure 3.4. Example of a dispersion map

To improve the system's performance, dispersion must be optimized. To do so, three degrees of freedom can be evaluated, these are: the amount of pre, post and in-line compensation. This gives place to a three dimension optimization space. In order to simplify the optimization process, a two dimensional space is explored.

The used variables are:

- *In-line residual dispersion*: $D_{res,IL} = D \cdot L + D_{IL}$ [ps/nm]
- *Total residual dispersion:* $D_{res,tot} = D_{pre} + D_{post} + (D \cdot L + D_{IL}) \cdot N_{span}$ [ps/nm]

By means of numerical simulation, a great amount of dispersion maps can be obtained in order to understand which values of dispersion yield the optimum results in terms of system performance (better BER). A contour plot of $\log_{10}$(BER) vs $D_{res,tot}$ and $D_{res,IL}$ can then be obtained to show the system's optimum regions. An example of such plot can be seen in *Figure 3.5*.

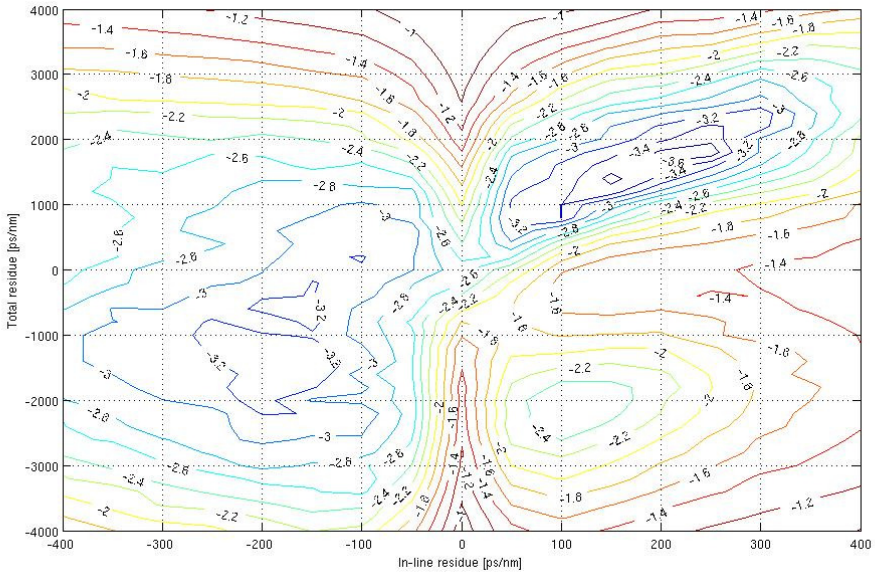

Figure 3.5. Contour plot of $\log_{10}$(BER) vs $D_{res,tot}$ and $D_{res,IL}$

It is important to point out that to every point of the contour plot shown in *Figure 3.5* corresponds a different dispersion map.

Due to the dependence on wavelength of dispersion, each dispersion map is valid for one channel only.

$$D(\lambda) = D_{\lambda_c} + \frac{\partial D}{\partial \lambda}\Delta\lambda \tag{3.9}$$

An example of this effect is shown in *Figure 3.6.*

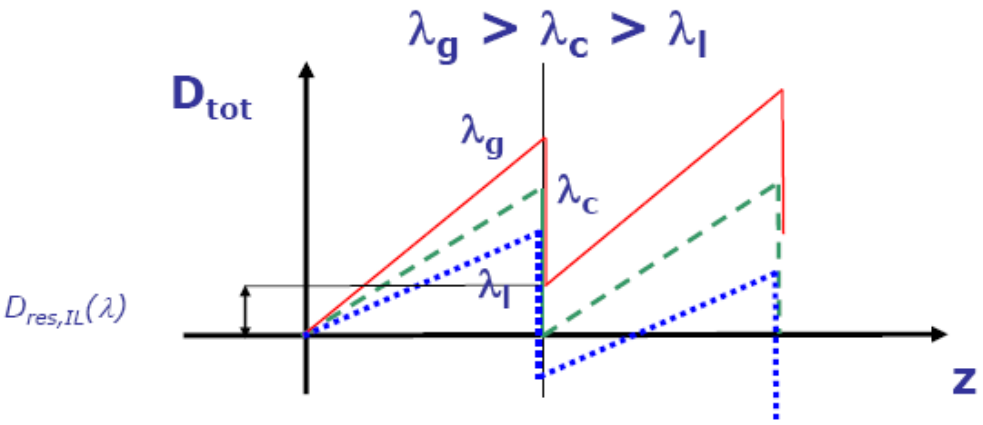

Figure 3.6. Dispersion map of a 3 channel system

3.1.3 Polarization mode dispersion (PMD)

In single mode fibers, two modes of the electromagnetic field polarized in orthogonal directions may be propagated. PMD is due to the difference in speed of these polarization modes. This difference in speed results from birefringence, a phenomenon where the refractive index differs from one input polarization state to another. Birefringence is caused by small defects in the manufacturing process, bends, and other mechanical stresses that may affect the circular fiber geometry [3].

The impact of PMD may generally be neglected in the transmissions at 10 Gbit/s, while it becomes a limiting factor at 40 Gbit/s.

3.2 Non linear effects

The transmission quality and capacity of a long distance optical system is certainly influenced by non-linear effects. These effects are: *Self Phase Modulation* (SPM), *Cross Phase Modulation* (XPM) and *Four Wave Mixing* (FWM).

The physical phenomenon that produces these effects is called Kerr effect, this is manifested when the refractive index of the material depends on the power of the signal which is being propagated through this material:

$$n(z) = n_L + \Delta n = n_L + n_2 \frac{P(z)}{A_e} \tag{3.10}$$

In the preceding formula n_L is the conventional refractive index, n_2 is the non-linear refractive index and A_e is the effective area of the fundamental mode which may be approximated by the core area. It can be observed then that the non-linear effects depend more on the power density per unit area than the absolute power.

- *Self phase modulation* (SPM)
  It consists in a phase modulation of the signal produced by variations of the power of the signal itself. Even if SPM by itself does not modify the width of the signal, this cannot be assured in the presence of dispersion, since when these two interact they might compensate each other or might cause the deterioration of the signal.
- *Cross phase modulation* (XPM)
  It consists in a phase modulation of the signal produced by variations of the power of spectrally adjacent channels. These phase fluctuations may be turned into amplitude fluctuations in the presence of dispersion causing a deterioration of the signal.

- *Four wave mixing* (FWM)

  It causes transfer of energy between the different channels and generates new frequencies. Each new frequency ω_i is created due to the contribution of 3 other frequencies ω_m, ω_n and ω_k according to the following rule:

$$\omega_i = \omega_m - \omega_n + \omega_k \tag{3.11}$$

  There are two types of *Four Wave Mixing:* Degenerate FWM, in which two of the three frequencies are the same ($\omega_m = \omega_k \neq \omega_n$) and Non degenerate FWM in which all three frequencies are different ($\omega_m \neq \omega_n \neq \omega_k$)

Chapter 4

Maximum likelihood sequence estimation (MLSE)

The maximum likelihood sequence estimation (MLSE) is an optimum sequence detection technique that minimizes the error probability in making a decision on the transmitted sequence. In this chapter the maximum likelihood principle, metric statistics and the Viterbi algorithm are discussed.

4.1 Maximum likelihood

Let's consider a model which gives the probability density function of observable random variable X as a function of a parameter θ. Then, for a specific value x of X, the function $L(\theta|x) = P(X=x|\theta)$ is a likelihood function of θ: it gives a measure of how "likely" any particular value of θ is, knowing that X has the value x. So, a likelihood function arises from a conditional probability distribution considered as a function of its second argument, holding the first one fixed.

In a sense, likelihood has an opposite behaviour than probability: if "probability" allows predicting unknown outcomes based on known parameters,

then "likelihood" allows determining unknown parameters based on known outcomes.

The extent to which the evidence supports one parameter value against another is equal to the ratio of their likelihoods. That is:

$$\Lambda = \frac{P(X = x \mid a)}{P(X = x \mid b)} \tag{4.1}$$

is the degree to which the observation x supports parameter value a against b. If this ratio is 1, the evidence is indifferent, and if greater or less than 1, the evidence supports a against b or vice versa.

The basis for the method of maximum likelihood is that the parameter value which maximizes the likelihood function is the value which is most strongly supported by the evidence.

All this can be applied to a transmission system. Let us suppose that we are to receive the signal vector $r = [r_0, r_1, ..., r_{N-1}]$, and considering that S_t represents one of all the possible transmitted sequences $[s_0, s_1, ..., s_{N-1}]$, the optimum decision rule is that the sequence S_t that maximizes the probability

$$p(S_t / r) = \frac{f(r \mid S_t) p(S_T)}{f(r)} \tag{4.2}$$

corresponds to the transmitted sequence S_T. This can be reduced to a maximum likelihood rule:

$$s(r) = \arg\max_{S_t} f(r \mid S_t) \tag{4.3}$$

where the functions $f(r / S_t)$ are the likelihood functions.

The sequence most likely to have been transmitted is the one associated with the minimum Euclidean distance (between the received signal r and the possible transmitted sequence S_t):

$$D(r, S_t) = \sum_{k=0}^{N-1} (r_k - s_k)^2 \tag{4.4}$$

This is called metric, and it can be rewritten as:

$$\Lambda(S_t) = \sum_{k=0}^{N-1} \lambda(x_k, x_{k+1}) \tag{4.5}$$

where x_k is the integer representation of the symbol vector $[s_{k-L+1}, s_{k-L+2}, ..., s_{k-1}]$ consisting of (L-1) consecutive data symbols.

Equation 4.5 expresses the optimal metric as the summation of partial metrics $\lambda(x_k, x_{k+1})$. The k-th of these terms, $\lambda(x_k, x_{k+1})$, depends on the vectors of consecutive trial symbols $[s_{k-L+1}, s_{k-L+2}, ..., s_{k-1}]$ and $[s_{k-L+2}, s_{k-L+3}, ..., s_k]$ respectively.

These considerations suggest a recursive formula for the evaluation of $\Lambda(S_t)$. So the following recursive relation is defined [4]:

$$\Lambda(s_k) = \Lambda(s_{k-1}) + \lambda(x_k, x_{k+1}) \tag{4.6}$$

with $s_i = [s_0, s_1, ..., s_i]$ $(s_{N-1} = S_t)$ and $\Lambda(s_0) = 0$, then, after N iterations:

$$\Lambda(S_t) = \Lambda(s_{N-1}) \tag{4.7}$$

A geometrical representation of the problem of searching over the optimal metric can be given as follows. A trellis diagram with N_s states is drawn as in *Figure 4.1*. In the k-th interval each trellis state represents one of the N_s possible values that x_k can take, and it is connected via M branches to the next state x_{k+1} (where M is the number of M-ary symbols). The branch connecting the states x_k and x_{k+1} is labeled by the trial symbol s_k and by the branch metric $\lambda(x_k, x_{k+1})$. In this way each trial sequence S_t has a one to one correspondence with a sequence of states in the trellis diagram. Looking for the optimal sequence decision is equivalent to searching for the path with minimum accumulated metric in the trellis. Such search would require an exhaustive analysis and comparison between all the possible trial sequences (trellis paths); in fact, for a sequence of N symbols, about M^N comparisons would have to be performed to select the most likely sequence, so the number of computations grows exponentially with respect to N. This technique would be unacceptable due to its excessive complexity; however, this can be

carried out recursively employing the *Viterbi algorithm*, where the number of computations necessary to select the most likely sequence grows only linearly. The Viterbi algorithm will be discussed later in section 4.3.

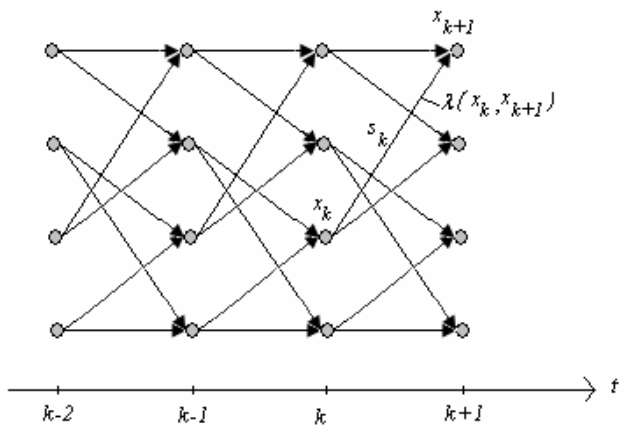

Figure 4.1. 4-state trellis diagram (M=2 is assumed)

4.2 Branch metric statistics

As it has been said before, the MLSE processor is implemented using the Viterbi algorithm. At each processor iteration, the following metric should be evaluated for each trellis branch:

$$M^{(n)} = -\sum_{k=1}^{K} \ln\left\{f_{y_{n,k}}(y)\right\} \tag{4.8}$$

where n is an index running from 1 to the total number of branches in the trellis, k is an index running from 1 to the total number K of samples per bit, $y_{n,k}$ is the random variable associated to the noisy signal, being the transmitted signal the one associated to the n-th branch of the k-th sample, $f_{y_{n,k}}(y)$ is the probability density function (pdf) of $y_{n,k}$ and y is the actual noisy signal sample taken on the photo-detected electrical signal $y(t)$.

It is seen that the metric expression takes account of the exact pdf's of the signal

samples. However, such pdf's are not analytically available in optical systems using post-detection filtering, and semi-analytical techniques based on Karhunen-Loève expansion [5] are needed to correctly evaluate them.

In order to reduce the computational complexity, in practice some other statistic models that approximate the signal statistic can be used to calculate the branch metrics.

Some of the models that approximate the signal statistic in an optical system are based on the assumption that the distribution of the received signal samples is Gaussian. In the following, two different metrics based on this assumption are described.

4.2.1 Gaussian metric

It is possible to simplify the metric evaluation procedures by assuming that the received signal samples are uncorrelated and follow a Gaussian distribution.

The Gaussian metric assumes an additive non-stationary Gaussian noise distribution. Its expression is the following:

$$M_{GAUSS}^{(n)} = -\sum_{k}\left\{\frac{(y_k - \mu_{n,k})^2}{\sigma_{n,k}{}^2} + \ln(\sigma_{n,k}{}^2)\right\} \tag{4.9}$$

where y_k is the k-th noisy received sample, and $\mu_{n,k}$ and $\sigma_{n,k}{}^2$ are the mean value and the variance of the k-th signal sample for the n-th trellis branch respectively.

The Gaussian metric correctly takes the noise variance non-stationarity into account, but as a consequence, a matrix $\sigma_{n,k}{}^2$ must be estimated and its values must be recalled at run-time to evaluate each signal sample contribution to the metric, which makes it very computationally intensive.

4.2.2 Square-root metric

The square-root metric is a simplified metric in which it is assumed that the square-root of the received signal follows a Gaussian distribution and that the variance of the square-root of the received signal samples is stationary [6].

Under these assumptions the square-root branch metric has the following expression:

$$M_{SQRT}^{(n)} = -\sum_{k}\left(\sqrt{y_k} - \mu'_{n,k}\right)^2 \tag{4.10}$$

where y_k is the k-th noisy received sample, and $\mu'_{n,k}$ is the mean value of the k-th signal sample for the n-th trellis branch.

This metric has the advantage that only the average value of the signal has to be calculated during the channel estimation procedure, and its expression can be written in a simple closed form.

4.3 Viterbi algorithm

The application of the Viterbi algorithm consists on finding, among the paths traversing the trellis from left to right (from time $k = 0$ until time $k = N$), the one with minimum metric. The metric associated with a path is the sum of the labels of the branches forming the path.

Formally, if x_k denotes the state at time k, taking values $\{X_i\}_{i=1}^{Ns}$, and $\lambda(x_k, x_{k+1})$ denotes the metric associated with the branch emanating from node x_k and joining node x_{k+1}, the algorithm tries to minimize the function:

$$\Lambda(x_0, x_1, ..., x_{N-1}) = \sum_{k=0}^{N-1} \lambda(x_k, x_{k+1}) \tag{4.11}$$

over the possible choices of the state sequences (x_0, … , x_{N-1}) compatible with the trellis structure.

The problem above could be solved by a brute-force approach, consisting of evaluating all the possible values of the function Λ and choosing the smallest. However, this would be too complex to develop due to the number of computations required and the storage needed, as they grow exponentially with the length N of the sequence.
The Viterbi algorithm solves the minimization problem without suffering from exponential complexity; actually its computational complexity grows only linearly with N.

The Viterbi algorithm achieves this by using a three key steps procedure: Add, Compare and Select (ACS). Consider *Figure 4.2* in which the trellis states at time k and $k+1$ are shown. The branches which link the states are labeled by the corresponding branch metrics, while the states are labeled by the *accumulated state metrics* which will be defined later. The add, compare and select procedure consists on the following:

- For each state x_{k+1}, examine the branches stemming from states x_k and leading to it. For these branches *add* the metric accumulated at the state x_k to the metric of the branch itself.
- *Compare* the results of these sums.
- *Select* the branch associated with the minimum value and discard all the other branches (if the quantities being compared are equal, either one of them can be chosen randomly). This minimum value is associated with the state x_{k+1} and forms its state accumulated metric (this value is stored only for the next ACS step and then discarded).

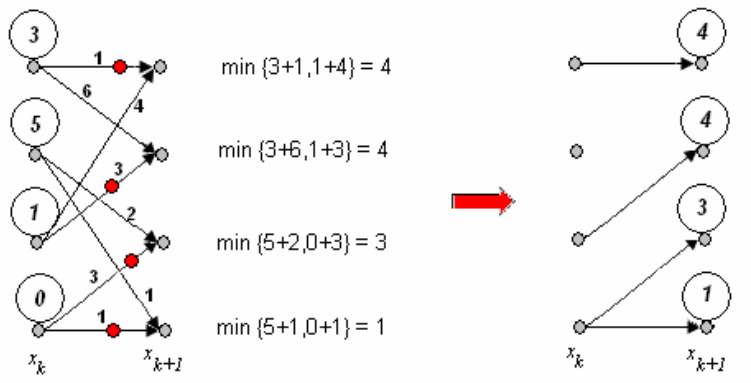

Figure 4.2. ACS step of Viterbi algorithm

The Viterbi algorithm consists of repeating the ACS from the first state of the trellis to the last state. After each ACS step for each state one value of accumulated metric and one path are retained. Thus, at any time k, for each x_k there is just a single survivor path left traversing the trellis from its first state to x_k and one value of accumulated metric. This survivor path is the minimum-metric path to the corresponding state. After N ACS steps, at the termination of the trellis, a single N-branch path and an accumulated metric are obtained, which are the minimum metric path and the minimum metric value respectively.

Figure 4.3 shows an example of the determination of the minimum metric path through a 4 states trellis using the Viterbi algorithm with N=6.

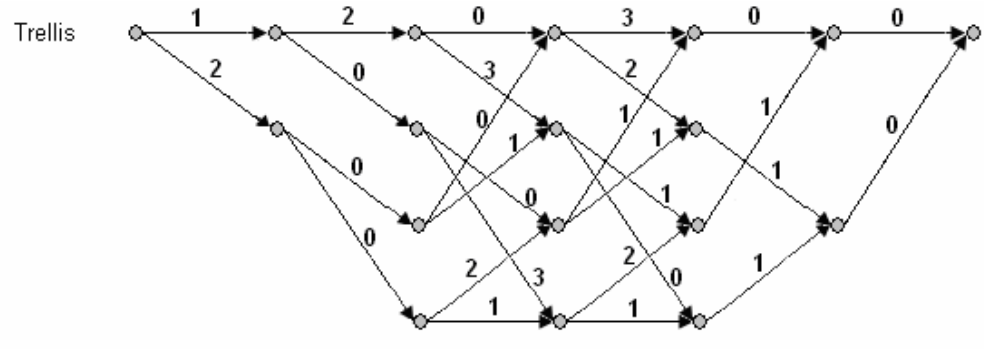

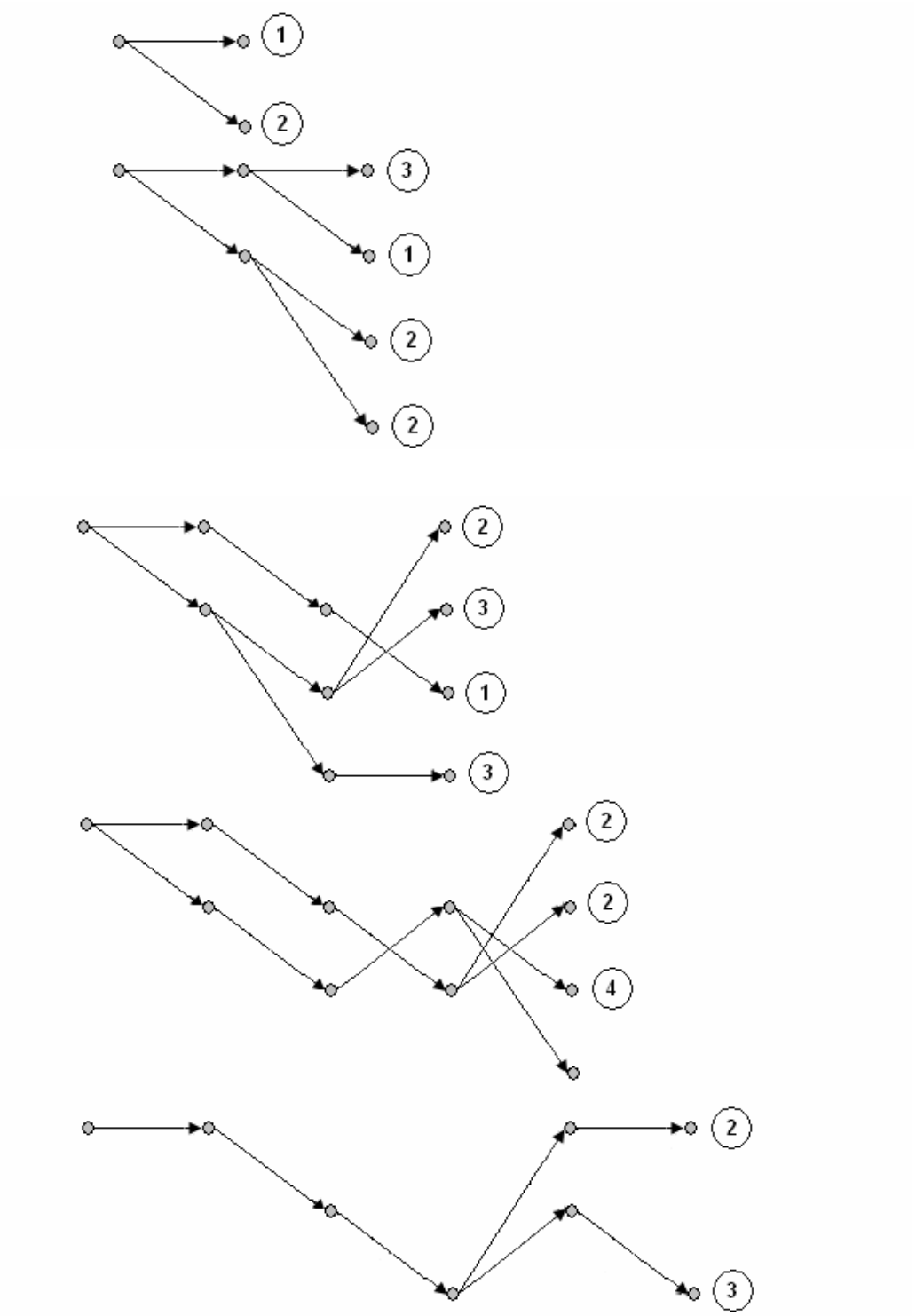
1
2
3
1
2
2
2
3
1
3
2
2
4
2
3

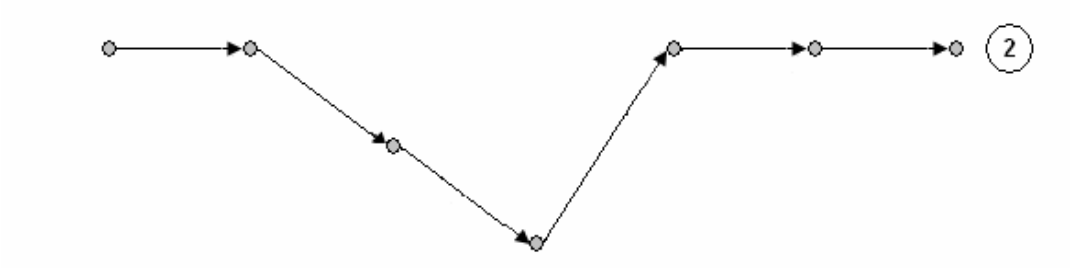

Figure 4.3. Determination of the minimum metric path using the Viterbi algorithm

4.4 MLSE receiver for DQPSK systems

Since the DQPSK modulation format generates at the receiver two parallel electrical signals $y^I(t)$ and $y^Q(t)$, the MLSE processor can adopt different configurations. There are three possible configurations: *Balanced single-input double-MLSE processor* (in which the RX is balanced and two binary MLSE processors are used, one for each signal quadrature), *Balanced double-input MLSE processor* (in which the RX is balanced and a single MLSE processor works on symbols composed by two parallel bits) and *Unbalanced quad-input MLSE processor* (where the electrical signals at the output of the lower and upper branches of the AMZ are not combined and are parallely fed to an MLSE processor working on symbols composed by two bits).

4.4.1 Balanced single-input double-MLSE processor

The system schematic is shown in *Figure 4.4*. A standard balanced DQPSK receiver generates the in-phase and quadrature electrical signals $y^I(t)$ and $y^Q(t)$, which enter a couple of ADC modules. The quantized signal samples y^I_k and y^Q_k are independently fed to two single-input MLSE processors.

The MLSE processors are based on the use of the Viterbi algorithm An example of a trellis structure with 16 states is shown in *Figure 4.5*.

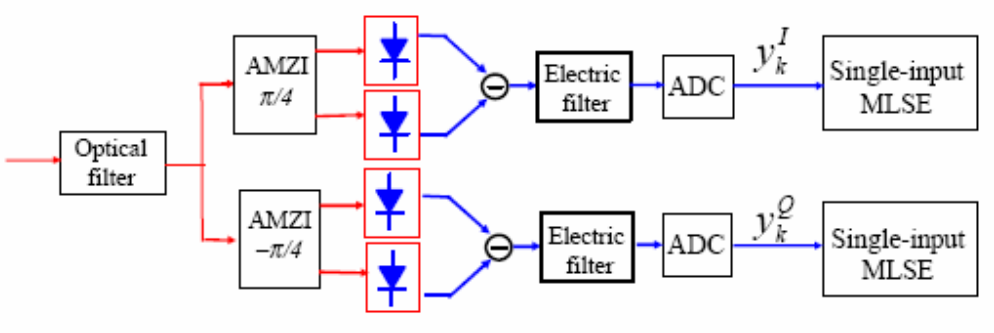

Figure 4.4. Balanced single-input double-MLSE processor schematic

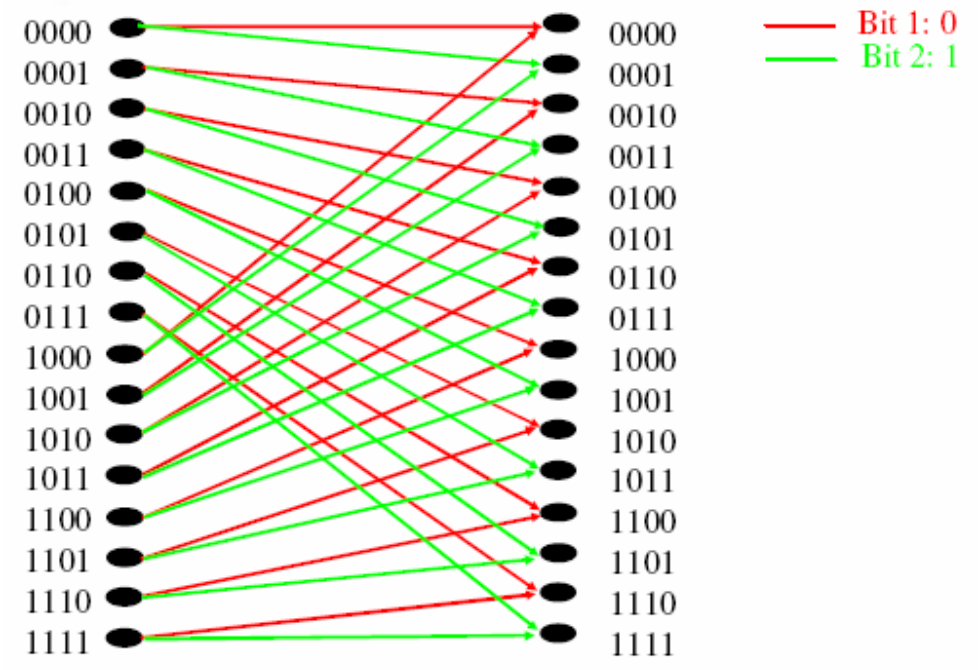

Figure 4.5. 16 states trellis for balanced single-input MLSE.

The trellis shown in *Figure 4.5* corresponds to a channel memory equal to 4, i.e. each trellis state is identified (and labeled) by the 4 past bits. Each state has 2 input branches and 2 output branches, corresponding to the current bit being a “0” or a “1”.

The branch metrics are evaluated as:

$$M^n_{DQPSK} = -\sum_{k=1}^{K} \log\left\{ f^{(n)}(y_k^{I,Q}) \right\} \tag{4.12}$$

where n is the branch number, K is the number of samples per bit and $f^{(n)}(y_k^{I,Q})$ is the probability density function (pdf) of the received sample taking on the value y^I_k (or y^Q_k), given that the n-th trellis branch was transmitted.

Assuming that the in-phase and quadrature signal samples have a Gaussian distribution, their pdf is given by:

$$f^{(n)}(y_k^{I,Q}) = \frac{1}{\sqrt{2\pi(\sigma^{I,Q}_{n,k})^2}} \cdot \exp\left\{ -\frac{(y_k - \mu^{I,Q}_{n,k})^2}{(\sigma^{I,Q}_{n,k})^2} \right\} \tag{4.13}$$

where the different μ and σ are respectively the mean value and the standard deviation of the k-th sample of the signal corresponding to the n-th trellis transition.

4.4.2 Balanced double-input MLSE processor

The system schematic is shown in *Figure 4.6.* A standard balanced DQPSK receiver generates the in-phase and quadrature electrical signals $y^I(t)$ and $y^Q(t)$, which enter a couple of ADC modules. The quantized signal samples y^I_k and y^Q_k are fed to a single MLSE processor which works on symbols composed by two parallel bits (one for each quadrature).

The MLSE processor is based on the use of the Viterbi algorithm An example of a trellis structure with 16 states is shown in *Figure 4.7*.

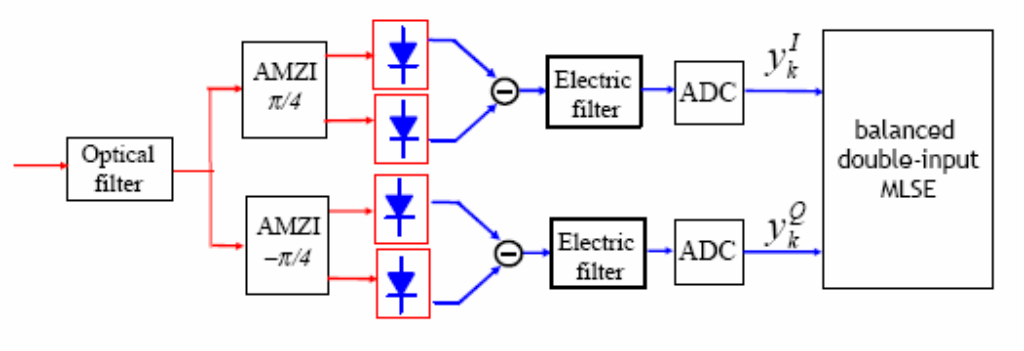

Figure 4.6. Balanced double-input MLSE processor schematic

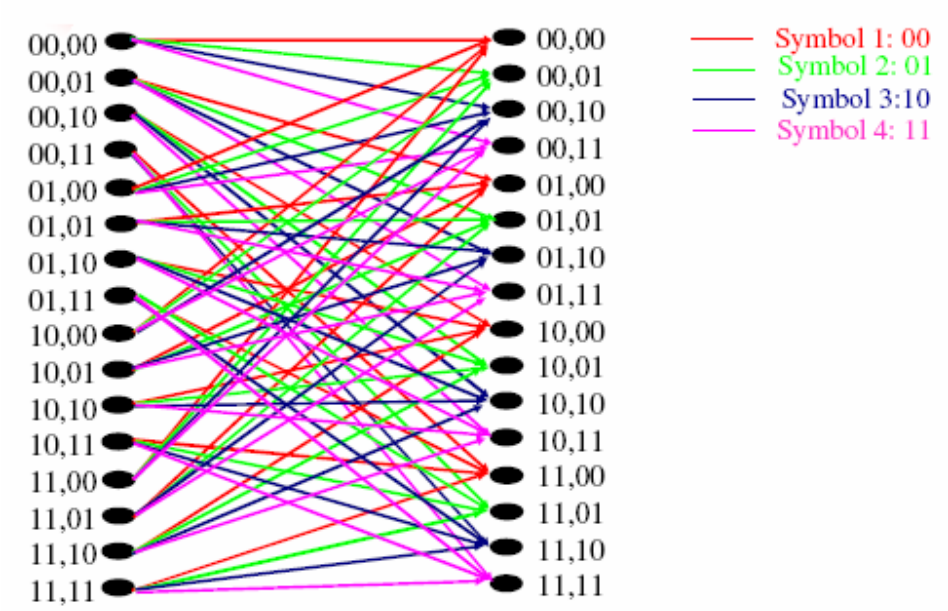

Figure 4.7. 16 states trellis for balanced double-input MLSE.

The trellis shown in *Figure 4.7* corresponds to a channel memory equal to 2, i.e. each trellis state is identified (and labeled) by the 2 past symbols. Each state has 4 input branches and 4 output branches, corresponding to the current symbol being “00”, “01”, “10” or “11”.

The branch metrics are evaluated as:

$$M^{n}_{DQPSK} = -\sum_{k=1}^{K} \log\left\{ f^{(n)}(y^{I}_{k}, y^{Q}_{k}) \right\} \tag{4.14}$$

where n is the branch number, K is the number of samples per bit and $f^{(n)}(y_k^I, y_k^Q)$ is the joint probability of receiving the two samples y^I_k and y^Q_k for the n-th trellis branch.

Assuming that the in-phase and quadrature signal samples are independent and follow a Gaussian distribution:

$$f^{(n)}(y^{I}_{k}, y^{Q}_{k}) = \frac{1}{\sqrt{2\pi(\sigma^{I}_{n,k})^2}} \cdot \exp\left\{ -\frac{(y_k - \mu^{I}_{n,k})^2}{(\sigma^{I}_{n,k})^2} \right\} \cdot \frac{1}{\sqrt{2\pi(\sigma^{Q}_{n,k})^2}} \cdot \exp\left\{ -\frac{(y_k - \mu^{Q}_{n,k})^2}{(\sigma^{Q}_{n,k})^2} \right\} \tag{4.15}$$

where the different μ and σ are respectively the mean value and the standard deviation of the k-th sample of the signal corresponding to the n-th trellis transition.

4.4.3 Unbalanced quad-input MLSE processor

The system schematic is shown in *Figure 4.8*. The four electrical signals at the output of the lower and upper branches of the two AMZs are not combined and parallely enter four ADC modules. The quantized signal samples $y_k^{I,up}$, $y_k^{I,low}$, $y_k^{Q,up}$ and $y_k^{Q,low}$ are fed to a single MLSE processor which works on symbols composed by two parallel bits (one for each quadrature).

The trellis structure is the same as for the balanced double-input MLSE (see *Figure 4.7*). Since in this case the signals on the BPD branches are no more bipolar (they assume mostly positive values), the SQRT metric can be used.

Assuming that the in-phase and quadrature signal samples on both the upper and lower branches are independent, the branch metrics can be evaluated as:

$$M_{DQPSK}^{n} = \sum_{k=1}^{K}\left(\sqrt{y_k^{I,low}} - \mu_{n,k}^{I,low}\right)^2 + \left(\sqrt{y_k^{I,up}} - \mu_{n,k}^{I,up}\right)^2 + \\ + \left(\sqrt{y_k^{Q,low}} - \mu_{n,k}^{Q,low}\right)^2 + \left(\sqrt{y_k^{Q,up}} - \mu_{n,k}^{Q,up}\right)^2 \tag{4.16}$$

where n is the branch number, K is the number of samples per bit and the different μ and σ are the mean values of the k-th sample of the signals corresponding to the n-th trellis transition.

The results shown in the following chapters were obtained using the *Balanced double-input MLSE processor*, since it represents the best trade-off between performance and complexity.

Chapter 5

Performance of the MLSE equalization in an optical communication system using the IMDD modulation format

In this chapter the results of a previous study on the effects of MLSE based receivers on a long-haul multi-channel dispersion-managed system are shown.

In [7] the performance of a MLSE receiver was compared, by simulation, with that of a standard optimized threshold receiver in a dispersion-managed multi-span multi-channel transmission system at 10.7 Gbit/s in the presence of fiber nonlinearities.

The system set-up is shown in *Figure 5.1*

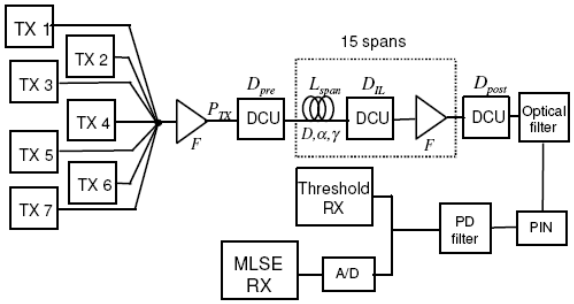

Figure 5.1 IMDD system set-up

5.1 IMDD system characteristics

Each transmitter (TX) is composed of a 10.7 Gbit/s $2^{16} - 1$ PN sequence generator, whose rectangular pulse output is passed through a 5-pole Bessel filter of -3 dB bandwidth equal to 7.5 GHz. Different PN sequence generators and slightly offset bit-rates (nominal bit rate ± 1.7%) were used for the seven transmitted channels, in order to obtain a better ensemble-estimate of inter-channel non-linear effects and, in particular, of XPM. The filtered signal is fed to an ideal chirpless Mach-Zehnder modulator which is driven exactly between full extinction and full transmission. The laser emission frequency for the center channel is 194 THz, and the channel frequency spacing is 50 GHz. The outputs of

the 7 transmitters are combined and input to an EDFA pre-amplifier which is used to tune the launch power to $P_{TX} = 7P_{ch}$, where P_{ch} is the average power per channel.

The transmission link is composed of 15 spans of SSMF, with loss coefficient α = 0.25 dB/km, dispersion parameter D = 16 ps/(nm·km), and nonlinear coefficient γ = 1.18 $W^{-1}km^{-1}$. Each fiber span is followed by an in-line dispersion compensating unit (DCU), which compensates an amount of CD equal to D_{IL}, and by an in-line EDFA amplifier, which completely recovers the span loss, with noise figure equal to 5.5 dB. It was assumed that the DCU would be inserted amidst a dual-stage EDFA, thus generating neither OSNR degradation nor further non-linearity. Pre and post-compensation units are present as well, with dispersion parameters equal to D_{pre} and D_{post} respectively.

At the receiver (RX) input there is a second-order super-gaussian optical filter with a -3 dB bandwidth of 35 GHz, a value that is realistic for commercial DWDM systems with channel spacing equal to 50 GHz. The optical filter is followed by an ideal photodetector, followed in turn by a 5-pole Bessel post-detection filter of bandwidth 7.5 GHz.

Two different types of receivers were used in the simulations:

- Threshold receiver: a standard receiver with adjustable threshold, used as reference;
- MLSE receiver: the post-detection filter is followed by a 5-bit A/D converter and a 32-state MLSE processor.

In the first case, the output of the post-detection filter is sampled (at a rate equal to the bit rate) and both the sampling instant and the decision threshold are optimized.

In the second case, the output of the post-detection filter is sampled at a rate equal to twice the bit rate and is sent to a MLSE processor. It consists of an A/D converter with 5 bits of resolution, whose samples are sent to a parallel bank of 64 branch metric computation stages. The extracted metric data is then sent to a 32-state Viterbi processor.

The MLSE processor employed the SQRT branch metric:

$$m_k = [\sqrt{y} - \mu_k]^2 \tag{5.1}$$

Where y is a sample of the RX signal, k is an index running over all possible branches and sampling instants, and μ_k is the mean value of those $\sqrt{y}$ that belong to the branch and sample corresponding to index k.

5.1.1 The testing procedure

The system OSNR due to ASE noise depends on the link parameters according to the well-known formula:

$$OSNR = \frac{P_{ch}}{2 \cdot N_o \cdot B}, \quad \text{with } N_o = n_{sp} h\nu (G-1) N_{span},\ F = 2n_{sp} \text{ and } G-1 \approx G$$

$$OSNR = \frac{P_{ch}}{2 \cdot n_{sp} \cdot h\nu (G-1) N_{span} B} = \frac{P_{ch}}{2 \cdot n_{sp} \cdot h\nu G N_{span} B} = \frac{P_{ch}}{F \cdot h\nu G N_{span} B}$$

Finally expressing it in dB and with $G = A_{span}$:

$$OSNR|_{dB} = P_{ch}|_{dBm} - A_{span}|_{dB} - F|_{dB} - 10\log_{10}(h\nu N_{span} B) \qquad (5.2)$$

where N_{span} is the number of spans, F is the noise figure of the EDFAs, h is Plank's constant, ν is the center channel frequency, B the OSNR noise bandwidth (0.1 nm throughout this study) and $A_{span}|_{dB}$ is the span loss.

From (5.2) it appears that, given a fixed OSNR, an increase in launch power would allow an identical increase in span loss. In linearity, this would also ensure no change in final BER, which would remain fixed at a, say, reference value BER_{ref}.

However, if non-linearity were present, an increase in $P_{ch}|_{dBm}$ might not allow the same increase in $A_{span}|_{dB}$. It could turn out that due to non-linear signal distortion BER > BER_{ref} even though the OSNR would be same as before.

If non-linearity were severe, it might happen that an increase in $P_{ch}|_{dBm}$ would require the span loss $A_{span}|_{dB}$ to decrease, in order for BER not to change.

Given this interplay between $P_{ch}|_{dBm}$ and $A_{span}|_{dB}$, which is revealing of how severe the impact of non-linearity is on a system, the following tests were carried out;

Given a fixed value of $P_{ch}|_{dBm}$ the value of $A_{span}|_{dB}$ which yielded a constant $BER_{ref} = 10^{-3}$ was estimated, over a large variety of dispersion maps. The dispersion maps were characterized using the in-line and total dispersion compensation residues, respectively defined as:

$$D_{res,IL} = D_{IL} + D \cdot L_{span} \qquad (5.3)$$
$$D_{res,tot} = D_{post} + D_{pre} + N_{span} \cdot D_{res,IL}$$

With such data the contour plots of $A_{span}|_{dB}$ vs. R_{IL} and R_{tot} were obtained. The higher the value of $A_{span}|_{dB}$, the better the map.

Two maps for each of the following values of $P_{ch}|_{dBm}$: 3, 4.5, 6, 7.5, 9 dBm were drawn. One map used the optimized threshold receiver and the other the MLSE receiver.

To improve readability and allow for a more intuitive appreciation of the results, the contour plots are not quoted directly in span loss $A_{span}|_{dB}$, but according to the derived quantity L_{tot}:

$$L_{tot} = \frac{N_{span}}{\alpha|_{dB/km}} \cdot A_{span}|_{dB} = 60 \cdot A_{span}|_{dB} \qquad (5.4)$$

L_{tot} would be the total system length theoretically reachable if all the span loss was due to span fiber. As shown above, given the set parameters of this study $N_{span} = 15$ and $\alpha|_{dB/km} = 0.25$, L_{tot} is exactly 60 times $A_{span}|_{dB}$.

As for pre-compensation, it was found that the contour plots were only marginally influenced by the value of Dpre. Therefore, the same configuration was used for all simulations, where Dpre = −300 ps/nm, a value which turned out to be approximately optimal for all values of launch power.

The obtained contour plots are shown in *Figures 5.2* thru *5.11* for increasing values of transmitted power.

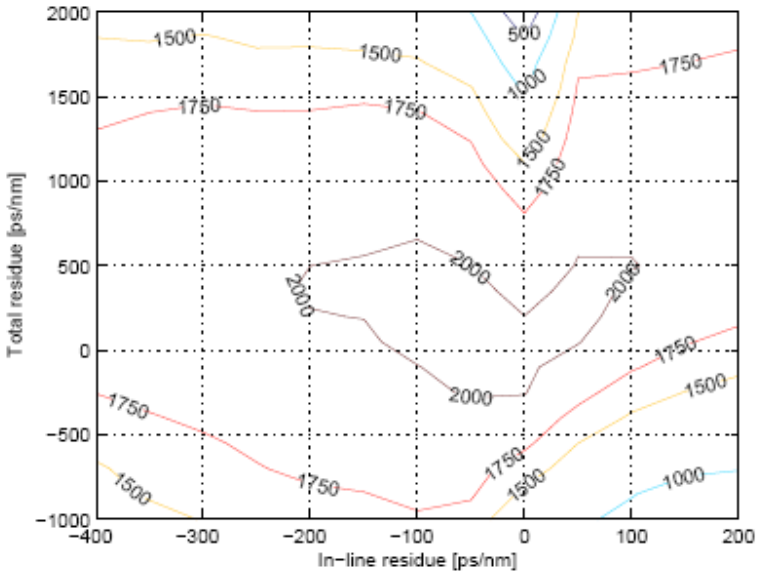

Figure 5.2 Contour plot of maximum reachable distance (in km) vs. in-line and total dispersion compensation residue for P_{ch}=3 dBm using a standard receiver and IMDD modulation

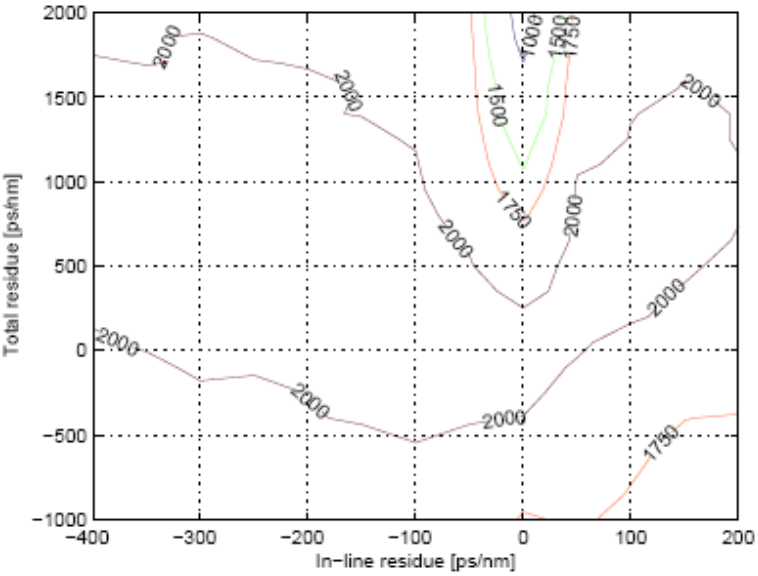

Figure 5.3 Contour plot of maximum reachable distance (in km) vs. in-line and total dispersion compensation residue for Pch=3 dBm using a MLSE receiver and IMDD modulation

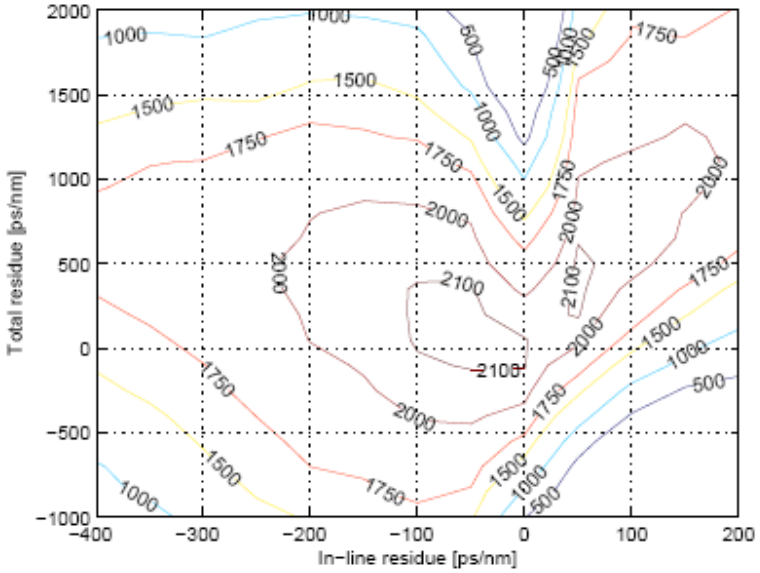

Figure 5.4 Contour plot of maximum reachable distance (in km) vs. in-line and total dispersion compensation residue for Pch=4.5 dBm using a standard receiver and IMDD modulation

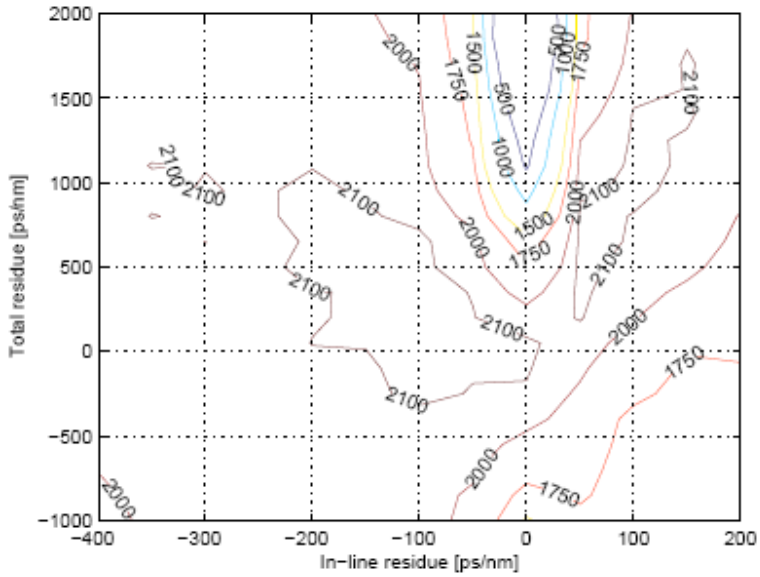

Figure 5.5 Contour plot of maximum reachable distance (in km) vs. in-line and total dispersion compensation residue for Pch=4.5 dBm using a MLSE receiver and IMDD modulation

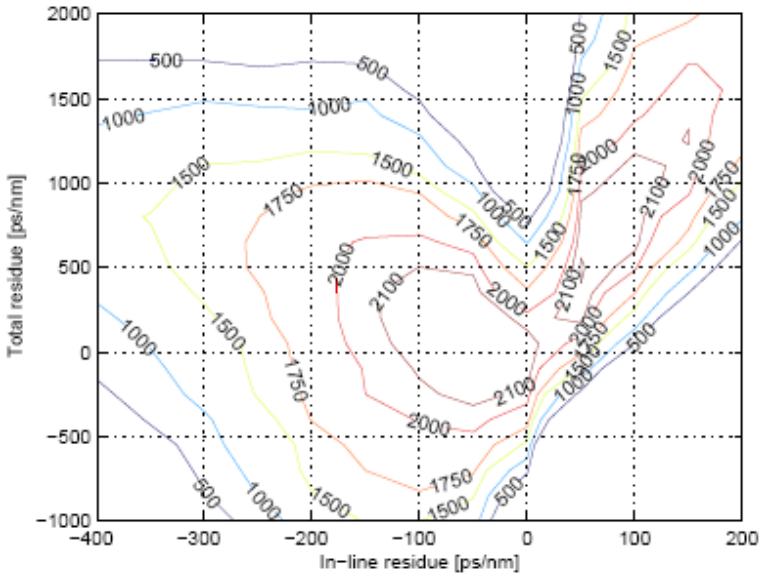

Figure 5.6 Contour plot of maximum reachable distance (in km) vs. in-line and total dispersion compensation residue for Pch=6 dBm using a standard receiver and IMDD modulation

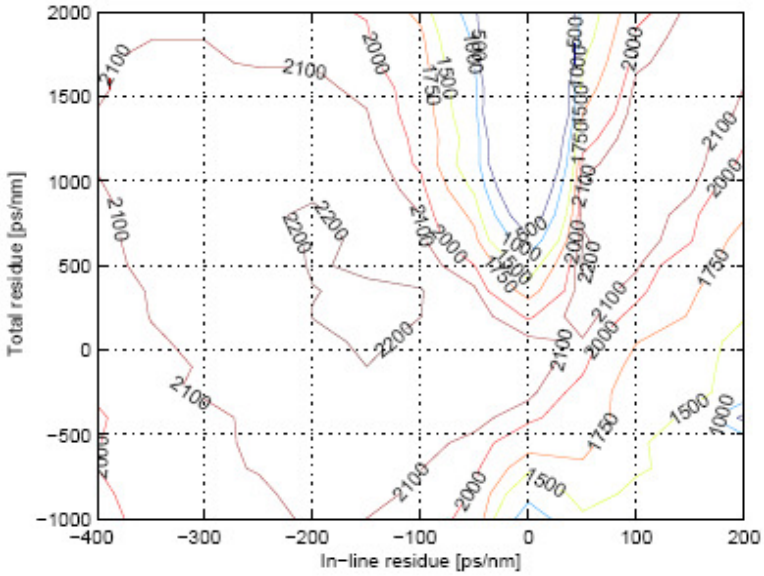

Figure 5.7 Contour plot of maximum reachable distance (in km) vs. in-line and total dispersion compensation residue for Pch=6 dBm using a MLSE receiver and IMDD modulation

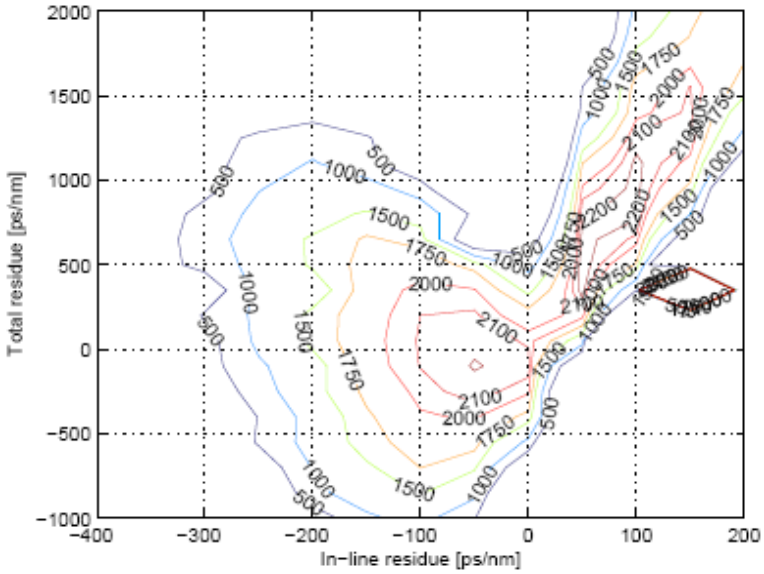

Figure 5.8 Contour plot of maximum reachable distance (in km) vs. in-line and total dispersion compensation residue for Pch=7.5 dBm using a standard receiver and IMDD modulation

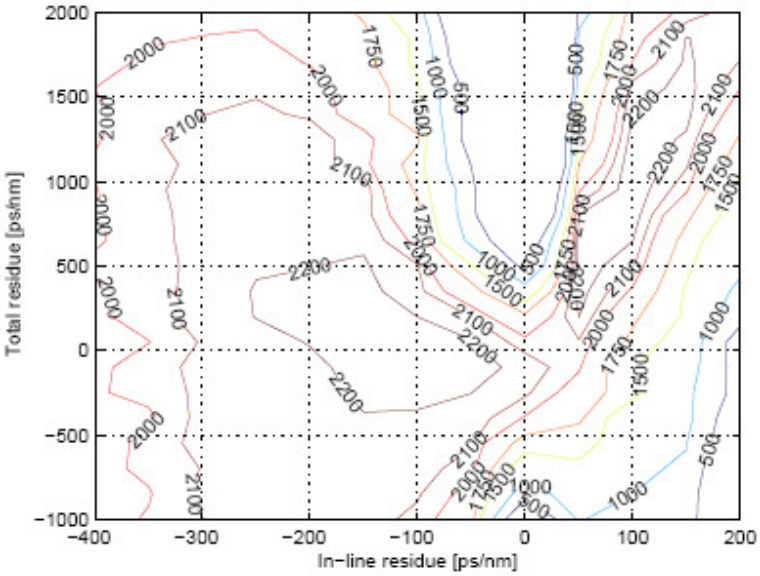

Figure 5.9 Contour plot of maximum reachable distance (in km) vs. in-line and total dispersion compensation residue for Pch=7.5 dBm using a MLSE receiver and IMDD modulation

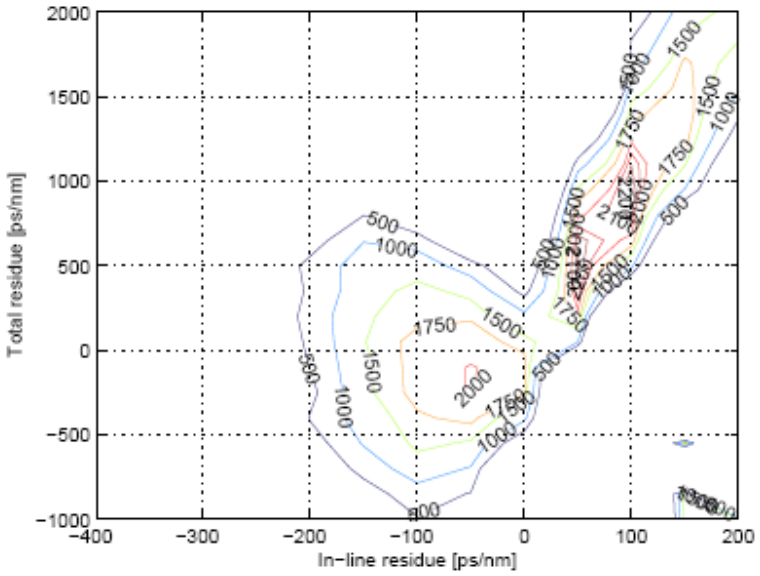

Figure 5.10 Contour plot of maximum reachable distance (in km) vs. in-line and total dispersion compensation residue for Pch=9 dBm using a standard receiver and IMDD modulation

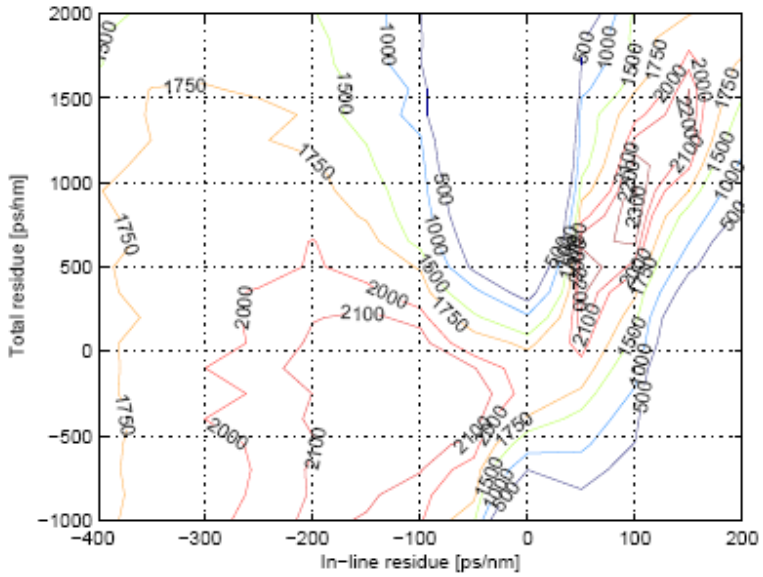

Figure 5.11 Contour plot of maximum reachable distance (in km) vs. in-line and total dispersion compensation residue for Pch=9 dBm using a MLSE receiver and IMDD modulation

5.1.2 Simulation results

For launch powers of 4.5 dBm and higher, two distinct optimum regions can be observed, for negative and positive values of the in-line residue, respectively. In all cases, a slightly larger theoretical L_{tot} (i.e., a marginally greater $A_{span|dB}$) is found for $D_{res,IL} > 0$. However, the optimal regions are typically much wider for $D_{res,IL} < 0$.

The great advantage of using an MLSE RX instead of a threshold RX is quite evident at all launched powers. The maximum L_{tot} is always somewhat larger with the MLSE receiver than without. More important, there is a very much increased tolerance to the values of in-line and total dispersion residues. As an example, for a launch power of 7.5 dBm, the contour of L_{tot} = 2100 km (see *Figures 5.8 and 5.9*) is reached over an extremely wide area with the MLSE receiver, both for $D_{res,IL} < 0$ and for $D_{res,IL} > 0$. The contour of L_{tot} = 2200 km still covers wide areas with MLSE whereas it is vanishing with the threshold receiver.

The maximum theoretical system total length is reported for all the transmitted power values and for both the standard and MLSE receivers in *Table 5.1*.

	Maximum System Total Length [km]	
P_{ch} [dBm]	**Standard RX**	**MLSE RX**
3	2030	2030
4.5	2110	2120
6	2190	2210
7.5	2230	2280
9	2260	2320

Table 5.1. Maximum system total length using IMDD modulation

The width of the $D_{res,IL}$ and $D_{res,tot}$ windows in which the maximum theoretical system length L_{tot} is greater than 2100 and 2200 km are reported in *Tables 5.2 and 5.3* for both receivers and for a launch power per channel ranging from 4.5 dBm to 9 dBm (a launch power equal to 3 dBm is not sufficient to reach such distances).

	Standard RX		**MLSE RX**	
P_{ch} [dBm]	**$D_{res,IL}$**	**$D_{res,tot}$**	**$D_{res,IL}$**	**$D_{res,tot}$**
4.5	± 50 ps/nm	± 300 ps/nm	± 70 ps/nm	± 500 ps/nm
6	± 70 ps/nm	± 400 ps/nm	± 160 ps/nm	± 1500 ps/nm
7.5	± 50 ps/nm	± 250 ps/nm	± 150 ps/nm	± 1400 ps/nm
9	± 10 ps/nm	± 100 ps/nm	± 130 ps/nm	± 500 ps/nm

Table 5.2. Dispersion windows for different values of launch power at a total distance of 2100 km for standard and MLSE receivers

	Standard RX		**MLSE RX**	
P_{ch} [dBm]	**$D_{res,IL}$**	**$D_{res,tot}$**	**$D_{res,IL}$**	**$D_{res,tot}$**
4.5	----------	----------	----------	----------
6	± 25 ps/nm	± 50 ps/nm	± 50 ps/nm	± 250 ps/nm
7.5	± 20 ps/nm	± 80 ps/nm	± 70 ps/nm	± 400 ps/nm
9	± 3 ps/nm	± 100 ps/nm	± 8 ps/nm	± 250 ps/nm

Table 5.3. Dispersion windows for different values of launch power at a total distance of 2200 km for standard and MLSE receivers

The optimum value of launch power, i.e. the one which yields the largest dispersion windows for the 2100 and 2200 km contours, is 6 and 7.5 dBm per channel, respectively. This is true for both the standard and the MLSE receivers, but the size of the regions is several times larger for the MLSE RX (10 to 15 times if areas are compared).

When the launch power becomes as high as 9 dBm, the maximum reachable distance slightly increases with respect to P_{ch} = 7.5 dBm, but the optimum map, found for the $D_{res,IL} > 0$ region, belongs to a region with excessively narrow and close contour lines.

To analyse how the MLSE receiver responds to XPM, a simulation of a system with the same characteristics as shown in section 5.1 was carried out, but transmitting one channel only (the central channel) with a launch power equal to 7.5 dBm. The obtained contour plots are shown in *Figures 5.12* and *5.13.*

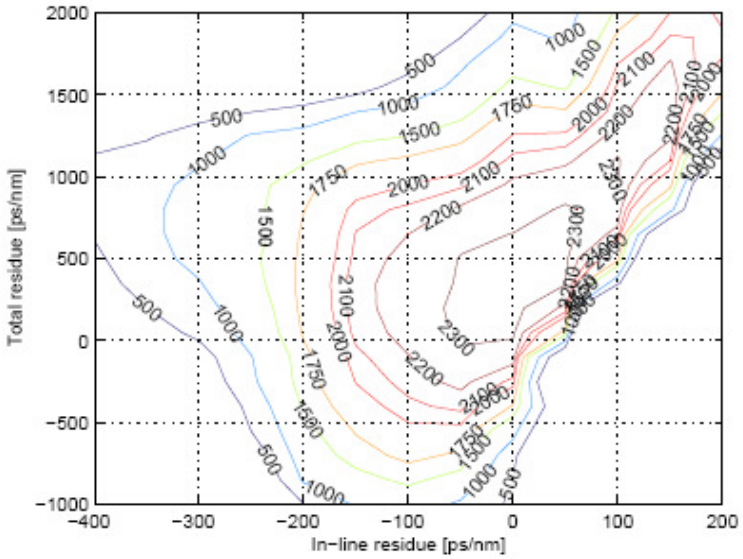

Figure 5.12 Contour plot of maximum reachable distance (in km) vs. in-line and total dispersion compensation residue for Pch=7.5 dBm using a standard receiver and IMDD modulation (only the central channel is transmitted)

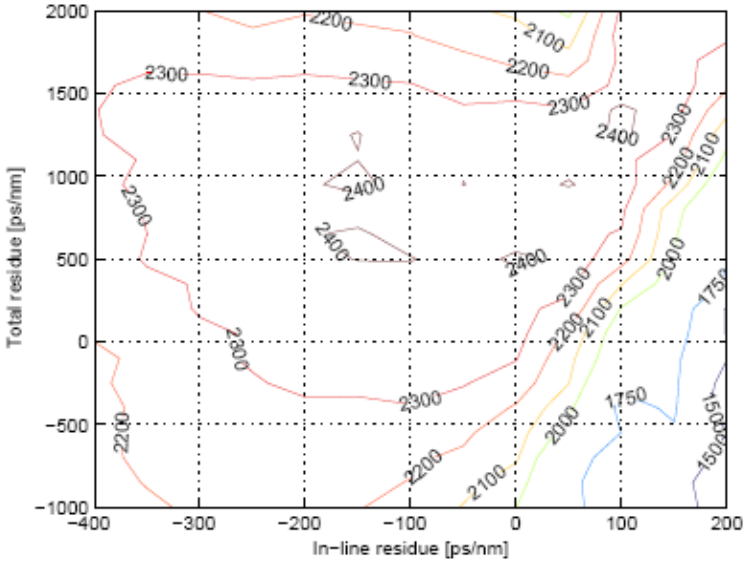

Figure 5.13 Contour plot of maximum reachable distance (in km) vs. in-line and total dispersion compensation residue for Pch=7.5 dBm using a MLSE receiver and IMDD modulation (only the central channel is transmitted)

There is no doubt that MLSE cannot mitigate XPM. Due to the high levels of launch power, needed to achieve sufficiently high OSNRs to reach a total link length as high as 2200 km, and to the tight channel spacing (50 GHz), XPM effects have a high impact on the performance of the analyzed system scenario.

Comparing *Figures 5.12* and *5.13* with *Figures 5.8* and *5.9*, it can be noticed that the presence of XPM reduces the maximum reachable distance from 2350 km to 2200 km and from 2420 km to 2250 km, when threshold and MLSE receivers are used, respectively.

MLSE can, however, by mitigating the penalty stemming from both suboptimal dispersion compensation and from intra-channel non-linearity, allow access to wide areas of the contour planes which are favorable for XPM but cannot be typically accessed by conventional systems due to the high single-channel penalties.

It is important to point out the great advantage that the use of a MLSE receiver brings to a WDM system. Due to the dispersion slope, different channels will "see" a different dispersion. If the optimum region is not wide enough, the lateral channels will not fit into it and suffer from different penalties which will make their reception impossible. When MLSE is used, the optimum regions are widened, providing a higher tolerance to chromatic dispersion which allows fitting the whole WDM comb in the same region, thus achieving the correct reception of all the channels.

Chapter 6

Performance of the MLSE equalization in an optical communication system using the Duobinary modulation format

In this chapter, the results of a study on the use of MLSE receivers on optical communications systems in the presence of chromatic dispersion and fiber nonlinearities are shown.

The system set-up is exactly the same as the one shown in chapter 5 but the modulation format considered is the Doubinary.

The simulations of the optical system were done using the software OptSim and the graphics were obtained using Matlab.

6.1 Duobinary System characteristics

The characteristics of the system set-up and simulation procedures are the following:

- The bit-rate is R_b = 10.7 Gbit/s
- The number of channels is 7 with spacing equal to 50 GHz
- The central channel frequency is 194 THz

- The Pseudo Random Bit Sequence generated for each channel is PRBS = 2^{16} -1 = 65535 bits
- Each bit is simulated using 60 samples
- The transmission electrical filter is a 5 pole Bessel filter with $B_{-3\ dB}$ = 2.89 GHz
- The channel is formed by 15 spans of SSMF followed by an in-line DCU and a EDFA
- The SMF has the following characteristics:
  - α = 0.25 dB/km
  - D = 16 ps/nm/km
  - γ = 1.18 1/W/km
- The EDFAs have a gain that completely recovers the span loss (G = $\alpha \cdot L_{span}$) and a noise figure equal to 5.5 dB
- The in-line DCU introduces a dispersion value equal to D_{IL} = $D_{res,IL} - D \cdot L_{span}$ ps/nm, where $D_{res,IL}$ is the In-Line residue
- The Pre and Post compensation units introduce dispersion values of:
  - Dpre = -300 ps/nm
  - Dpost = $D_{res,tot} - D_{res,IL} \cdot$Nspan – Dpre ps/nm, where $D_{res,tot}$ is the total residue at the end of the link
- The receiver is composed by a 2^{nd} order SuperGaussian optical filter with B_{-3dB} = 35 GHz followed by an ideal photodetector and finally a 5 pole Bessel electrical filter with B_{-3dB} = 7.5 GHz.
- The receiver is followed by a 32-states Viterbi MLSE processor.
- The SQRT metric is used.
- 2 samples per bit are used for the branch metric evaluation.

6.1.1 The testing procedure

By simulation, a large amount of dispersion maps were analyzed for both the standard and MLSE receivers at three different lengths and five different transmitted power levels. The lengths considered were: 1700, 1900 and 2100 km and the transmitted powers: 3, 4.5, 6, 7.5 and 9 dBm per channel.

The dispersion maps were characterized using the in-line and total dispersion compensation residues respectively defined as:

$$D_{res,IL} = D_{IL} + D \cdot Lspan \qquad (6.1)$$

$$D_{res,tot} = Dpost + Dpre + Nspan \cdot D_{res,IL}$$

As an example, the contour plots of *log_{10}(BER) vs. in-line and total dispersion residue* found for P_{ch} = 3 dBm are shown in *Figures 6.1* thru *6.6*.

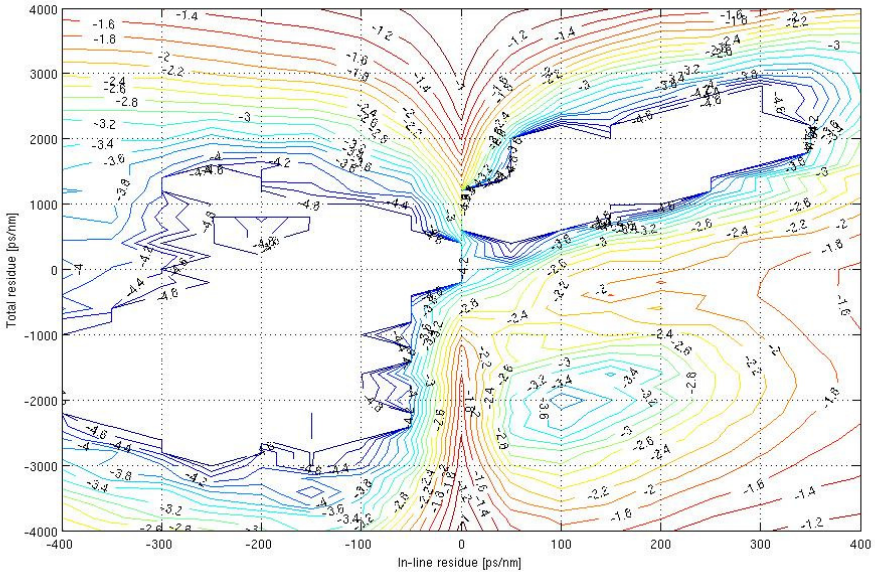

Figure 6.1 Contour plot of log_{10}BER vs. in-line and total dispersion residue for P_{ch} = 3dBm at 1700 km using a standard receiver and Duobinary modulation

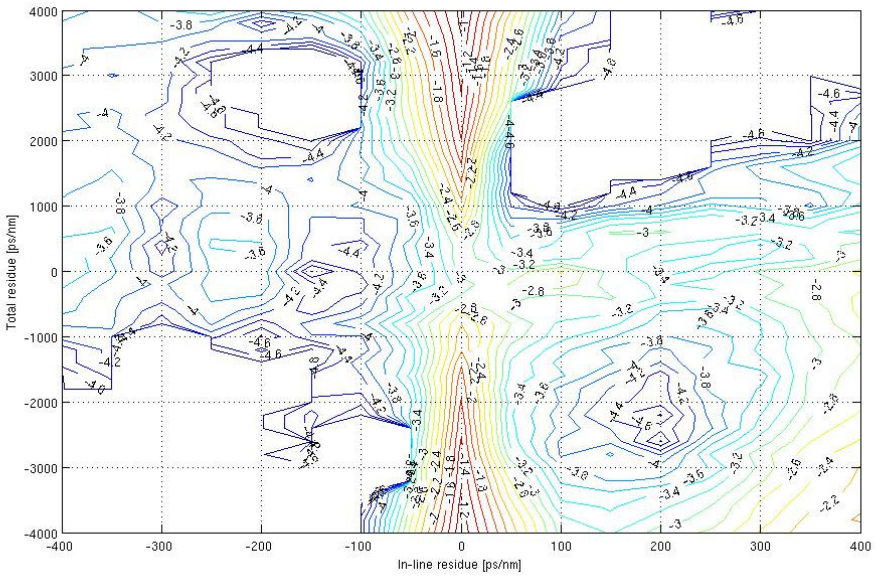

Figure 6.2 Contour plot of log10BER vs. in-line and total dispersion residue for Pch = 3dBm at 1700 km using a MLSE receiver and Duobinary modulation

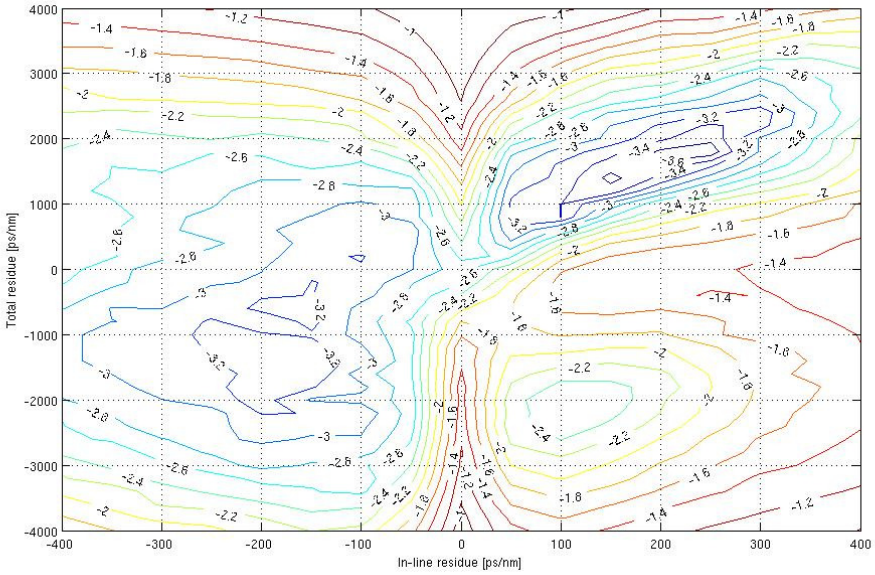

Figure 6.3 Contour plot of log_{10}BER vs. in-line and total dispersion residue for P_{ch} = 3dBm at 1900 km using a standard receiver and Duobinary modulation

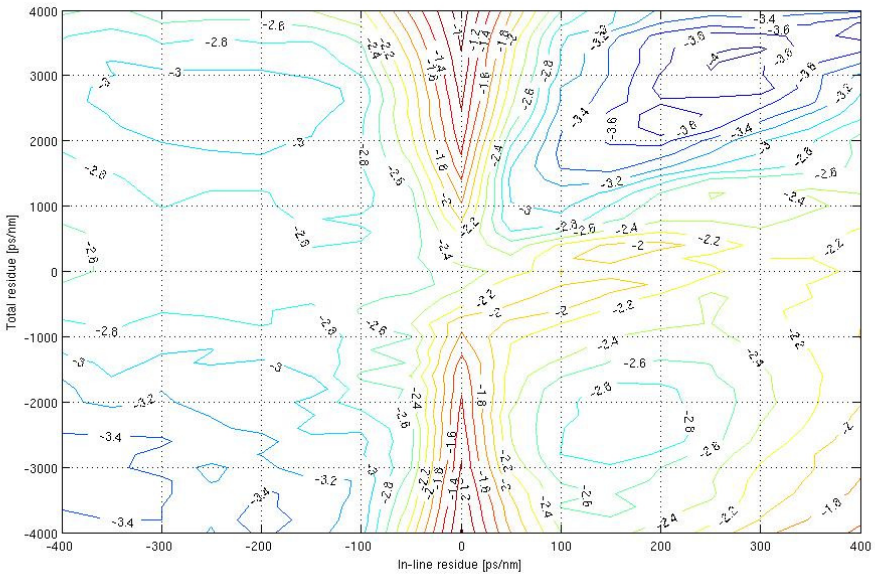

Figure 6.4 Contour plot of log10BER vs. in-line and total dispersion residue for Pch = 3dBm at 1900 km using a MLSE receiver and Duobinary modulation

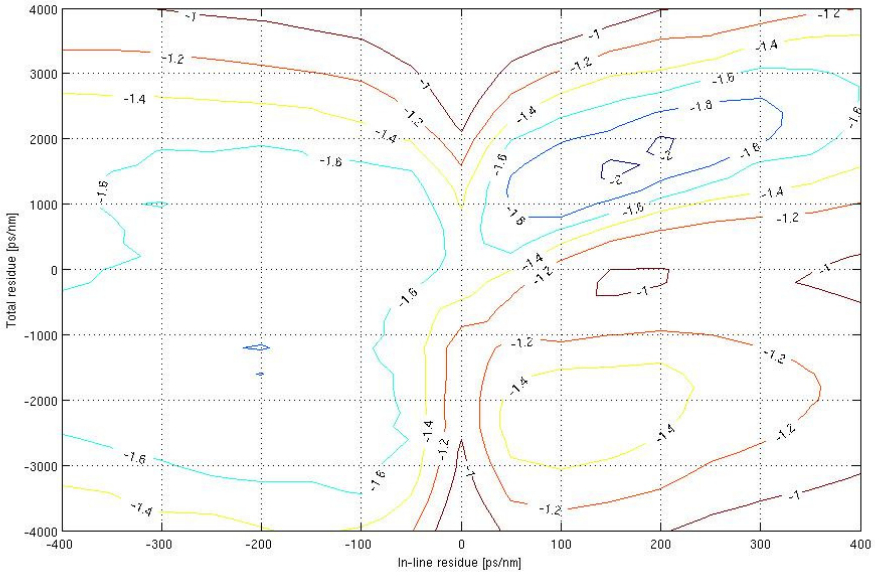

Figure 6.5 Contour plot of log_{10}BER vs. in-line and total dispersion residue for P_{ch} = 3dBm at 2100 km using a standard receiver and Duobinary modulation

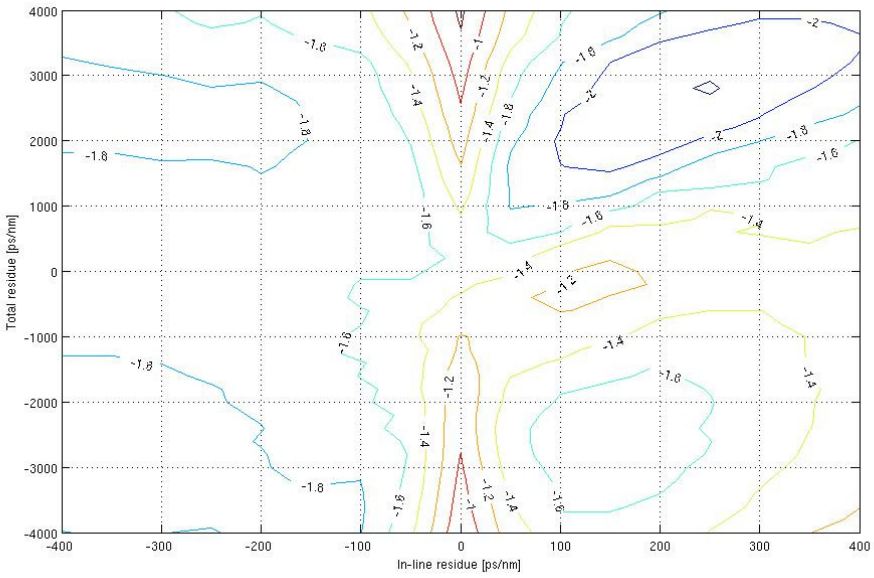

Figure 6.6 Contour plot of log_{10}BER vs. in-line and total dispersion residue for P_{ch} = 3dBm at 2100 km using a MLSE receiver and Duobinary modulation

These graphics show the system BER for different values of in-line and total compensation residue. However, the results would be easier to read and more intuitive if the graphics were quoted in total system length instead of BER. To do so, the graphics for each of the three lengths must be combined in some way.

First, the reference BER is set to 10^{-3} to ensure the operation beneath the FEC threshold. Then, to each couple of values of $D_{res,IL}$ and $D_{res,tot}$ a particular value of $\log_{10}$(BER) is associated, which is represented in the preceding graphics. So taking this value for the same couple of $D_{res,IL}$ and $D_{res,tot}$ over each of the three simulated system lengths we can plot the curve *log_{10}[-log_{10}(BER)] vs. total system length* which is a very good approximation of a straight line. Now a linear interpolation of these three couples of values (one for each length) can be done in order to find the length that corresponds to the chosen reference BER. An example of this is shown in *Figure 6.7*. Repeating this procedure over all the possible couples of $D_{res,IL}$ and $D_{res,tot}$ found on the *log_{10}BER vs. in-line and total dispersion residue* contour plots, we obtain the total system lengths reachable at a

BER equal to 10^{-3}. This has been done for both the standard and MLSE receivers. The obtained graphics are shown in *Figures 6.8* thru *6.17*.

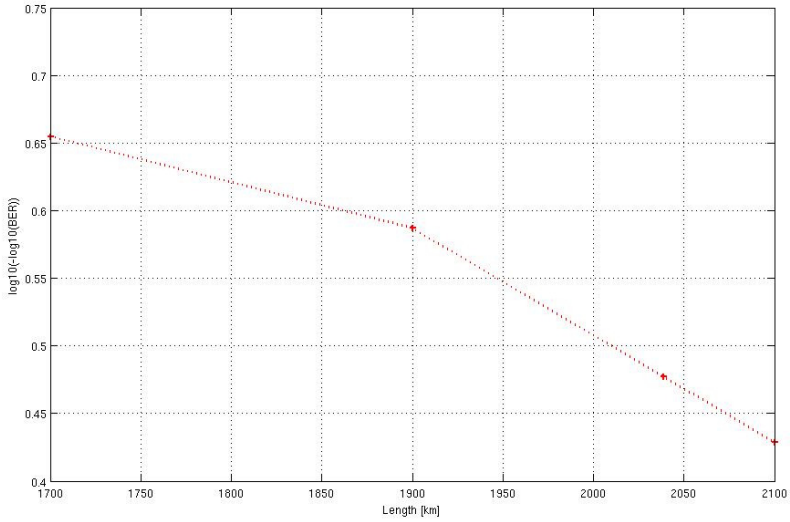

Figure 6.7. log10[-log10(BER)] vs. total system length, example of the interpolation procedure

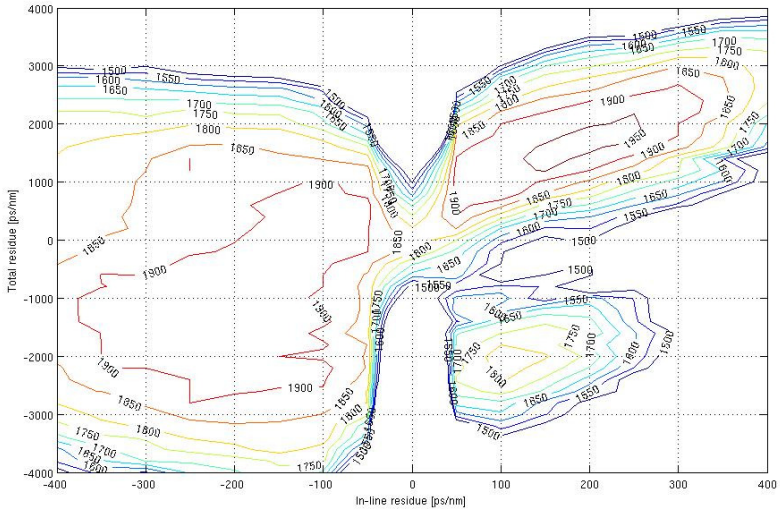

Figure 6.8. Contour plot of maximum reachable distance (in km) vs. in-line and total dispersion compensation residue for P_{ch}=3 dBm using a standard receiver and Duobinary modulation

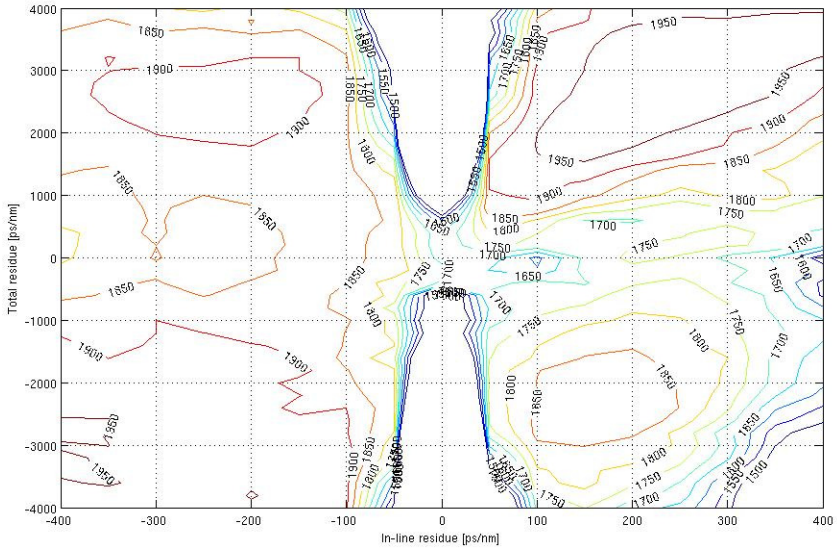

Figure 6.9. Contour plot of maximum reachable distance (in km) vs. in-line and total dispersion compensation residue for P_{ch}=3 dBm using a MLSE receiver and Duobinary modulation

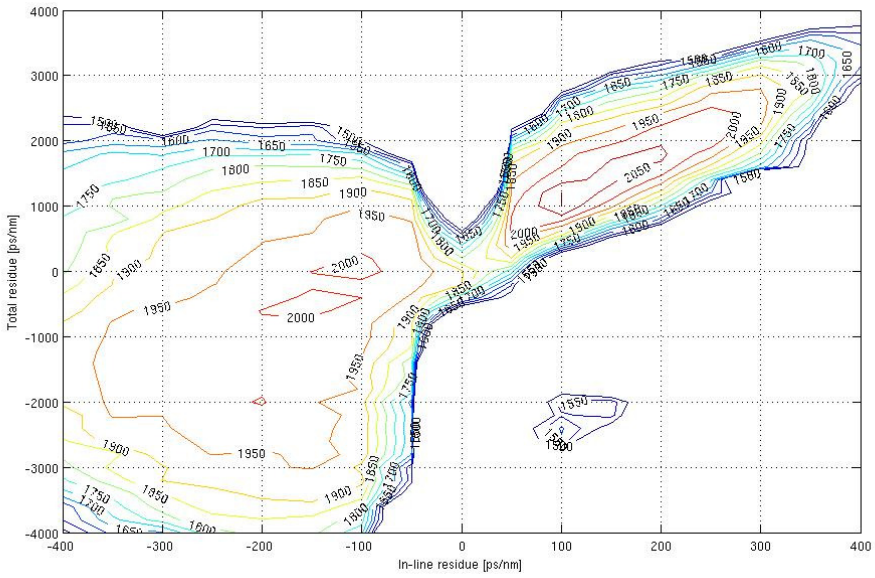

Figure 6.10. Contour plot of maximum reachable distance (in km) vs. in-line and total dispersion compensation residue for P_{ch}=4.5 dBm using a standard receiver and Duobinary modulation

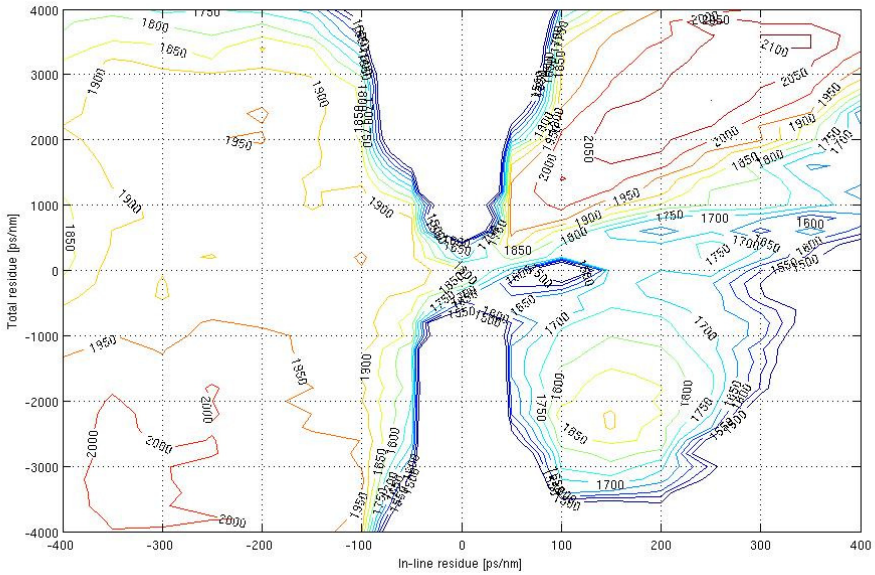

Figure 6.11. Contour plot of maximum reachable distance (in km) vs. in-line and total dispersion compensation residue for P_{ch}=4.5 dBm using a MLSE receiver and Duobinary modulation

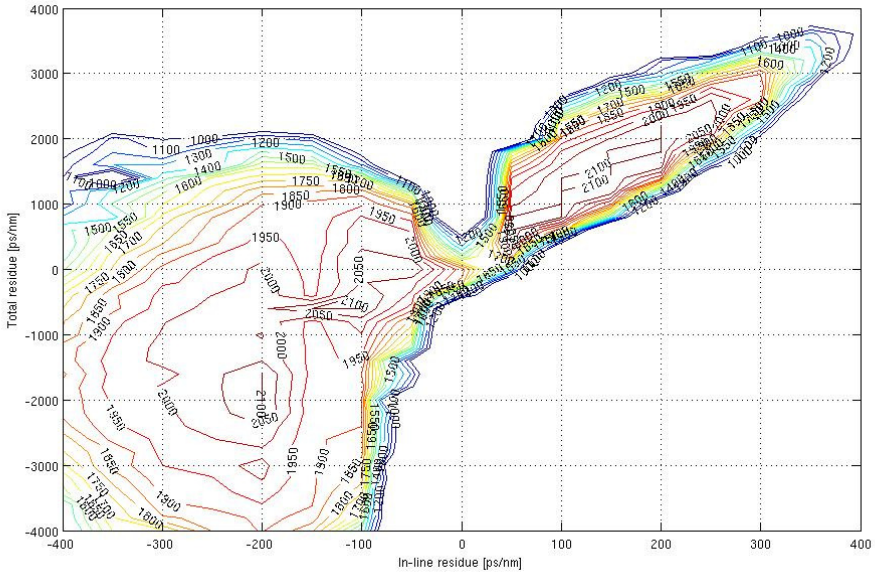

Figure 6.12. Contour plot of maximum reachable distance (in km) vs. in-line and total dispersion compensation residue for P_{ch}=6 dBm using a standard receiver and Duobinary modulation

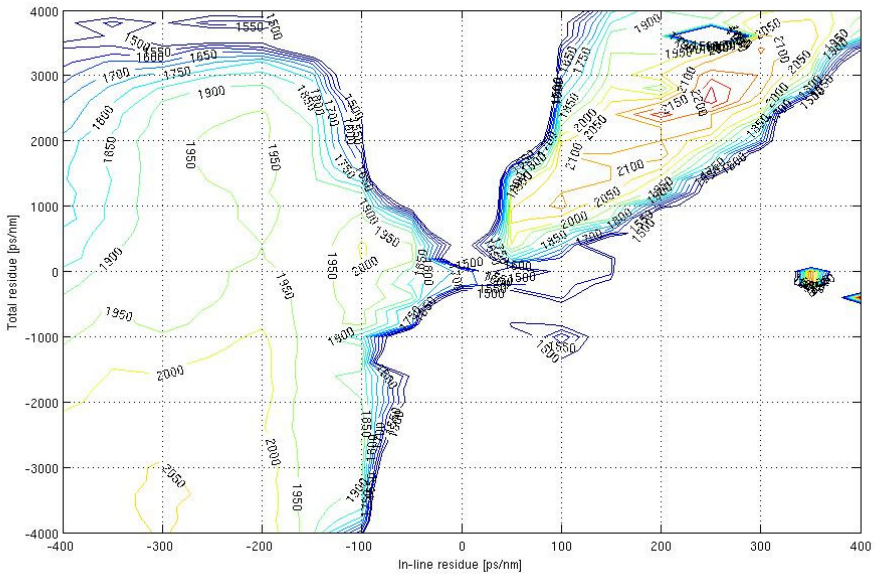

Figure 6.13. Contour plot of maximum reachable distance (in km) vs. in-line and total dispersion compensation residue for P_{ch}=6 dBm using a MLSE receiver and Duobinary modulation

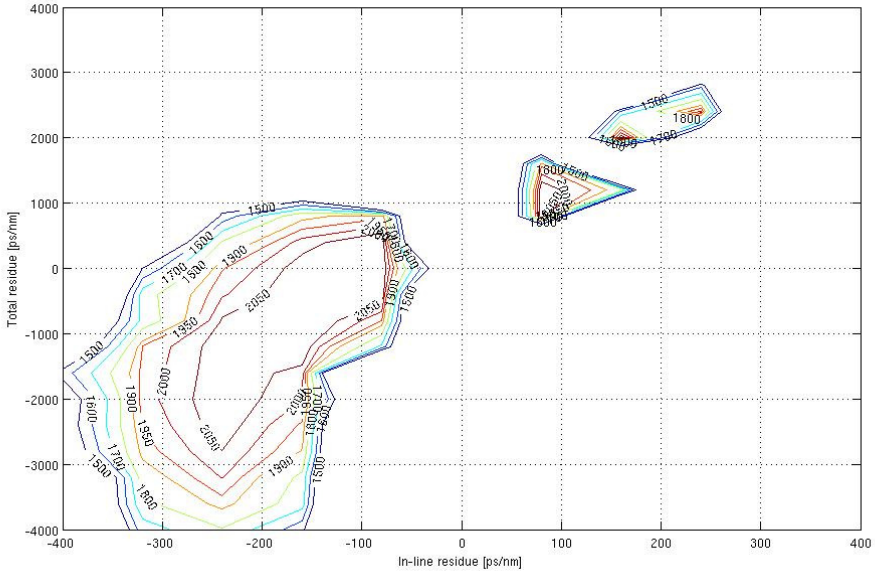

Figure 6.14. Contour plot of maximum reachable distance (in km) vs. in-line and total dispersion compensation residue for Pch=7.5 dBm using a standard receiver and Duobinary modulation

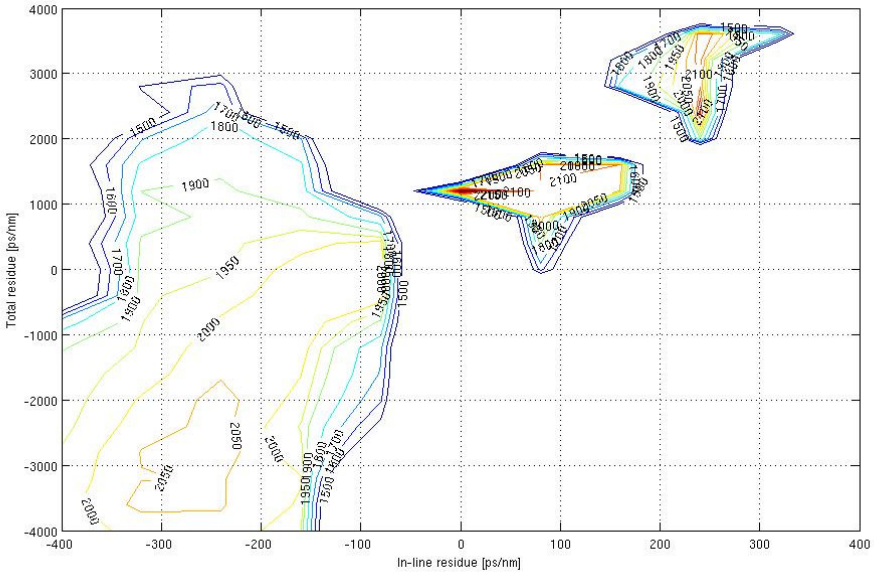

Figure 6.15. Contour plot of maximum reachable distance (in km) vs. in-line and total dispersion compensation residue for P_{ch}=7.5 dBm using a MLSE receiver and Duobinary modulation

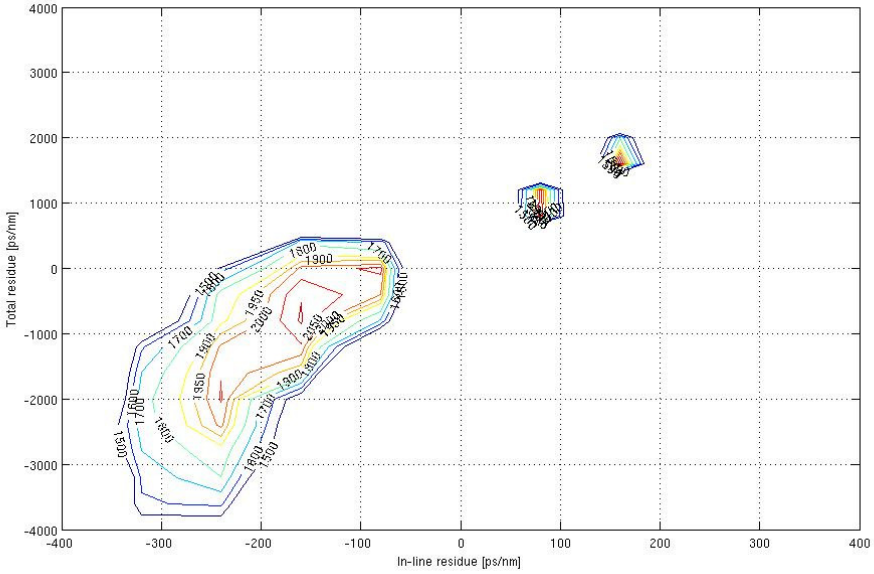

Figure 6.16. Contour plot of maximum reachable distance (in km) vs. in-line and total dispersion compensation residue for P_{ch}=9 dBm using a standard receiver and Duobinary modulation

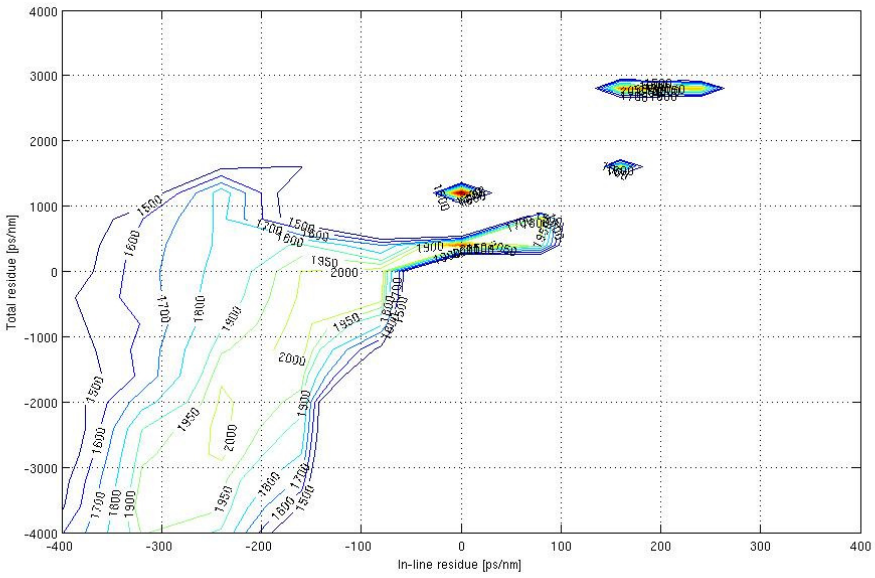

Figure 6.17. Contour plot of maximum reachable distance (in km) vs. in-line and total dispersion compensation residue for P_{ch}=9 dBm using a MLSE receiver and Duobinary modulation

6.1.2 Simulation results

For all the transmitted power values, two distinct optimum regions can be observed for negative and positive values of the in-line residue respectively. Also in all the cases, a slightly higher system length is reached for the region located on the positive end of the in-line residue. However, the optimum regions on the negative end of the in-line residue are wider.

The maximum theoretical system total length is reported for all the transmitted power values and for both the standard and MLSE receivers in *Table 6.1*.

	Maximum System Total Length [km]	
P_{ch} [dBm]	**Standard RX**	**MLSE RX**
3	1960	1990
4.5	2100	2120
6	2110	2270
7.5	2130	2340
9	2160	2400

Table 6.1. Maximum system total length using Duobinary modulation

Even though slightly greater total system distances, compared to the IMDD modulation format, can be achieved with Duobinary modulation, the optimum regions for which they are reached are extremely narrow.

The width of the $D_{res,IL}$ and $D_{res,tot}$ windows in which the maximum theoretical system length L_{tot} is greater than 2000 km are reported in *Table 6.2* for both the standard and MLSE receivers and for transmitted channel powers ranging from 4.5 dBm to 9 dBm (a launch power equal to 3 dBm is not sufficient to reach such distance).

	Standard RX		MLSE RX	
P_{ch} [dBm]	**$D_{res,IL}$**	**$D_{res,tot}$**	**$D_{res,IL}$**	**$D_{res,tot}$**
4.5	± 40 ps/nm	± 200 ps/nm	± 50 ps/nm	± 450 ps/nm
6	± 60 ps/nm	± 1000 ps/nm	± 100 ps/nm	± 1500 ps/nm
7.5	± 35 ps/nm	± 900 ps/nm	± 60 ps/nm	± 1000 ps/nm
9	± 20 ps/nm	± 300 ps/nm	± 30 ps/nm	± 350 ps/nm

Table 6.2. Dispersion windows for different values of launch power at a total distance of 2000 km for standard and MLSE receivers

The optimum value of launch power (the one which yields the largest window for the 2000 km contour) is 6 dBm for both receivers.

By comparing these results against those obtained with IMDD, shown in chapter 5, it is evident that the system's performance, in terms of maximum total length and

tolerance to chromatic dispersion, when using IMDD is better. However, Duobinary modulation is theoretically more robust to chromatic dispersion, so at first glance it doesn't seem right that its performance is inferior to that of IMDD. This can be attributed to the fact that the optimized band of the optical reception filter is narrow (under 10 GHz), while the band of the optical filter used in the simulations is wide (35 GHz).

To analyze the effect of XPM, a simulation of a system with the same characteristics as shown in section 6.1 was carried out, but transmitting one channel only (the central channel) with a launch power equal to 6 dBm. The obtained contour plots are shown in *Figures 6.18* and 6.*19*.

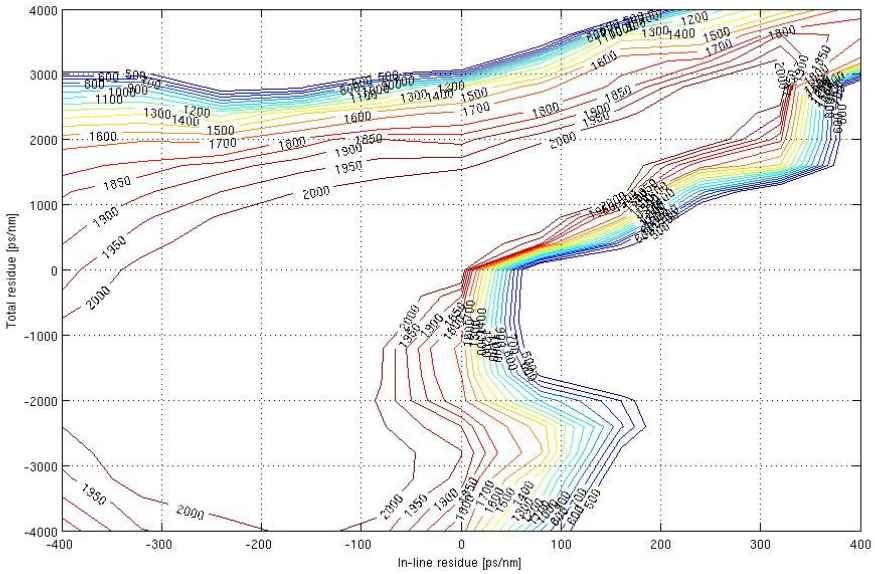

Figure 6.18 Contour plot of maximum reachable distance (in km) vs. in-line and total dispersion compensation residue for Pch=6 dBm using a standard receiver and Duobinary modulation (only the central channel is transmitted)

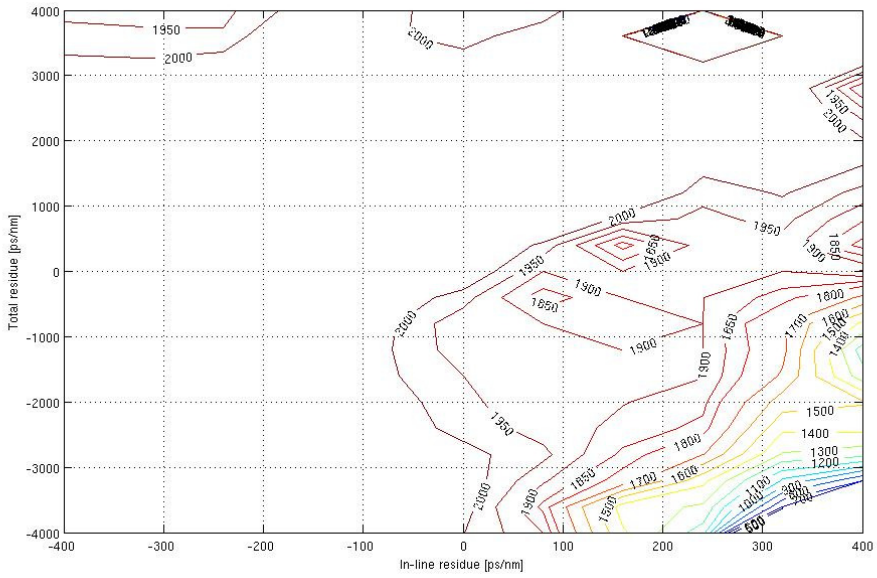

Figure 6.19 Contour plot of maximum reachable distance (in km) vs. in-line and total dispersion compensation residue for Pch=6 dBm using a MLSE receiver and Duobinary modulation (only the central channel is transmitted)

When comparing *Figures 6.12* and *6.13* with *Figures 6.18* and 6.*19*, it is evident how XPM affects the system's performance. This is due to the high launch power needed to reach a maximum link length as high as 2000 km, and the tight channel spacing (50 GHz).

As seen in the graphics, MLSE cannot mitigate XPM. However, as said in chapter 5, by mitigating the penalty stemming from both suboptimal dispersion compensation and from intra-channel non-linearity, MLSE can allow access to wide areas of the contour planes which are favorable for XPM but cannot be typically accessed by conventional systems due to the high single-channel penalties.

It is important to point out the great advantage that the use of a MLSE receiver brings to a WDM system. Due to the dispersion slope, different channels will "see" a different dispersion. If the optimum region is not wide enough, the lateral channels will

not fit into it and suffer from different penalties which will make their reception impossible. When MLSE is used, the optimum regions are widened, providing a higher tolerance to chromatic dispersion which allows fitting the whole WDM comb in the same region, thus achieving the correct reception of all the channels.

Chapter 7

Performance of the MLSE equalization in an optical communication system using the DPSK modulation format

It is known that the DPSK modulation format has a better sensitivity with respect to the IMDD and has also a reduced impact on fiber nonlinearities.

In this chapter, the results of a study on the use of MLSE receivers on optical communications systems in the presence of chromatic dispersion and fiber nonlinearities are shown.

The system set-up is exactly the same as the one shown in the previous two chapters but the modulation format considered is the DPSK.

The simulations of the optical system were done using the software OptSim and the graphics were obtained using Matlab.

7.1 DPSK System characteristics

The characteristics of the system set-up and simulation procedures are the following:

- The bit-rate is R_b = 10.7 Gbit/s
- The number of channels is 7 with spacing equal to 50 GHz

- The central channel frequency is 194 THz
- The Pseudo Random Bit Sequence generated for each channel is PRBS = 2^{16} -1 = 65535 bits
- Each bit is simulated using 60 samples
- The transmission electrical filter is a 5 pole Bessel filter with $B_{-3\ dB}$ = 8 GHz
- The channel is formed by 15 spans of SSMF followed by an in-line DCU and a EDFA
- The SMF has the following characteristics:
  - α = 0.25 dB/km
  - D = 16 ps/nm/km
  - γ = 1.18 1/W/km
- The EDFAs have a gain that completely recovers the span loss ($G = \alpha \cdot L_{span}$) and a noise figure equal to 5.5 dB
- The in-line DCU introduces a dispersion value equal to $D_{IL} = D_{res,IL} - D \cdot L_{span}$ ps/nm, where $D_{res,IL}$ is the In-Line residue
- The Pre and Post compensation units introduce dispersion values of:
  - Dpre = -300 ps/nm
  - Dpost = $D_{res,tot} - D_{res,IL} \cdot$Nspan – Dpre ps/nm, where $D_{res,tot}$ is the total residue at the end of the link
- The receiver is composed by a 2^{nd} order SuperGaussian optical filter with B_{-3dB} = 35 GHz followed by an ideal DPSK receiver and finally a 5 pole Bessel electrical filter with B_{-3dB} = 7.5 GHz.
- The receiver is followed by a 32-states Viterbi MLSE processor.
- The Gaussian metric is used because the DPSK signal can take negative values.
- 2 samples per bit are used for the branch metric evaluation.

7.1.1 The testing procedure

In this case the testing procedure is exactly the same as explained in chapter 6, with the exception that the MLSE processor uses the Gaussian metric due to the nature of the DPSK signal which can take negative values.

The contour plots of maximum system length (@BER=10^{-3}) vs. in-line and total residue were obtained for launch power values equal to 3, 4.5, 6, 7.5 and 9 dBm and for both the standard and MLSE receivers. These graphics are shown in *Figures 7.1* thru *7.10.*

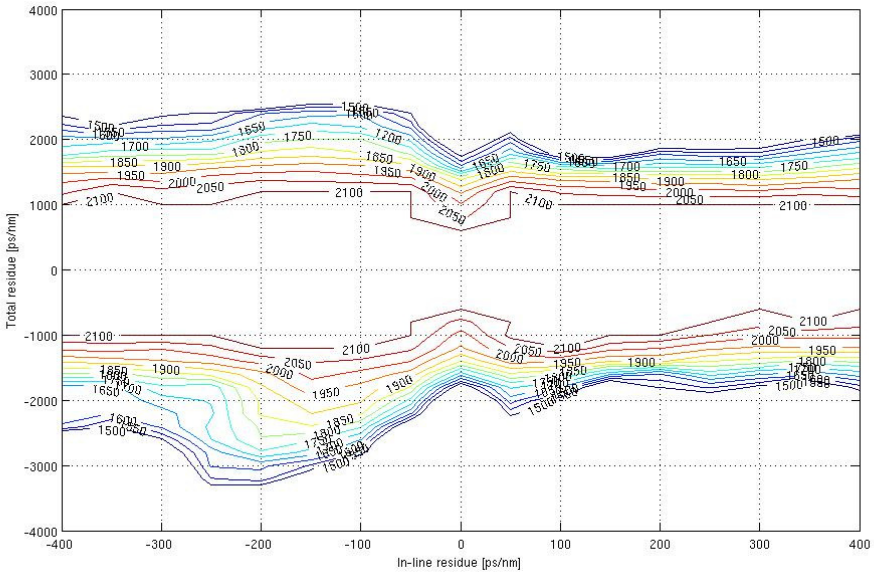

Figure 7.1. Contour plot of maximum reachable distance (in km) vs. in-line and total dispersion compensation residue for P_{ch}=3 dBm using a standard receiver and DPSK modulation

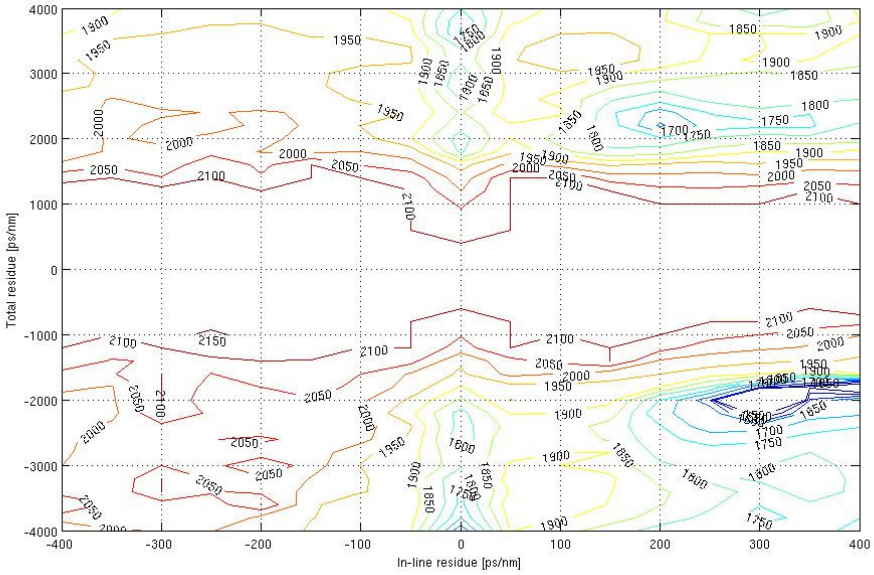

Figure 7.2. Contour plot of maximum reachable distance (in km) vs. in-line and total dispersion compensation residue for P_{ch}=3 dBm using a MLSE receiver and DPSK modulation

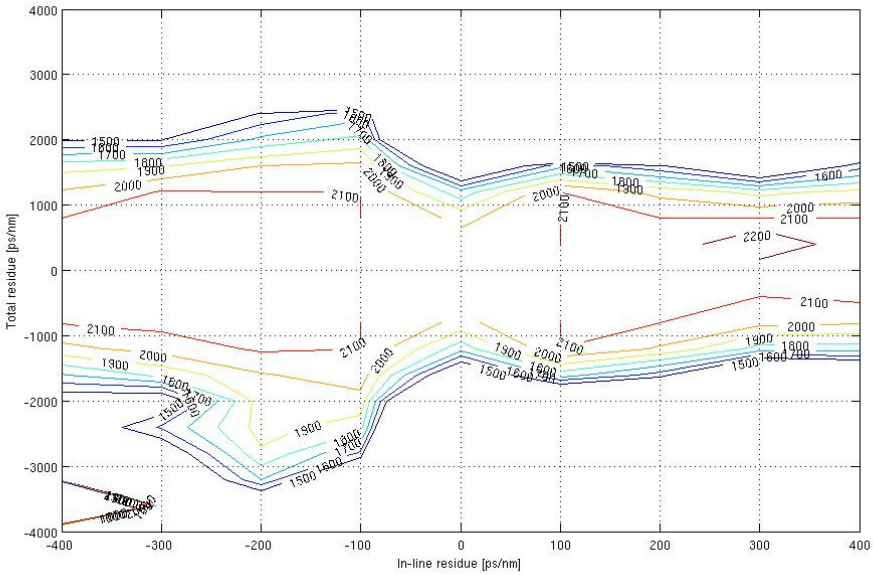

Figure 7.3. Contour plot of maximum reachable distance (in km) vs. in-line and total dispersion compensation residue for P_{ch}=4.5 dBm using a standard receiver and DPSK modulation

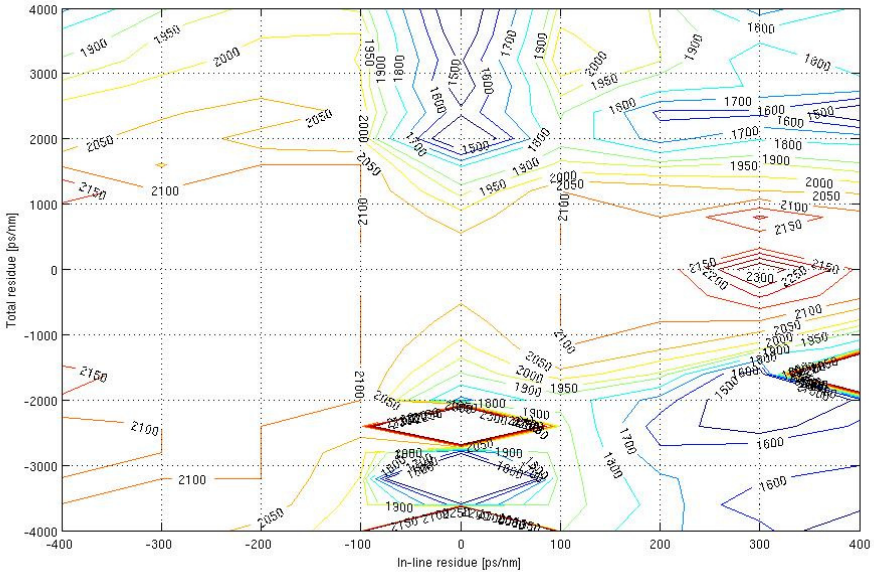

Figure 7.4. Contour plot of maximum reachable distance (in km) vs. in-line and total dispersion compensation residue for P_{ch}=4.5 dBm using a MLSE receiver and DPSK modulation

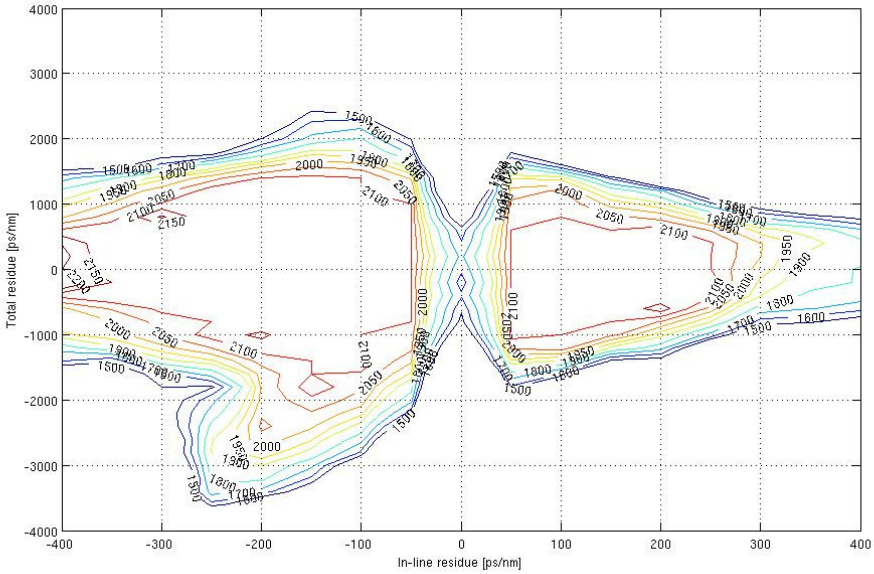

Figure 7.5. Contour plot of maximum reachable distance (in km) vs. in-line and total dispersion compensation residue for P_{ch}=6 dBm using a standard receiver and DPSK modulation

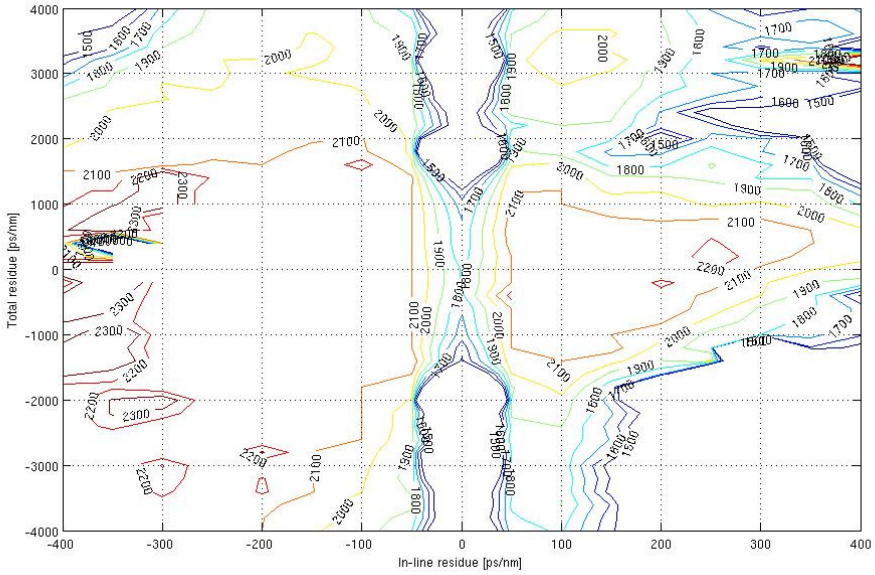

Figure 7.6. Contour plot of maximum reachable distance (in km) vs. in-line and total dispersion compensation residue for P_{ch}=6 dBm using a MLSE receiver and DPSK modulation

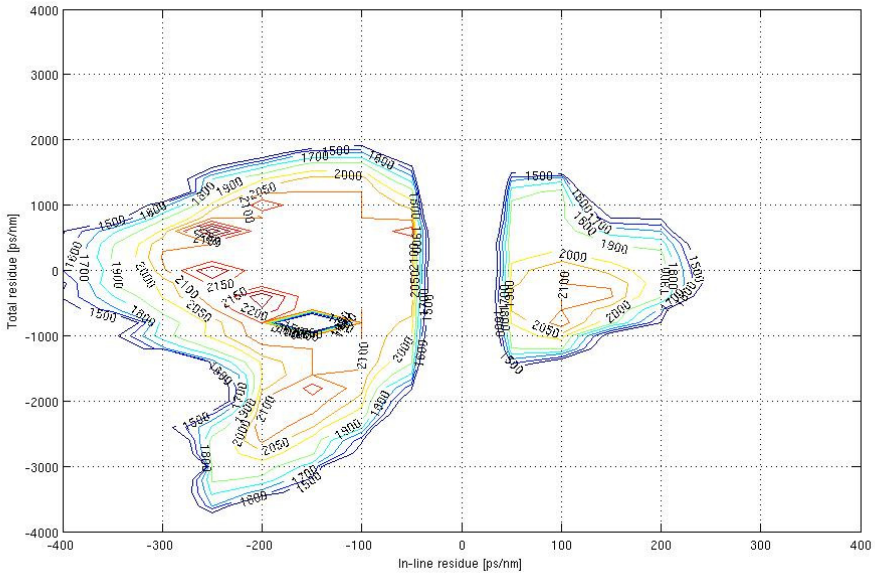

Figure 7.7. Contour plot of maximum reachable distance (in km) vs. in-line and total dispersion compensation residue for P_{ch}=7.5 dBm using a standard receiver and DPSK modulation

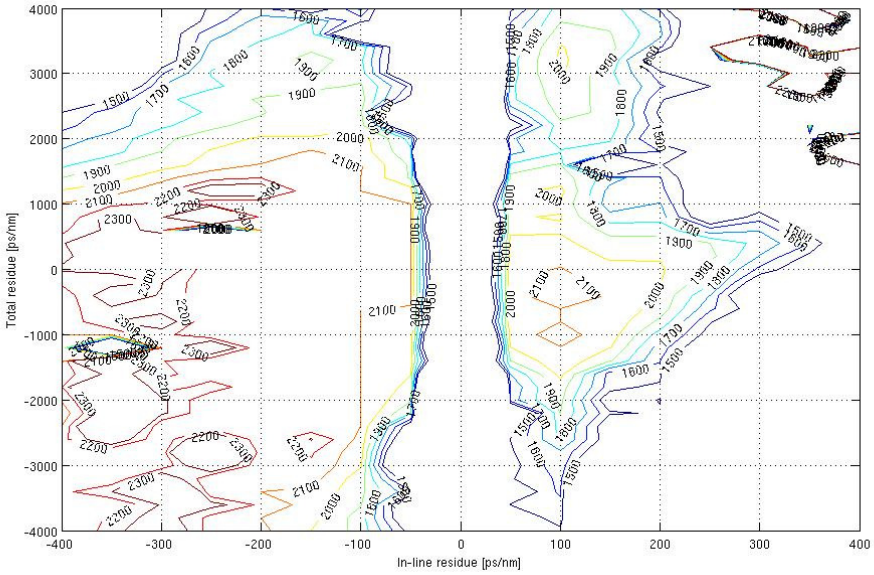

Figure 7.8. Contour plot of maximum reachable distance (in km) vs. in-line and total dispersion compensation residue for P_{ch}=7.5 dBm using a MLSE receiver and DPSK modulation

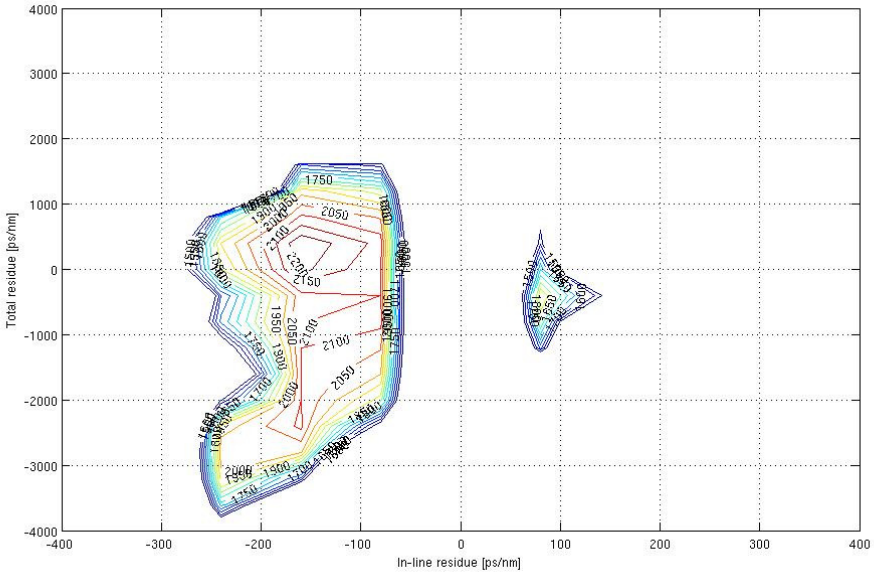

Figure 7.9. Contour plot of maximum reachable distance (in km) vs. in-line and total dispersion compensation residue for P_{ch}=9 dBm using a standard receiver and DPSK modulation

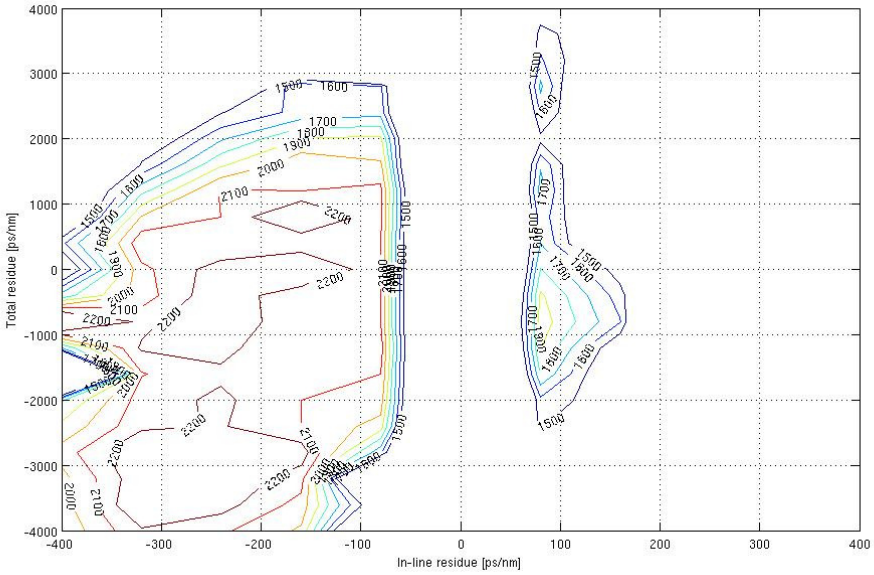

Figure 7.10. Contour plot of maximum reachable distance (in km) vs. in-line and total dispersion compensation residue for Pch=9 dBm using a MLSE receiver and DPSK modulation

7.1.2 Simulation results

In this case, for a launch power equal to 3 dBm, one large optimum region ($D_{res,tot}$ ±600 ps/nm and $D_{res,IL}$ ±400 ps/nm) is observed. For launch powers of 4.5 dBm and higher, two distinct optimum regions can be observed for negative and positive values of in-line residue respectively. Contrary to what happens with IMDD and Duobinary, a higher system distance is reached for $D_{res,IL} < 0$. The optimum regions are larger for $D_{res,IL} < 0$.

The maximum theoretical system total length is reported for all the transmitted power values and for both the standard and MLSE receivers in *Table 7.1*.

	Maximum System Total Length [km]	
P_{ch} [dBm]	**Standard RX**	**MLSE RX**
3	2115	2175
4.5	2140	2270
6	2275	2395
7.5	2340	2470
9	2240	2480

Table 7.1. Maximum system total length using DPSK modulation

For all launch powers and for both the standard and MLSE receivers, the maximum reachable system distance is greater than that achieved with Duobinary and IMDD modulation formats. The optimum regions are wider as well.

The width of the $D_{res,IL}$ and $D_{res,tot}$ windows in which the maximum theoretical system length L_{tot} is greater than 2100 and 2200 km are reported in *Tables 7.2* and *7.3* for both the standard and MLSE receivers and for transmitted channel powers ranging from 3 dBm to 9 dBm.

	Standard RX		**MLSE RX**	
P_{ch} [dBm]	**$D_{res,IL}$**	**$D_{res,tot}$**	**$D_{res,IL}$**	**$D_{res,tot}$**
3	± 400 ps/nm	± 600 ps/nm	± 200 ps/nm	± 1000 ps/nm
4.5	± 100 ps/nm	± 1000 ps/nm	± 150 ps/nm	± 1500 ps/nm
6	± 125 ps/nm	± 850 ps/nm	± 150 ps/nm	± 1700 ps/nm
7.5	± 60 ps/nm	± 800 ps/nm	± 140 ps/nm	± 2000 ps/nm
9	± 50 ps/nm	± 500 ps/nm	± 110 ps/nm	± 1000 ps/nm

Table 7.2. Dispersion windows for different values of launch power at a total distance of 2100 km for standard and MLSE receivers

	Standard RX		MLSE RX	
P_{ch} [dBm]	**$D_{res,IL}$**	**$D_{res,tot}$**	**$D_{res,IL}$**	**$D_{res,tot}$**
3	----------	----------	----------	----------
4.5	----------	----------	± 20 ps/nm	± 100 ps/nm
6	± 7 ps/nm	± 100 ps/nm	± 50 ps/nm	± 800 ps/nm
7.5	± 6 ps/nm	± 130 ps/nm	± 50 ps/nm	± 600 ps/nm
9	± 14 ps/nm	± 160 ps/nm	± 30 ps/nm	± 500 ps/nm

Table 7.3. Dispersion windows for different values of launch power at a total distance of 2200 km for standard and MLSE receivers

The optimum value of launch power, i.e. the one which yields the largest window for the 2100 and 2200 km contours, is 7.5 and 6 dBm per channel respectively for both receivers.

By comparing these results against those obtained with IMDD and Duobinary modulations, it can be seen that the DPSK modulation format is more robust to chromatic dispersion and impact of non-linear effects.

To analyze the effect of XPM, a simulation of a system with the same characteristics as shown in section 7.1 was carried out, but transmitting one channel only (the central channel) with a launch power equal to 7.5 dBm. The obtained contour plots are shown in *Figures 7.11* and 7.*12.*

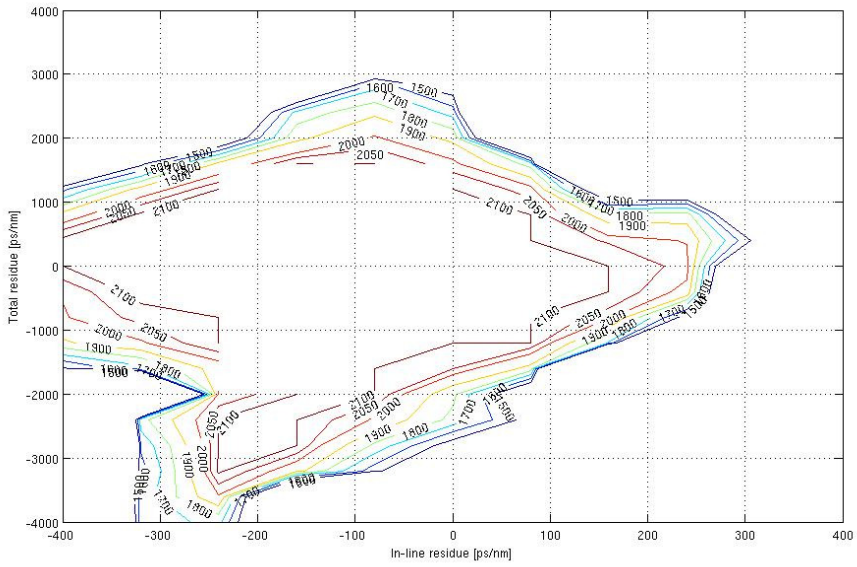

Figure 7.11 Contour plot of maximum reachable distance (in km) vs. in-line and total dispersion compensation residue for Pch=7.5 dBm using a standard receiver and DPSK modulation (only the central channel is transmitted)

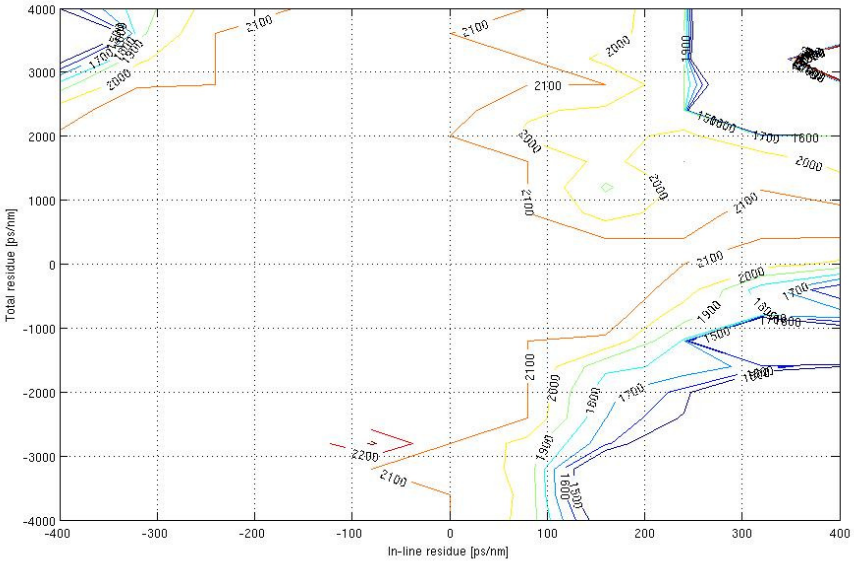

Figure 7.12 Contour plot of maximum reachable distance (in km) vs. in-line and total dispersion compensation residue for Pch=7.5 dBm using a MLSE receiver and DPSK modulation (only the central channel is transmitted)

When comparing *Figures 7.7* and *7.8* with *Figures 7.11* and 7.*12*, it is evident how XPM affects the system's performance. This is due to the high launch power needed to reach a maximum link length as high as 2200 km, and the tight channel spacing (50 GHz).

As seen in the graphics, MLSE cannot mitigate XPM. However, as said in chapter 5, by mitigating the penalty stemming from both suboptimal dispersion compensation and from intra-channel non-linearity, MLSE can allow access to wide areas of the contour planes which are favorable for XPM but cannot be typically accessed by conventional systems due to the high single-channel penalties.

It is important to point out the great advantage that the use of a MLSE receiver brings to a WDM system. Due to the dispersion slope, different channels will "see" a different dispersion. If the optimum region is not wide enough, the lateral channels will not fit into it and suffer from different penalties which will make their reception impossible. When MLSE is used, the optimum regions are widened, providing a higher tolerance to chromatic dispersion which allows fitting the whole WDM comb in the same region, thus achieving the correct reception of all the channels.

Chapter 8

Performance of the MLSE equalization in an optical communication system using the DQPSK modulation format

The DQPSK modulation format uses a four level signal that has a reduced band occupancy (half the bit-rate), which makes it more robust to chromatic dispersion. Also, the fact that the transmitted power is constant makes it more resistant against non-linear effects.

In this chapter, the results of a study on the use of MLSE receivers on optical communications systems in the presence of chromatic dispersion and fiber nonlinearities are shown.

The system set-up is exactly the same as the one shown in the previous three chapters but the modulation format considered is the DQPSK. In this case, the transmitter and receiver are substituted with their corresponding DQPSK equivalent. The DQPSK transmitter and receiver implemented on the simulations are shown in *Figures 8.1* and *8.2* respectively.

The simulations of the optical system were done using the software OptSim and the graphics were obtained using Matlab.

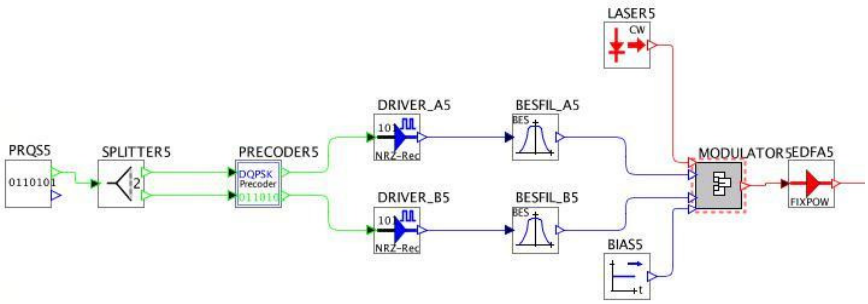

Figure 8.1. DQPSK transmitter scheme

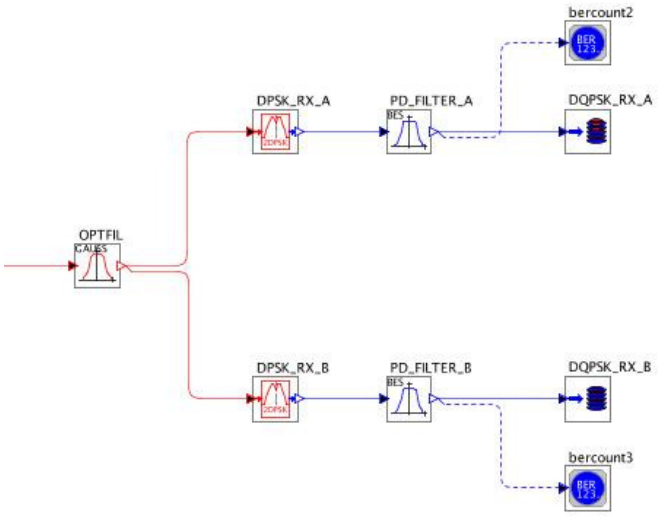

Figure 8.2. DQPSK receiver scheme

8.1 DQPSK System characteristics

The characteristics of the system set-up and simulation procedures are the following:

- The symbol-rate is R_s = 5.35 GBaud
- The number of channels is 7 with spacing equal to 50 GHz
- The central channel frequency is 194 THz

- The Pseudo Random Bit Sequence generated for each channel is PRBS = 2^{16} -1 = 65535 bits
- Each bit is simulated using 80 samples
- The electrical filters of the transmitter are 5 pole Bessel filters with $B_{-3\ dB}$ = 3 GHz
- The channel is formed by 15 spans of SSMF followed by an in-line DCU and a EDFA
- The SMF has the following characteristics:
  - α = 0.25 dB/km
  - D = 16 ps/nm/km
  - γ = 1.18 1/W/km
- The EDFAs have a gain that completely recovers the span loss ($G = \alpha \cdot L_{span}$) and a noise figure equal to 5.5 dB
- The in-line DCU introduces a dispersion value equal to $D_{IL} = D_{res,IL} - D \cdot L_{span}$ ps/nm, where $D_{res,IL}$ is the In-Line residue
- The Pre and Post compensation units introduce dispersion values of:
  - Dpre = -300 ps/nm
  - Dpost = $D_{res,tot} - D_{res,IL} \cdot$Nspan – Dpre ps/nm, where $D_{res,tot}$ is the total residue at the end of the link
- The receiver is composed by a 2^{nd} order SuperGaussian optical filter with B_{-3dB} = 35 GHz followed by two ideal DPSK receivers (see *Figure 8.2*), each DPSK receiver if followed by a 5 pole Bessel electrical filter with B_{-3dB} = 7.5 GHz.
- The receiver is followed by a 64-states balanced double-input MLSE processor.
- The used metric is as shown in section 4.4.2 of chapter 4.
- 2 samples per bit are used for the branch metric evaluation.

8.1.1 The testing procedure

In this case the testing procedure is exactly the same as explained in chapter 6, with the exception that a balanced dual-input MLSE processor is used. In the previous two chapters the MLSE processor was implemented directly on OptSim, while in this case, BER calculation for the MLSE receiver was implemented on MatLab.

The contour plots of maximum system length (@BER=10^{-3}) vs. in-line and total residue were obtained for launch power values equal to 3, 4.5, 6 and 7.5 dBm and for both the standard and MLSE receivers. These graphics are shown in *Figures 8.3* thru 8.*10*.

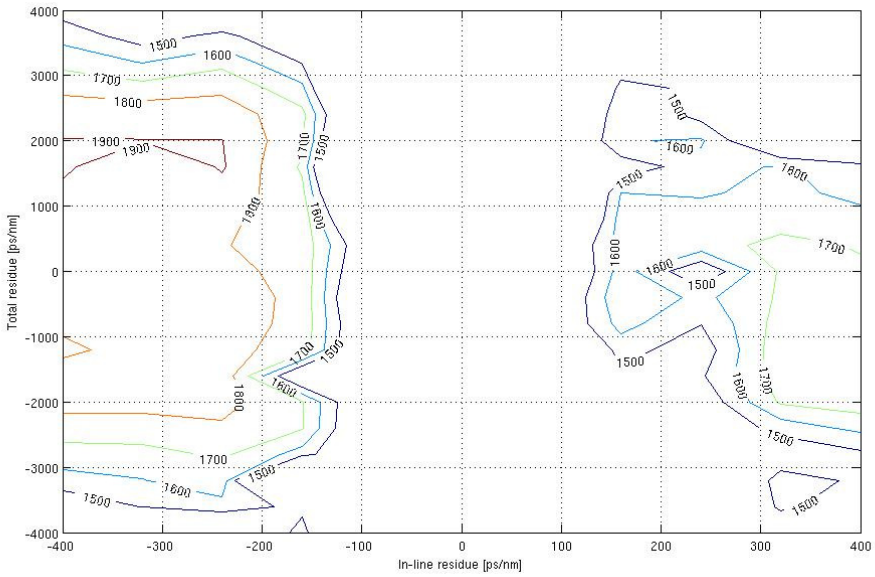

Figure 8.3. Contour plot of maximum reachable distance (in km) vs. in-line and total dispersion compensation residue for P_{ch}=3 dBm using a standard receiver and DQPSK modulation

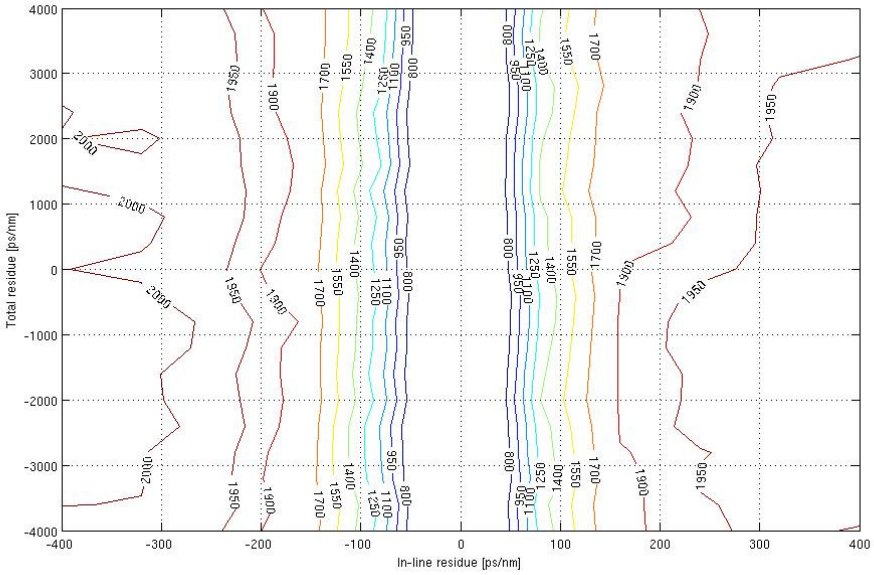

Figure 8.4. Contour plot of maximum reachable distance (in km) vs. in-line and total dispersion compensation residue for P_{ch}=3 dBm using a MLSE receiver and DQPSK modulation

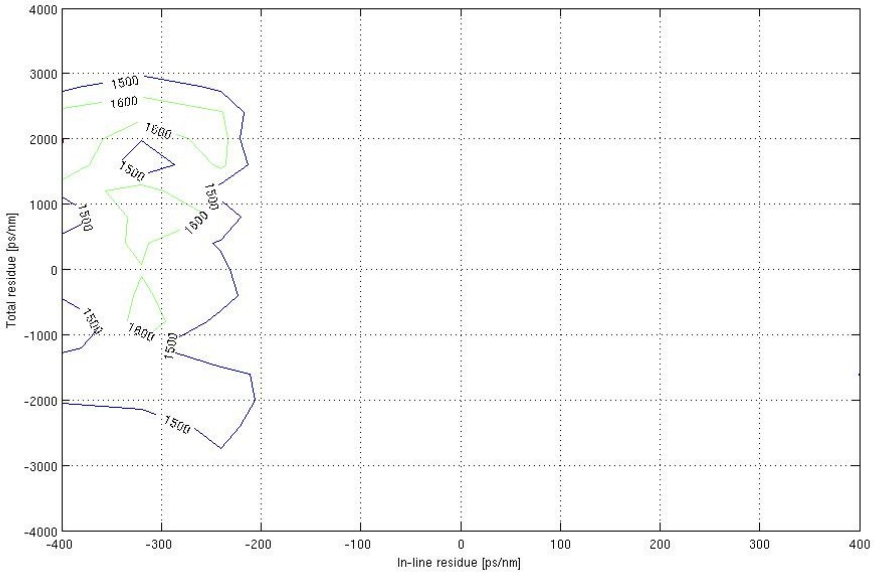

Figure 8.5. Contour plot of maximum reachable distance (in km) vs. in-line and total dispersion compensation residue for P_{ch}=4.5 dBm using a standard receiver and DQPSK modulation

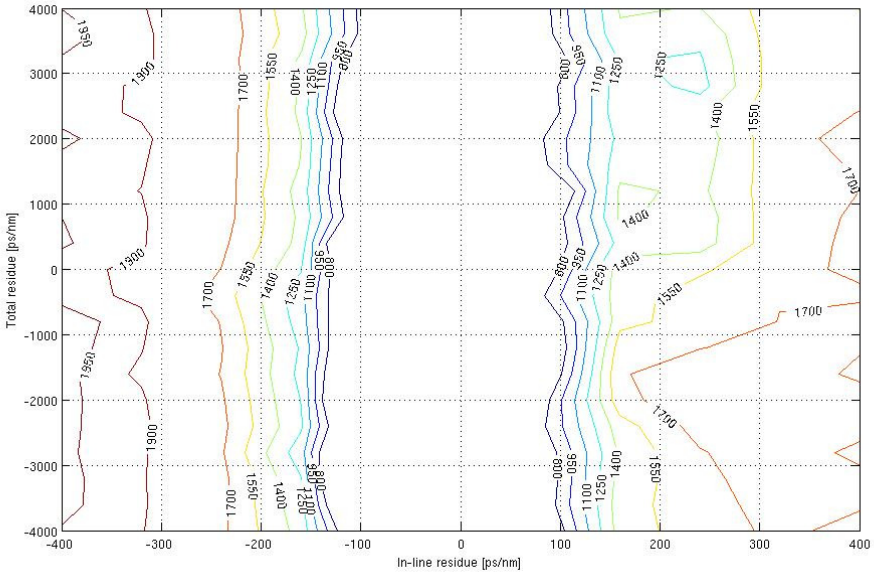

Figure 8.6. Contour plot of maximum reachable distance (in km) vs. in-line and total dispersion compensation residue for P_{ch}=4.5 dBm using a MLSE receiver and DQPSK modulation

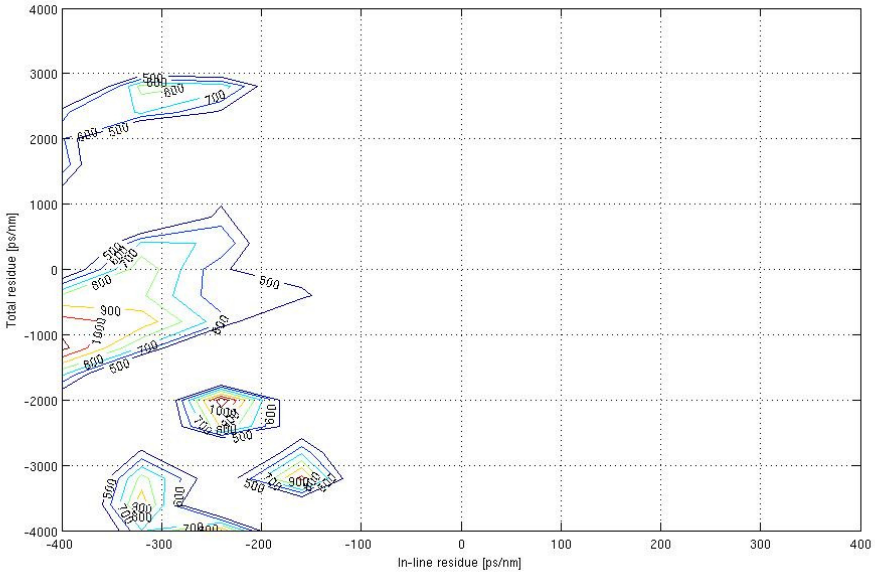

Figure 8.7. Contour plot of maximum reachable distance (in km) vs. in-line and total dispersion compensation residue for P_{ch}=6 dBm using a standard receiver and DQPSK modulation

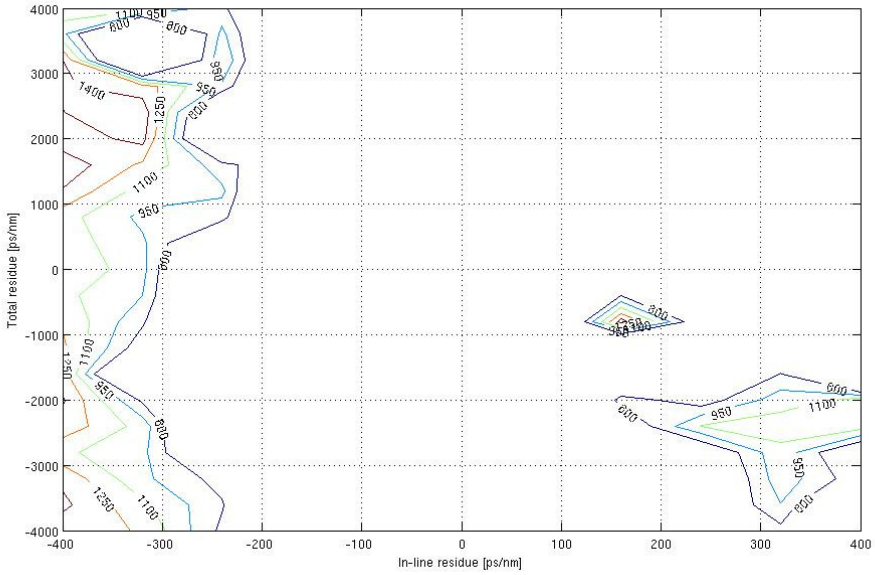

Figure 8.8. Contour plot of maximum reachable distance (in km) vs. in-line and total dispersion compensation residue for P_{ch}=6 dBm using a MLSE receiver and DQPSK modulation

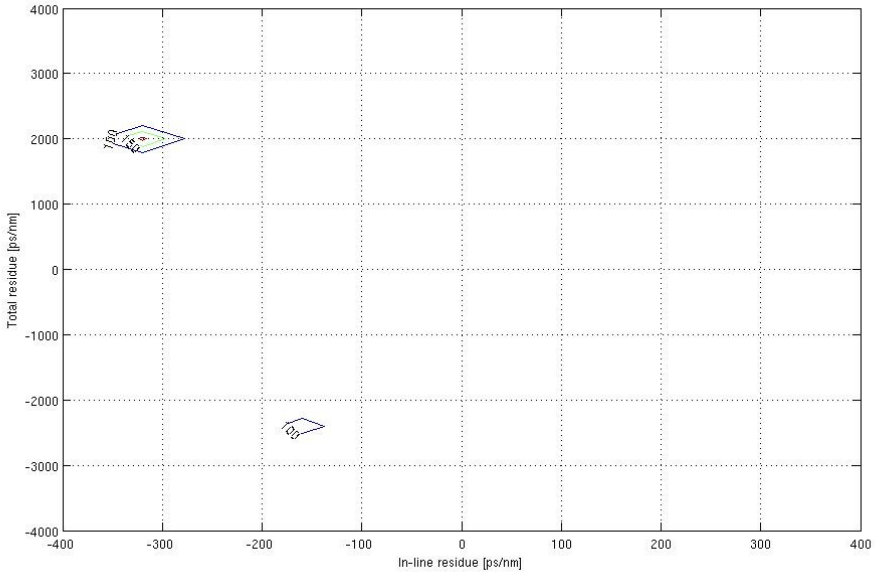

Figure 8.9. Contour plot of maximum reachable distance (in km) vs. in-line and total dispersion compensation residue for P_{ch}=7.5 dBm using a standard receiver and DQPSK modulation

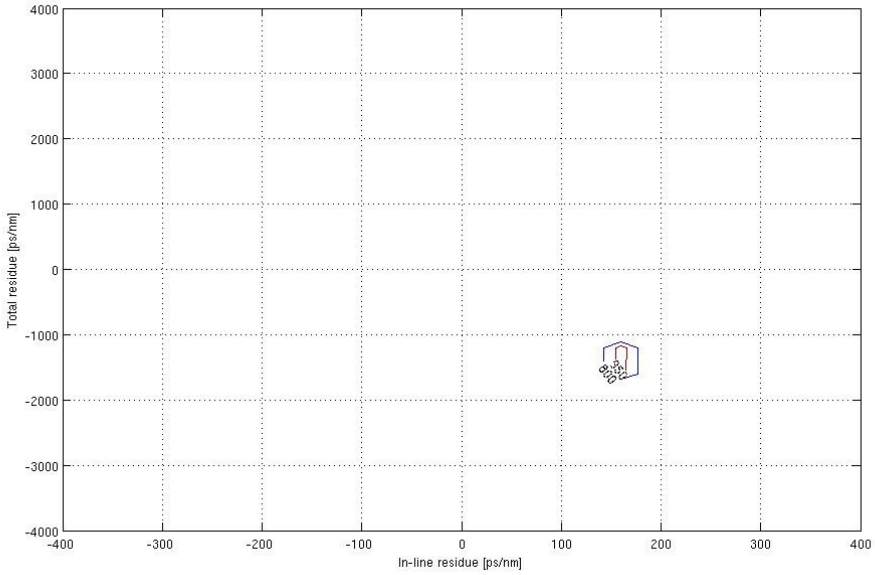

Figure 8.10. Contour plot of maximum reachable distance (in km) vs. in-line and total dispersion compensation residue for P_{ch}=7.5 dBm using a MLSE receiver and DQPSK modulation

8.1.2 Simulation results

For launch powers from 3 to 6 dBm, two distinct optimum regions can be observed for negative and positive values of in-line residue respectively. While for 7.5 dBm, the effect of XPM strongly limits the system performance. Contrary to what happens with IMDD and Duobinary, a higher system distance is reached for $D_{res,IL} < 0$. The optimum regions are larger for $D_{res,IL} < 0$.

The maximum theoretical system total length is reported for all the transmitted power values and for both the standard and MLSE receivers in *Table 8.1*.

	Maximum System Total Length [km]	
P_{ch} [dBm]	**Standard RX**	**MLSE RX**
3	1920	2030
4.5	1740	1980
6	1175	1500
7.5	210	1020

Table 8.1. Maximum system total length using DQPSK modulation

It can be seen how XPM strongly impairs the system performance as launch power increases. However, as expected, the use of a MLSE receiver increases the maximum reachable distance and widens the optimum regions.

The optimum value of launch power in this case is 3 dBm, since the system performance decreases dramatically for increasing values of launch power.

The performance of the system when DQPSK modulation is used is not better than that obtained with the modulation formats studied in the previous chapters (IMDD, Duobinary and DPSK).

To show just how strong the impact of XPM is on this system set-up, a simulation of a system with the same characteristics as shown in section 8.1 was carried out, but transmitting one channel only (the central channel) with a launch power equal to 6 dBm. The obtained contour plots are shown in *Figures 8.11* and 8.*12.*

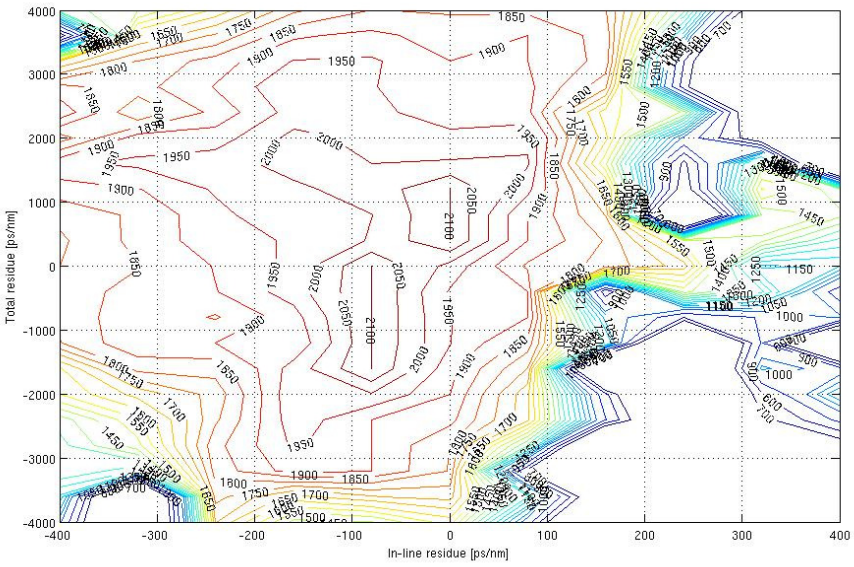

Figure 8.11 Contour plot of maximum reachable distance (in km) vs. in-line and total dispersion compensation residue for Pch=6 dBm using a standard receiver and DQPSK modulation (only the central channel is transmitted)

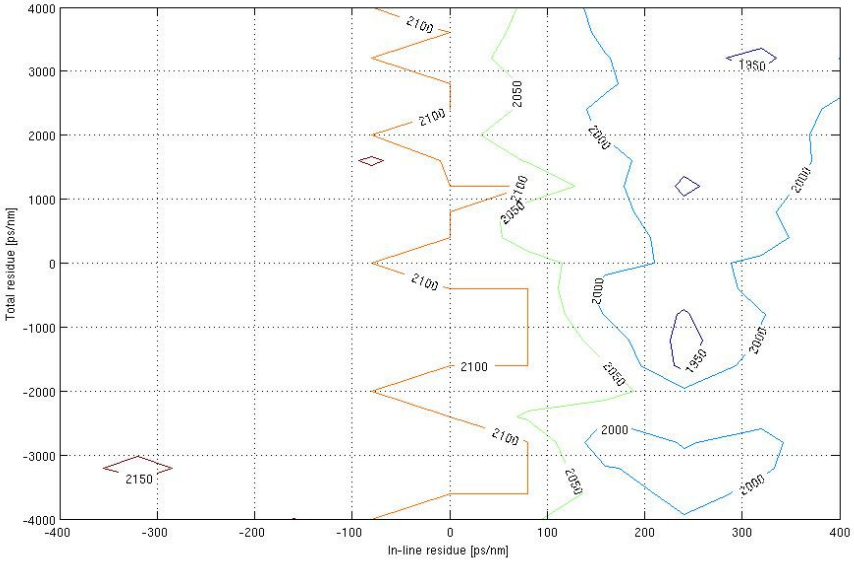

Figure 8.12 Contour plot of maximum reachable distance (in km) vs. in-line and total dispersion compensation residue for Pch=6 dBm using a MLSE receiver and DQPSK modulation (only the central channel is transmitted)

When comparing *Figures 8.7* and *8.8* with *Figures 8.11* and 8.*12*, it is evident how XPM strongly affects the system's performance. It can be seen how XPM reduces the maximum reachable distance from 2100 to 1175 km when a standard receiver is used, and from 2190 to 1500 km when a MLSE receiver is used.

These results were obtained using standard values for the electrical filter bands at the transmitter and receiver. The performance can improve if these bands were to be optimized.

As seen in the graphics, MLSE cannot mitigate XPM. However, as said in chapter 5, by mitigating the penalty stemming from both suboptimal dispersion compensation and from intra-channel non-linearity, MLSE can allow access to wide areas of the contour planes which are favorable for XPM but cannot be typically accessed by conventional systems due to the high single-channel penalties.

It is important to point out the great advantage that the use of a MLSE receiver brings to a WDM system. Due to the dispersion slope, different channels will "see" a different dispersion. If the optimum region is not wide enough, the lateral channels will not fit into it and suffer from different penalties which will make their reception impossible. When MLSE is used, the optimum regions are widened, providing a higher tolerance to chromatic dispersion which allows fitting the whole WDM comb in the same region, thus achieving the correct reception of all the channels.

Conclusions

Since its beginnings, optical communication systems have implemented the IMDD modulation format. Nevertheless, it has been shown that the use of alternative modulation schemes such as Duobinary, DPSK and DQPSK can be effective in mitigating the phenomenon of chromatic dispersion, allowing the reaching of greater distances. Another interesting alternative which has proven to be very effective in the compensation of chromatic dispersion is the use of a MLSE receiver as an electronic compensation system.

For the system analyzed in this study, it has been found that for all the modulation formats used and for all launch power values, the use of a MLSE receiver yields a greater total system reachable length than that achieved with a standard threshold receiver. The optimum regions of the contour plots of maximum reachable distance (in km) vs. in-line and total dispersion compensation residue widen as well when the MLSE receiver is used. This substantially increases dispersion map design tolerance.

Regarding XPM, the use of MLSE certainly cannot mitigate it. However, by mitigating the penalty stemming from both suboptimal dispersion compensation and from intra-channel non-linearity, it allows access to wide areas of the contour planes which are favorable for XPM but cannot be typically accessed by conventional systems due to the high single-channel penalties.

Four modulation formats were studied: IMDD, Duobinary, DPSK and DQPSK. Given the results obtained from the simulated system, the modulation format which yields the best performance in terms of maximum reachable distance and tolerance to

chromatic dispersion is the DPSK, followed by IMDD, Duobinary and finally DQPSK. As an additional comment, the maximum system reachable length is found in the region corresponding to $D_{res,IL}>0$ for the intensity modulation formats i.e. IMDD and Duobinary, whereas it is found for $D_{res,IL}<0$ for the phase modulation formats i.e. DPSK and DQPSK. In all four cases, the optimum regions are wider for $D_{res,IL}<0$.

The sub-optimal performance of the Duobinary and DQPSK systems can be attributed to the fact that the bands of the filters were not optimized.

The carried out experiments show that the use of a reasonable complexity (32 states) MLSE processor, together with a relatively simple metric such as the Gaussian metric (in the case of DPSK), can greatly help in enhancing system robustness to dispersion map parameters, even in presence of significant XPM impact. To a certain extent, also the system top performance, in terms of theoretical total length, is improved. This represents a great advantage to WDM systems, where due to the non-zero dispersion slope; different channels experience different in-line dispersion values, since the use of MLSE widens the optimum regions providing a higher tolerance to chromatic dispersion which allows fitting the whole WDM comb in the same region, thus achieving the correct reception of all the channels.

The techniques here studied may be introduced in an optical communication system without touching the fiber already installed, and from the results here obtained, it may be observed that they are very effective in counteracting the effects produced by chromatic dispersion.

References

[1] "A Brief History of Fiber Optical Technology" [online], *FI*. 2005. 22 Aug. 2007. <http://www.fiber-optics.info/fiber-history.htm>.

[2] "Types of Optical Fiber" [online], *FI.* 2005. 22 Aug. 2007. <http://www.fiber-optics.info/articles/fiber-types.htm>.

[3] A. Girard, "Polarization of Light in Fiber Causes Signal Dispersion", Canada, Exfo Electro-optical Engineering, 2000.

[4] I. Karminow and L. Tingye, "Optical fiber telecommunications IVB: systems and impairements", San Diego, Academic Press, 2002.

[5] N. Alic, G. C. Papen, R. E. Saperstein, L. B. Milstein and Y. Fainman, "Signal statistics and maximum likelihood sequence estimation in intensity modulated fiber optic links containing a single optical preamplifier", Opt. Exp., Vol. 13, issue 5, pp. 4568-4579, Jun 2005.

[6] G. Bosco, P. Poggiolini and M. Visintin, "Performance Analysis of MLSE Receivers Based on the Square Root Metric", *ECOC 2007*, Berlin, Germany, 16-20 Sep. 2007.

[7] G. Bosco and P. Poggiolini "Long-Haul WDM IMDD Transmission at 10.7 Gbit/s in a Dispersion-Managed Multispan System Using MLSE Receivers" To be published in IEEE Journal of Lightwave Technology

[8] S. Chandrasekhar and A.H. Gnauck, "Performance of MLSE receiver in a dispersion-managed experiment at 10.7 Gb/s under non-linea transmission", *IEEE Photon. Technol. Lett., vol. 18, no. 23, pp. 2448-2450, Dec. 2006.*

[9] P. Poggiolini, G. Bosco and M. Visintin, "MLSE receivers and their applications in optical transmission systems", in Proc. LEOS, Oct. 21-25, 2007, pp. 216-217.

Bibliography

- O. E. Agazzi, M. R. Hueda, H. S. Carrer and D. E. Crivelli, "Maximum Likelihood Sequence Estimation in Dispersive Optical Channels", *IEEE Journal of Lightwave Technology,* ISBN: 0733-8724, Vol. 23, pp 749–763, Feb. 2005.
- G. Bosco, "Performance analysis of optical communication systems" (PhD. Thesis), Torino: Politecnico di Torino, XIV Ciclo.
- G. Bosco, I. Cano, V. Curri, P. Poggiolini, "Optimization of Branch Metric Exponent and Quantization Range in MLSE Receivers for Duobinary Systems".
- G. Bosco, P. Poggiolini, M. Visintin, "Performance Analysis of MLSE Receivers Based on the Square-Root Metric".
- G. Bosco, V. Curri and P. Poggiolini "Long Haul Multi-Channel IMDD Transmission at 10.7 Gbit/s in a Dispersion-Managed Multispan System Using a MLSE Receiver" To be published on *J. Lightw. Technol*
- C. Dorschky et al., "Measurement of the Dispersion Tolerance of Optical Duobinary with an MLSE-Receiver at 10.7 Gb/s", *Optical Society of America*, 2005.
- G.D. Forney JR, "The Viterbi Algorithm", *Proceedings of the IEEE*, Vol. 61, No. 3, pp. 268-278, Mar. 1973.
- R. Gaudino, P. Poggiolini, "Reti in fibra ottica", Torino, Politeko, 2005.
- G. Bosco and P. Poggiolini, "Long-distance Effectiveness of MLSE IMDD Receivers", *IEEE Photonics Technology Letters*, Vol. 18, Issue 9, pp. 1037–1039, May 2006.

- O. Koufopavlou, I. Tomkos, A. Tychopoulos, “FEC IN OPTICAL COMMUNICATIONS” *IEEE Circuits & Devices Magazine*, pp. 79-86, Nov./Dec. 2006.
- E. Roffé, “Use of MLSE receivers in optical communications” (Thesis), Torino: Politecnico di Torino, 2007.
- “History of fiber optics” [online]. *Timbercon*. 22 Aug. 2007. <http://www.timbercon.com/History-of-Fiber-Optics/index.html>.
- “Advantages of fiber optics” [online] May 2008 <http://www.doc.ic.ac.uk/~nd/surprise_97/journal/vol4/sm27/adv.html>